

博士論文

Modeling urban growth prediction in Yangon, Myanmar
considering flood and earthquake vulnerabilities

(洪水と地震脆弱性を考慮したミャンマーヤンゴンの
都市成長予測モデル)

スリータラーピパット タナコーン

37-147192

A Dissertation Submitted in Partial Fulfillment

of the Requirements for the Degree of

Doctor of Philosophy

Department of Civil Engineering

Graduate School of Engineering

The University of Tokyo

Tokyo, Japan

September 2017

Modeling urban growth prediction in Yangon, Myanmar
considering flood and earthquake vulnerabilities

(洪水と地震脆弱性を考慮したミャンマーヤンゴンの
都市成長予測モデル)

Examination Committee

Associate Professor Wataru Takeuchi

Associate Professor Akiyuki Kawasaki

Associate Professor Kazuo Oki

Associate Professor Yoshihide Sekimoto

Associate Professor Yudai Honma

Tanakorn Sritarapipat

A dissertation submitted to

Department of Civil Engineering, The University of Tokyo

Abstract

(論文の内容の要旨)

Modeling urban growth prediction in Yangon, Myanmar considering
flood and earthquake vulnerabilities

(洪水と地震脆弱性を考慮したミャンマーヤンゴンの都市成長予測モデル)

Tanakorn Sritarapipat

Yangon, formerly known as Rangoon, is the largest city in Myanmar, formerly known as Burma. Yangon is the major of country's economic areas with more than five million population, and the urban areas have significantly increased. However, Yangon has suffered from the series of floods with almost every 1-2 years. In flooding case of 2014, Yangon had losses of more than 8.5 million US dollars with affected 63,082 people, 18 schools, 17 miles of road, 8 bridges and 56,486 acres of farmland. Yangon city also had faced the effect of the earthquake in 1930. In that time, an earthquake with the magnitude of 7.0 occurred in Bago region and caused the extensive damage including 500 killed people. In Yangon city, there were 50 died people with the population of 400,000. As a result, Yangon is at the high risks of flood and earthquake. In order to reduce the impacts of flood and earthquake in the future, the disaster risk assessment and disaster risk reduction in the term of economic loss relating to the gross domestic product in Yangon, Myanmar are necessary.

The objectives of this research are (1) to reduce flood and earthquake risks in Yangon from 2020 to 2040, and (2) to assess the flood and earthquake risks in term of economic loss relating to the regional gross domestic product (GRDP) with multiple-scenarios in Yangon from 2020 to 2040. To achieve the objectives, we have done mainly six steps as follows.

Firstly, the assessment of flood vulnerability in Yangon, Myanmar has been conducted base on the multi-criteria analysis modeling. We used the seven factors with (1) land cover types, (2) elevation, (3) slope, (4) soil types, (5) flow accumulation, (6) the distance from the drainage network, (7) rainfall. We combined the empirical model linking with the historical water surface to estimate the coefficients in the flood vulnerability assessment. Then, the flood vulnerability map in Yangon was computed based on the empirical model with the historical water surface.

Secondly, the assessment of earthquake vulnerability in Yangon, Myanmar has been performed base on the multi-criteria analysis modeling. We used the factors of (1) the seismic intensity, (2) soil type (3) slope (4) the height of the building, (4) the material of the building and (5) the age of the building. Then, the earthquake building vulnerability maps with the multiples cases by varying the earthquake probabilities and the materials were provided.

Thirdly, the estimation of land price based on the empirical model in Yangon, Myanmar has been done. The defined factors are (1) building types, (2) land cover change, (3) elevation, (4) the distance from railways. The empirical model was used to relate to land price information at the township scale to estimate the parameters in the land price estimation. Then, Land price map base on the empirical model was provided.

Fourthly, urban expansion model has been proposed in order to predict the urban areas in the future in Yangon, Myanmar by using the dynamic statistical model. The defined factors are (1) the distance from the multi-center of the urban areas, (2) the distance from the urban areas in the past, (3) the distance from roads, (4) the distance from railways, (5) the class translation, (6) elevation, (7) separated lands by rivers. The maximum likelihood estimator was employed with the defined factors to estimate the urban expansion.

Fifthly, by relating the prediction of urban expansion, enhanced with the master plan as future dataset, to the assessments of flood and earthquake vulnerabilities, the predicted urban growths by considering flood and earthquake vulnerabilities in order to reduce the damage of the flood and

earthquake from 2020 to 2040 with multi-scenarios were proposed.

Finally, by relating the predicted urban expansion, merged with land price estimation and the predicted economic growth relating to the regional gross domestic product (GRDP), to the assessments of flood and earthquake vulnerabilities, the assessments of flood and earthquake risks in term of economic loss relating to the GRDP from 2020 to 2040 with multiple-scenarios were proposed.

For the experimental result of urban expansion modeling, our method estimated urban areas in 1990, 2000, 2010, and 2020 with the averaged accuracy of 93% with the averaged TPR of 73% and the averaged TNR of 95%.

By using master plan as future dataset in the prediction of urban expansion, we found that the predicted urban expansion by using the master plan has more distribution than without the master plan. Unfortunately, by using the master plan, we found that some of predicted urban areas are located on the high venerable areas. By integrating flood and earthquake risk reductions with the prediction of urban expansion, the predicted urban areas can escape from the high flood and earthquake vulnerable areas effectively.

For assessment of flood economic risk, the total flood economic losses in 2020, 2030, and 2040 in Yangon by using Master plan are 687 million US dollars, 1,728 million US dollars, and 3049 million US dollars, respectively. By integrating with flood risk reduction, the flood economic losses can be reduced from 4 to 28 million US dollars. At the township scale, the five highest flood economic losses are Thanlyin, Twante, Haingtharyar, Mingalardon, Dagonmyothit (South).

For assessment of earthquake economic risk, the earthquake economic losses with the safest case of the probability of 10% and RC 2500psi in 2020, 2030, and 2040 in Yangon are 1,029 million US dollars, 2,613 million US dollars, 4,673 million US dollars, respectively. By integrating with earthquake risk reduction, the earthquake economic losses with the safest case can be reduced from 1 to 7 million US dollars. The earthquake economic losses with the worst

case of the probability of 2% and RC 1250psi in 2020, 2030, and 2040 in Yangon are 1,702 million US dollars, 4,595 million US dollars, 8,673 million US dollars, respectively. By integrating with earthquake risk reduction, the earthquake economic losses with the worst case can be reduced from 10 to 64 million US dollars. At the township scale, the five highest earthquake economic losses with the worst case are Thanlyin, Hlaingtharyar, Mingalardon, Dagonmyothit (South), Dagonmyothit (East).

By using the different features with the prediction model, multi-scenarios of predicted urban areas can be available to support for decision-making or policy for reducing disaster risk.

In this research, we used the various products analyzed from remotely sensed data. The validations of the products were performed. The validated results confirmed that our products by using remotely sensed data are reliable to be used in this research.

Acknowledgement

I would like to express my heartfelt appreciation to those who have all given me invaluable supports during my Ph.D. study.

I thought that I had precious experiences for studying Civil Engineering and doing research in Takeuchi Laboratory. I would like to express my deepest gratitude to Associate Professor Wataru Takeuchi, my supervisor, for always giving me constant encouragement, valuable suggestions, useful comments, and great supports to graduate the Ph.D. course. Under supervision of Takeuchi-sensei, I have many chances to attend the international remote sensing conferences that offered me to obtain the highly academic experiences and the deep knowledges of Remote Sensing with wide ranges. I also would like to express my sincere gratitude to Associate Professor Akiyuki Kawasaki, Associate Professor Kazuo Oki, Associate Professor Yoshihide Sekimoto, and Associate Professor Yudai Honma for their time, valuable comments and suggestions to improve considerably my research.

I am thankful to all members in Takeuchi laboratory. I am grateful to Ms. Yoko Yoshimura for her kind support in handling many documents. I would like to thank Ms. Nakasano and Mr. Arai for thier valuable suggestions and comments to enhance my research. I also would like to thank Mr. Prakhar, Mr. Anjar, Mr. Ark, Ms. Pegah, Ms. Trang, Ms. Tita, Mr. Arbad, Ms. Uchida, Mr. Inoue, Mr. Arif, Mr. Trung, Mr. yang, Ms.Li, Ms. Park, Mr. Sho, Mr. Katayama, Mr. Jonai for having great time together with various enjoyable activities.

I would like to thank Japan Science and Technology Agency (JST)/ Japan International Cooperation Agency (JICA), Science and Technology Research Partnership for Sustainable Development Program (SATREPS) for supporting this research. Finally, I would like to express my deepest appreciation to my family for their affection and support during my Ph.D. study.

September 2017

Contents

Abstract.....	III
Acknowledgement	VII
Contents	VIII
List of Figure	XII
List of Table.....	XIX
Chapter1. Introduction.....	1
1.1 Background	1
1.2 Objective of this study.....	10
1.3 Originality of this study.....	11
1.4 Outline of this study.....	12
Chapter2. Assessment of flood vulnerability	16
2.1 Background	16
2.2 Methodology.....	17
2.2.1 Defining flood vulnerability assessment	17
2.2.2 Preparing data.....	18
2.2.3 Defining flood vulnerability index	20
2.2.4 Estimating the weights of flood vulnerability index	21
2.3 Results and discussions	22
2.3.1 The assessment of flood vulnerability map	22
2.3.2 The validation of historical water surface	25
2.3.3 The validation of land cover image and SRTM DEM.....	28
2.4 Remarks	29

Chapter3.	Assessment of earthquake vulnerability	30
3.1	Background	30
3.2	Methodology.....	31
3.2.1	Defining earthquake vulnerability assessment	31
3.2.2	Preparing data.....	32
3.2.3	Calculating ground shaking map.....	33
3.2.4	Computing earthquake building vulnerability map.....	36
3.3	Results and discussions	40
3.3.1	The results of earthquake building vulnerability maps.....	40
3.3.2	The validation of the heights of buildings and digital surface model	42
3.4	Remarks	43
Chapter4.	Estimation of land price.....	44
4.1	Background	44
4.2	Methodology.....	45
4.2.1	Defining land price model.....	45
4.2.2	Preparing data.....	46
4.2.3	Defining land price index.....	47
4.2.4	Estimating the weights of land price index.....	49
4.3	Results and Discussions	50
4.3.1	The estimation of land price index	50
4.3.2	The validation of land price index.....	51
4.3.3	The validation of the building classification.....	53
4.4	Remarks	53
Chapter5.	Modeling urban expansion.....	55
5.1	Background	55
5.2	Methodology.....	56

5.2.1 Modeling urban expansion	56
5.2.2 Preparing data.....	57
5.2.3 Monitoring urban expansion with defined factors	58
5.2.4 Estimation of urban expansion.....	65
6.2.5 Prediction of urban expansion	67
5.3 Results and discussion.....	69
5.4 Remarks	72
Chapter6. Prediction urban expansion with consideration on flood and earthquake vulnerabilities	73
6.1 Reviews.....	73
6.2 Prediction of urban expansion with master plan	74
6.3 Prediction of urban expansion with consideration on flood vulnerability.....	76
6.4 Prediction of urban expansion with consideration on earthquake vulnerability	79
6.5 Remarks	83
Chapter7. Assessments of flood and earthquake risks interm of economic loss	84
7.1 Reviews.....	84
7.2 Converting land cover areas into economic areas	86
7.3 Calculating flood and earthquake risks in term of economic loss relating to GRDP.	88
7.4 Results of flood and earthquake risks in term of economic loss relating to GRDP ...	90
7.4.1 Results of flood risk in term of economic loss relating to GRDP	90
7.4.2 Results of earthquake risk in term of economic loss relating to GRDP	94
7.5 Remarks	107
Chapter8. Investigation of the high-rise buildings growth.....	108
8.1 Reviews.....	108
8.2 Observing the estimated building types with nighttime light data	108

8.3 Detecting the high rise building growth.....	109
8.4 Discussions.....	112
8.5 Remarks	113
Chapter9. Conclusions and recommendations	114
9.1 Conclusions	114
9.2 Recommendations	116
Reference	118
Appendix.....	127

List of Figure

Figure 1.1 The framework of this research.....	13
Figure 2.1 Flowchart of flood vulnerability assessment.....	18
Figure 2.2 The flood vulnerability map based on the empirical model (30 meters-resolution)	23
Figure 2.3 The flood vulnerability map based on AHP by expert opinions (30 meters-resolution).....	23
Figure 2.4 The flood vulnerability map based on flooding caused by cyclone Nargis using HydroSHEDS by ICHARM, 2016 (450 meters-resolution)	24
Figure 2.5 The flood vulnerability map based on the costal flood by Cyclone Nargis with the rainfall (100-year flood) by using RRI Model by ICHARM, 2016 (450 meters-resolution)	24
Figure 2.6 The historical water surface map using NDVI-time series from 2001 to 2015 (250 meters-resolution).....	26
Figure 2.7 The averaged LSWC map using AMSR-E and AMSR-2 from 2001 to 2015 (9 kilometers-resolution)	26
Figure 2.8 MODIS NDVI 8 days composition image during the flood event in 2008 (250 meters-resolution).....	27
Figure 2.9 The actual flooded areas map in the flood event in 2008 by UNOSAT	27
Figure 2.10 The estimated flooded areas map in the flood event in 2008 by MODIS NDVI 8 days composition image	28
Figure 3.1 Flowchart of earthquake vulnerability assessment	32

Figure 3.2 The earthquake amplitude map	34
Figure 3.3 The seismic intensity maps in term of PGA with the earthquake probabilities of (a) 2% and (b) 10%	35
Figure 3.4 The ground shaking maps in term of PGA with the earthquake probabilities of (a) 2% and (b) 10%	36
Figure 3.5 The fragility curves with (1) low-rise building with RC 2500psi, (2) high-rise building with RC 2500psi (3) low-rise building with RC 1250psi, (4) high-rise building with RC 1250psi.....	37
Figure 3.6 The simulated building damages with (a) the probability of 10% and RC 2500psi, (b) the probability of 10% and RC 1250psi, (c) the probability of 2% and RC 2500psi, (d) the probability of 2% and RC 1250psi.....	39
Figure 3.7 The earthquake building vulnerability map with (a) the probability of 10% and RC 2500psi, (b) the probability of 10% and RC 1250psi, (c) the probability of 2% and RC 2500psi, (d) the probability of 2% and RC 1250psi	41
Figure 4.1 The flowchart of land price estimation.....	46
Figure 4.2 The estimation of land price in Yangon.....	50
Figure 4.3 The estimated land price map at the township scale in 2012.....	51
Figure 4.4 The actual land price map at the township scale in 2012.....	51
Figure 4.5 The comparison between the estimated and actual land prices in 2012 at the township scale.....	52
Figure 4.6 The mean absolute error of the estimated and actual land prices in 2012 at the township scale.....	52

Figure 5.1 The flowchart of molding urban expansion	57
Figure 5.2 The 18 regions of the multi-centers of urban areas	59
Figure 5.3 The bar graphs of the means of the Euclidean distance from the multi-centers of urban areas in each region from 1978 to 2009 (Pixels).....	60
Figure 5.4 The histograms of the Euclidean distance from the multi-centers of urban areas in the region of the center #1 in the years of (a) 1978→1990, (b) 1990→2000, (c) 2000→2009 (Pixels).....	60
Figure 5.5 The bar graphs of the means of the Euclidean distance from the urban areas in the past from 1978 to 2009 (Pixels).....	61
Figure 5.6 The histogram of the Euclidean distances from the roads (Pixels).....	62
Figure 5.7 The bar graphs of the means of the Euclidean distance from the railways from 1978 to 2009 (Pixels).....	63
Figure 5.8 The bar graphs of the means of the elevation from 1978 to 2009 (Pixels)	64
Figure 5.9 The class translation in the region of the center #1 from 1978 to 2009 (Pixels)	65
Figure 5.10 The estimated Euclidean distance from the railways from 2020 to 2040 (Pixels)	68
Figure 5.11 The estimated class translation in the region of the center #1 from 2020 to 2040 (Pixels).....	68
Figure 5.12 (a) Referenced land cover image in 1990, (b) Referenced land cover image in 2000, (c) Referenced land cover image in 2009, (d) Estimated land cover image in 1990, (e) Estimated land cover image in 2000, (f) Estimated land cover image in 2009	69
Figure 5.13 (a) The unseen land cover image in 2015, (b) Predicted land cover image in	

2020, (c) Predicted land cover image in 2030, (d) Predicted land cover image in 2040	70
Figure 6.1 The flowchart of prediction of urban expansion considering on flood and earthquake vulnerabilities	74
Figure 6.2 The master plan in Yangon, Myanmar by JICA Team, 2016	75
Figure 6.3 (a) Predicted land cover image in 2020 with the master plan, (b) Predicted land cover image in 2030 with the master plan, (c) Predicted land cover image in 2040 with the master plan.	76
Figure 6.4 (a) Predicted land cover image in 2020 with the master plan and flood vulnerability map, (b) Predicted land cover image in 2030 with the master plan and flood vulnerability map, (c) Predicted land cover image in 2040 with the master plan and flood vulnerability map.....	77
Figure 6.5 Comparing total flood loss in term of the area on urban between using master plan, and using master plan and flood risk reduction in Yangon from 2020 to 2040.....	78
Figure 6.6 (a) Predicted land cover image in 2020 with the master plan and earthquake vulnerability map, (b) Predicted land cover image in 2030 with the master plan and earthquake vulnerability map, (c) Predicted land cover image in 2040 with the master plan and earthquake vulnerability map	80
Figure 6.7 Comparing total earthquake loss in term of the area on urban between using master plan, and using master plan and earthquake risk reduction in Yangon from 2020 to 2040.....	81
Figure 7.1 The flowchart of assessments of flood and earthquake risks in term of economic loss relating to GRDP	85

Figure 7.2 (a) economic area image in 2020, (b) economic area image in 2030 (c) economic area image in 2040 using the master plan.....	87
Figure 7.3 (a) economic area image in 2020, (b) economic area image in 2030 (c) economic area image in 2040 using the master plan and flood risk reduction	87
Figure 7.4 (a) economic area image in 2020, (b) economic area image in 2030 (c) economic area image in 2040 using the master plan and earthquake risk reduction	88
Figure 7.5 Comparing total flood losses in term of economic relating to GRDP between (1) using master plan and (2) using master plan and flood risk reduction in Yangon from 2020 to 2040 (Million US dollars).....	90
Figure 7.6 Total flood loss in term of economic relating to GRDP in Yangon from 2020 to 2040 by using master plan at the township scale (Million US dollars)	92
Figure 7.7 Total flood loss in term of economic relating to GRDP in Yangon from 2020 to 2040 by using master plan and flood risk reduction at the township scale (Million US dollars)	93
Figure 7.8 Total flood loss in term of economic relating to GRDP in Yangon in 2040 by using master plan at the township scale (US dollars).....	94
Figure 7.9 The earthquake building vulnerability indexes with master plan (a), (b), (c) in 2020, 2030, and 2040 and with earthquake risk reduction (d), (e), (f) in 2020, 2030, and 2040 with the probability of 10% and RC 2500psi	95
Figure 7.10 The earthquake building vulnerability indexes with master plan (a), (b), (c) in 2020, 2030, and 2040 and with earthquake risk reduction (d), (e), (f) in 2020, 2030, and 2040 with the probability of 10% and RC 1250psi	96

Figure 7.11 The earthquake building vulnerability indexes with master plan (a), (b), (c) in 2020, 2030, and 2040 and with earthquake risk reduction (d), (e), (f) in 2020, 2030, and 2040 with the probability of 2% and RC 2500psi97

Figure 7.12 The earthquake building vulnerability indexes with master plan (a), (b), (c) in 2020, 2030, and 2040 and with earthquake risk reduction (d), (e), (f) in 2020, 2030, and 2040 with the probability of 2% and RC 1250psi98

Figure 7.13 Comparing total earthquake losses in term of economic relating to GRDP between (1) using master plan and (2) using master plan and earthquake risk reduction in Yangon from 2020 to 2040 with the probability of 10% and RC 2500psi (Million US dollars)99

Figure 7.14 Comparing total earthquake losses in term of economic relating to GRDP between (1) using master plan and (2) using master plan and earthquake risk reduction in Yangon from 2020 to 2040 with the probability of 10% and RC 1250psi (Million US dollars)100

Figure 7.15 Comparing total earthquake losses in term of economic relating to GRDP between (1) using master plan and (2) using master plan and earthquake risk reduction in Yangon from 2020 to 2040 with the probability of 2% and RC 2500psi (Million US dollars)101

Figure 7.16 Comparing total earthquake losses in term of economic relating to GRDP between (1) using master plan and (2) using master plan and earthquake risk reduction in Yangon from 2020 to 2040 with the probability of 2% and RC 1250psi (Million US dollars)102

Figure 7.17 Earthquake risks in term of economic loss relating to GRDP from 2020 to 2040 with the probability of 2% and RC 1250psi by using master plan at the township scale (Million US dollars).....	104
Figure 7.18 Earthquake risks in term of economic loss relating to GRDP from 2020 to 2040 with the probability of 2% and RC 1250psi by using master plan and earthquake risk reduction at the township scale (Million US dollars).....	105
Figure 7.19 Earthquake risks in term of economic loss relating to GRDP in 2040 with the probability of 2% and RC 1250psi by using master plan at the township scale (US dollars)	106
Figure 8.1 The histogram of nighttime light.....	109
Figure 8.2 VIIRS nighttime light (a) in 2012 and (b) in 2015.....	110
Figure 8.3 Changed areas from low to high nighttime light	110
Figure 8.4 Histograms of elevation with (a) commercial buildings and (b) change areas, histograms of distance from railway with (c) commercial buildings and (d) change areas, and histograms of past urban areas with (e) commercial buildings and (f) change areas..	112
Figure A.1 Land cover image in 2015	127
Figure A.2 Land use map in 2012 by JICA	127
Figure A.3 Building height map in 2013.....	128
Figure A.4 The six regions of surveying building heights in 2015	129
Figure A.5 Building type map in 2013	130
Figure A.6 Building use map in 2012 by JICA	130

List of Table

Table 1.1 Remotely sensed dataset.....	14
Table 1.2 GIS dataset	15
Table 1.3 Supplement dataset.....	15
Table 2.1 The defined parameters of flood vulnerability index.....	21
Table 2.2 The weights of flood vulnerability index based on the empirical model	22
Table 2.3 The weights of flood vulnerability index based on AHP by expert opinions	22
Table 3.1 The defined parameters of earthquake amplitude index.....	34
Table 3.2 The cases of the simulated building damage	38
Table 3.3 The defined parameters of earthquake building vulnerability index.....	40
Table 4.1 The land price index of urban, cropland, and forest	48
Table 4.2 The defined parameters of land price index	49
Table 4.3 The weights of land price index based on the empirical model.....	49
Table 5.1 The means and variances of the Euclidean distance from the multi-centers of urban areas in each region from 1978 to 2009 (Pixels).....	59
Table 5.2 The means and variances of the Euclidean distance from the urban areas in the past from 1978 to 2009 (Pixels).....	61
Table 5.3 The means and variances of the Euclidean distance from the railways from 1978 to 2009 (Pixels).....	62
Table 5.4 The means and variances of the elevation from 1978 to 2009 (Pixels)	63

Table 5.5 The class translation in the region of the center #1 from 1978 to 2009 (Pixels)..	64
Table 5.6 The accuracies of the estimation of urban expansion	71
Table 6.1 The total flood losses in term of the area between using master plan, and using master plan and flood risk reduction in Yangon from 2020 to 2040 (km ²)	78
Table 6.2 The total earthquake losses in term of the area between using master plan, and using master plan and earthquake risk reduction in Yangon from 2020 to 2040 (km ²).....	81
Table 7.1 The prediction of economic growth relating to GRDP by JICA (US dollars)	86
Table 7.2 The statistics of total flood losses in term of economic relating to GRDP between (1) using master plan and (2) using master plan and flood risk reduction in Yangon from 2020 to 2040 (Million US dollars)	91
Table 7.3 The statistics of total earthquake losses in term of economic relating to GRDP between (1) using master plan and (2) using master plan and earthquake risk reduction in Yangon from 2020 to 2040 with the probability of 10% and RC 2500psi (Million US dollars)	99
Table 7.4 The statistics of total earthquake losses in term of economic relating to GRDP between (1) using master plan and (2) using master plan and earthquake risk reduction in Yangon from 2020 to 2040 with the probability of 10% and RC 1250psi (Million US dollars)	100
Table 7.5 The statistics of total earthquake losses in term of economic relating to GRDP between (1) using master plan and (2) using master plan and earthquake risk reduction in Yangon from 2020 to 2040 with the probability of 2% and RC 2500psi (Million US dollars)	101

Table 7.6 The statistics of total earthquake losses in term of economic relating to GRDP between (1) using master plan and (2) using master plan and earthquake risk reduction in Yangon from 2020 to 2040 with the probability of 2% and RC 1250psi (Million US dollars)	102
Table 8.1 The statistical of mean and variance of nighttime light	109
Table 8.2 The comparison between commercial buildings and change areas relating to elevation, distance from railways and urban areas in the past.....	111
Table A.1 The confusion matrix between land cover image in 2015 and land use map in 2012 by JICA (km ²)	128
Table A.2 The comparison between the estimated building heights in 2013 with the surveying building heights in 2015	129
Table A.3 The confusion matrix between building type map in 2013 and building use map in 2012 by JICA (km ²)	131

Chapter1. Introduction

1.1 Background

A natural disaster is a negative event causing from natural processes of the Earth. A natural disaster causes the principal problem around the world. It has made huge destruction to life, property, and the economy of the affected areas and surrounding areas (Neumayer and Barthel, 2011; Neumayer et.al, 2014). Due to the climate change, the damage and frequency of the disasters have become higher. Since 1970, there have been more than 9,800 natural disasters worldwide, more than 3.7 million died people, more than 5.8 billion affected people, and more than 1.7 trillion US dollars of the economic losses and the amounts of the effects have been continually increased (emdat.be/database, 2016).

There are many kinds of the natural disaster such as flood, earthquake, drought, typhoon, volcanic eruption etc. Flood, cyclone, and drought related to extreme weather events have frequently occurred. Whereas, earthquake and volcanic eruption related to extreme earth geology have rarely happened. Possibly, some disasters effects to cause the other disasters. For the instance, after a cyclone occurred, a flood can occur, or after an earthquake happened, a landslide can happen (pitt.edu, 2015). In this research, we focused on the natural disasters of flood and earthquake.

A flood is an overflow of water from rivers, oceans or lakes that submerge land. There are various kinds of flood disasters as follows. Overbank flood is caused by overflowing water from the river. Flash flood is affected by rapidly rising water of fast moving water in a short time. Coastal flood is caused by another natural disaster such as storm, hurricane, and tsunami. Catastrophic flood is affected by infrastructural failures such as ruin of a dam. Floods can make severely damaged levels and cause huge destruction human and their properties in the affected areas (punditcafe.com, 2015).

An earthquake is a rapid discharge of energy in the Earth's crust affected by tectonic plate movements. The movement generates seismic waves and causes a shaking of the Earth's surface that can destroy buildings or human in the affected areas. While the earthquake is caused by rupture of geological faults, they can also be affected by volcanic activity, landslide, mine blasts and nuclear tests. The epicenter is the point on the ground above the origin of the tremor and is also the worst affected area. The magnitude of an earthquake is commonly measured using the Richter Scale. The current measurement indicated that 500,000 earthquakes occur each year around the world (punditcafe.com, 2015).

The implications of the disasters are different effects depending on various factors such as the damaged level of the disaster (low or high damages) and the affected areas of the disaster (high or low values) etc. Especially, when a disaster occurs in the urban areas that have the characteristics of the high population density with very important human activities, it makes huge damages with direct and indirect losses and it might spread the impact thought out the city or the country (Riggs et.al, 2008; Notaro et.al, 2014). In order to reduce the damage of the disaster in the future, the disaster risk management is required (Horita et.al, 2015).

The Red Cross and Red Crescent societies defined that disaster management is the organization and management of resources and responsibilities for dealing with all humanitarian aspects of emergencies, especially; preparedness, response, and recovery in order to reduce the impact of disasters (ifrc.org, 2015). Disaster prevention refers to the activities designed to provide sustainable protection from disasters. Disaster preparedness refers to the activities designed to minimize the loss of life and damage. Disaster relief is a coordinated multi-agency response to reduce the impact of a disaster and its long-term results. Disaster recovery is the recovering activities including re-building infrastructure, health care and rehabilitation (wcpt.org, 2015). As a result, in order to support the activities of the disaster management, the disaster risk assessment and the disaster risk reduction are required. Disaster risk assessment is a process or method to identify the potential hazard and

analyze what can happen if a disaster occurs (ready.gov, 2015). Disaster Risk Reduction is a process to reduce the damage caused by natural hazards (unisdr.org, 2015).

In scientific aspect for the assessment of the disaster risk, according to Kron's research (Kron, 2005), disaster risk is the product of a hazard and its consequences. Where there are no human or valuable things that can be affected by a natural disaster, there is no risk at all. In the other hand, a disaster risk can occur when the people and their properties are harmed or damaged. Therefore, disaster risk can be expressed in terms of (1) hazard, (2) vulnerability and (3) value as the below equation.

$$\text{Disaster Risk} = \text{Hazard} * \text{Vulnerability} * \text{Value} \quad (1.1)$$

The hazard refers to the threatening natural disaster event including its frequency of occurrence and its level of damage. For instance, a flood has occurred frequently but has taken on a low damage, while an earthquake has rarely happened but has taken on a high damage. Then, the vulnerability can refer to the prone areas that high lacking the resistance to damaging and destructive forces. Next, the value or value at risk can refer to the buildings, items, humans, properties that are present at the location involved (Kron, 2005).

Disaster risk reduction is the process or method to reduce the terms of (1) hazard, (2) vulnerability and (3) value. Disaster risk reduction can be expressed as the below equation.

$$\text{Disaster risk reduction} = \text{reducing Hazard} * \text{Vulnerability} * \text{Value} \quad (1.2)$$

According to equation 2, disaster risk reduction can be performed with the several ways. For the instance, firstly, we can reduce the disaster risk by reducing the hazard of a natural disaster. Since the hazard of natural disaster can be affected by climate change caused by carbon dioxide emission, the activities that reduce carbon dioxide emission causing of the natural hazard can be performed such as alternative driving, reuse and recycle (Disaster and Climate Change, 2016). Secondly, we can reduce the disaster risk by reducing

the vulnerability of the affected areas. For the example, for flooding, we can install the high-quality drainage system to reduce the flood vulnerable areas (Lee et.al, 2016). Thirdly, we can reduce the disaster risk by reducing the value. For the example, the important buildings such as commercial buildings should be located in the low vulnerable areas or safe areas.

Sustainable Development Goals (SDG) known as the Global Goals are a universal call to action to end poverty, protect the planet and ensure that all people enjoy peace and prosperity by United Nations. In the goal number of 11.5, it was written that “by 2030, significantly reduce the number of deaths and the number of people affected and substantially decrease the direct economic losses relative to global gross domestic product caused by disasters, including water-related disasters, with a focus on protecting the poor and people in vulnerable situations” (pwc.com, 2017). As a result, the disaster risk reduction that reduces the economic losses in term of the gross domestic product caused by disasters can be considered as the significant solution for the sustainable development goals to protect people from disasters. The economic loss means changes in wealth caused by damage to structures or other physical assets. There is a direct loss (those resulting from building and infrastructure damage) and an indirect loss (those that follow on from physical damage) (Ahmad, 2015).

Myanmar, formerly known as Burma, is the second largest land areas (more than 260,000 square miles) of South East Asia countries with a population from 28.9 million people in 1973 to 60 million people in 2009 (World Bank, 2017). Despite strong growth in recent years, Myanmar has been one of the poorest countries in Southeast Asia with a GDP per capita of 1,204 us dollars. In recently years, the growth has been urged by economic reforms, public consumption, and private investment. However, it has been decreased to 7 percent in 2015–2016 because of there were heavy floods and landslides (World Bank, 2016; Estimate depends on the methodology used, 2014).

Myanmar has frequently had the problem with the disaster that negatively impacts on livelihoods and Government resources. Myanmar is ranked 2nd out

of 187 countries in the 2016 Global Climate Risk Index (GermanWatch, 2016) and is ranked 9th out of 191 countries in the Index for Risk Management (INFORM) (INFORM (Index for Risk Management), 2016). Considering the past 25 years, Myanmar has faced 24 disaster events that affected more than 4 million people and lost about 4.7 billion US dollars (EM-DAT database, 2016). A preliminary financial risk assessment estimated that expected annual economic losses are more than 184 million US dollars (0.9 % of GDP) due to natural disasters (World Bank and Global Facility for Disaster Reduction and Recovery, 2012).

Yangon, formerly known as Rangoon, is located on between 17°06' N and 16°35'N latitudes and between 95°58' E and 96°24'E longitudes. Yangon is the largest city in Myanmar (triple the size of the country's second largest city, Mandalay) with more than five million population (Morley, 2013; United Nations, 2015). Yangon is the economic center of the country with 12% of the national population and 22% of Gross Domestic Products (GDP) in the country (based on the data from Planning Department, Ministry of National Planning and Economic Development (MNPED, 2010-2011). Yangon is considered as country's commercial and financial hub, also the gateway for tourism. Yangon is expected to continue capturing a dominant share of Myanmar's economic growth. Yangon had rapidly increased population growth in the past decade. The average growth rate of population in Yangon City between 1998 (3.69 million population) and 2011 (5.14 million population) is 2.58% annually whereas, the national population growth rate of 0.9%. JICA Team estimated that the growth rate per year is around 8% with the GRDP of 17.6 billion US dollars in 2016 and the GRDP of 75.9 billion US dollars in 2035. As increasing population and economic development in Yangon, urban has rapidly increased (JICA, 2013).

Yangon has suffered from the series of floods with almost every years such as 2008, 2010, 2013, 2014 and 2015. In flooding case of 2014, Yangon had losses of more than 8.5 million US dollars with affected 63,082 people, 18 schools, 17 miles of road, eight bridges and 56,486 acres of farmland (mmtimes.com, 2016). In the extreme case, the flood has occurred 6 to 10 times a year when heavy

rainfall comes with high tides during the monsoon season (World Bank, 2017).

Yangon city also had faced the effect of the earthquake in 1930. In that time, an earthquake with the magnitude of 7.0 occurred in Bago region and caused the extensive damage including 500 killed people. In Yangon city, there were 50 died people with the population of 400,000 (mmtimes.com, 2016). Yangon is also highly earthquake-prone, located along the active Sagaing fault system and built on weak surface geological conditions associated with an alluvial delta (World Bank, 2017).

Yangon is unprepared in many ways for its growth. In the absence of a comprehensive land use and infrastructure plan, spatial expansion has been rapid and fragmented and is not coordinated with infrastructure provision. While the city adopted 'A Strategic Urban Development Plan for Greater Yangon' in 2013, translating the plan into comprehensive land use and infrastructure investments remains a challenge. Recently, The Government has since formed a committee of relevant agencies, including YCDC and the national government's Department of Urban and Housing Development, to develop a land use plan and prepare Planning Guidelines and Building Regulations (World Bank, 2017).

According to the previous information, Yangon is at risk of the flood and earthquake and is need to prepare for a land used plan. In order to support preparation for the land use plan, the multiple scenarios of the predicted land cover in the future in Yangon, Myanmar by using disaster risk assessment and disaster risk reduction are required to reduce the impacts of flood and earthquake in the future.

This research aims to reduce the damage of flood and earthquake in the future by locating high-value areas in the future on the low vulnerable areas or the safe areas with considering the mechanism of the urban expansion, and to assess the flood and earthquake risks in term of economic loss relating to GDP in the future with the multiple-scenarios.

To achieve the objectives of this research, the four fundamental aspects of (1)

flood vulnerability assessment, (2) earthquake vulnerability assessment, (3) land price estimation, (4) urban prediction modeling are necessary to be investigated.

The assessment of flood vulnerability was widely introduced by many works (Meja-Navarro et.al, 1994; Black and Burns, 2002). The assessment of flood hazard map has been developed by using the rainfall and run-off model (Schumann et.al, 2000). The methodology based on the statistical analysis to evaluate flood vulnerability map has been done (Tehrany et.al, 2013). The multi-criteria index based on the Analytical Hierarchy Process (AHP) model has been introduced (Kazakis et.al, 2015).

The Assessment of earthquake risk in Tabriz, Iran was introduced (Karimzadeh et.al, 2014) by using GIS information including soil's type and ground water. The assessment of earthquake-induced land slides was proposed (Song et.al, 2012) by using the Bayesian network with GIS data to estimate earthquake risk areas.

The estimations of land price have been widely introduced in various research works (Ihlanfeldt, 2007; Tsutsumi et.al, 2011). Xu and Li (, 2014) proposed the empirical model of land price in urban residential development by using GIS data including land use areas such as residential, commercial and industrial areas. The model of land price distribution was developed (Hu et.al, 2013) by using the multifractal inverse distance weighted interpolation with sampled land price data.

Many urban expansion models have been widely developed in order to understand the system of urban expansion and predict the urban areas in the future. Urban land-use model based on spatial interaction model was developed by Lowry (, 1964). The statistical model was used for introducing urban expansion model (Sklar and Costanza, 1991). An Urban growth model based on automata cellular was proposed by Batty (, 1997). Moreover, by using multi-agent-based model, the residential distribution estimation was developed (Benenson, 1998).

Here, the fundamental processes have been investigated with (1) the assessment of flood vulnerability (2) the assessment of earthquake vulnerability (3) the estimation of land price, (4) prediction of urban expansion in Yangon. After that, In order to calculate the reduction process of assess flood and earthquake risk and compute the assessment process of flood and earthquake risk in term of economic relating to GDP. The integrating processes are necessary with (1) the prediction of urban expansion by reducing flood and earthquake risks (2) the assessment of flood and earthquake risks in term of economic loss relating to GDP.

Remotely sensed data were widely employed in many applications since sensing technology can observe wide areas with long time and frequent monitoring. Thus, remotely sensed data can be used as the supporting information for disaster risk assessment and disaster risk reduction.

Landsat has monitored the world's longest continuously. By using Landsat imagery, various applications in several aspects have been conducted such as agriculture, geology, forestry, regional planning, education, mapping, and global change research (landsat.usgs.gov, 2015). In this research, we used the Landsat images to provide the land cover images from 1978 to 2015. GeoEye is able to acquire the imagery with 0.46 meter for panchromatic image and 1.84 meters for the multispectral image. By using stereo mode, the high-resolution Digital Surface Model (DSM) can be evaluated (satimagingcorp.com, 2015). We used SRTM DEM as elevation data. The SRTM DEM, produced by NASA originally, is a digital elevation map of the world, and provides high quality elevation data for large portions of the tropics and other areas of the developing world (Jarvis et.al, 2008). We employed the stereo GeoEye images to obtain the building heights. MODIS (Moderate Resolution Imaging Spectroradiometer) is an instrument aboard the Terra (and Aqua satellites. Terra and Aqua MODIS can monitor the entire Earth's surface every 1 to 2 days and provide the imagery with 36 spectral bands. By using the imagery, we can obtain more understanding of global dynamics and processes occurring on the land and in the oceans (modis.gsfc.nasa.gov, 2015). We used the MODIS surface reflectance 8 days composition to detect the surface water from 2001 to 2015. Tropical

Rainfall Measuring Mission (TRMM) is the mission, a joint space mission between NASA and the Japan Aerospace, to measuring tropical and subtropical rainfall through microwave and visible infrared sensors (earthobservatory.nasa.gov, 2016). We used the TRMM data to obtain the monthly rainfall images. VIIRS (Visible Infrared Imaging Radiometer Suite) provides daily multi-spectral observations for the land surface at regional to global scales. These data can be employed for the applications to monitor fire and air quality monitoring, agriculture monitoring and production modeling, carbon modeling and flood and sea ice mapping (earthdata.nasa.gov, 2015). In this research, VIIRS nighttime light can use to provide the different nighttime light activities.

A geographic information system (GIS) is a system designed to capture, store, manipulate, analyze, manage, and present spatial or geographic data. Infrastructural data such as road and railways can be used as In this research, GIS dataset were used to support the disaster risk reduction and disaster risk assessment in Yangon. Infrastructure dataset such as road and railways were used to provide the information for the transportation. The soil map by Myanmar Agriculture Service, 2002 was used as the one factor to calculate flood and earthquake vulnerabilities. The simulated seismic map by Thant was employed in earthquake vulnerability assessment. The population density map was applied in the land price estimation. The master plan by JICA was extracted the future dataset to enhance the prediction of urban expansion.

Supplementary dataset was involve1d in this research to support the disaster risk reduction and disaster risk assessment in Yangon. The surveying elevation information was used as the validated data for the estimated elevation from the remotely sensed data. The surveying building information was applied to validate the estimated building heights. For validating the land cover image, we used a land use map to compare the estimated land cover from Landsat images. Also, we used the land use map to validate the estimated building types (Sritarapipat and Takeuchi, 2017a). Land price information was employed to calculate the coefficient parameters in the land price estimation and also was compared with the estimated land price map. The predicted

economic growth relating to GRDP by JICA was applied with the calculating process of the economic areas.

1.2 Objective of this study

- To reduce flood and earthquake risks in term of economic loss in Yangon, Myanmar from 2020 to 2040.
 - o To assess flood vulnerability (Chapter 2)
 - o To assess earthquake vulnerability (Chapter 3)
 - o To predict urban expansion (Chapter 5)
 - o To predict urban expansion considering flood and earthquake vulnerabilities (Chapter 6)
- To assess flood and earthquake risks in term of economic loss relating to Gross Regional Domestic Product (GRDP) with multiples-scenarios in Yangon from 2020 to 2040.
 - o To estimate land price (Chapter 4)
 - o To calculate flood and earthquake risks in term of economic loss relating to GRDP (Chapter 7)

1.3 Originality of this study

In this research, the various remotely sensed data have been employed as the input data to support the disaster risk assessment and the disaster risk reduction in Yangon, Myanmar; especially under the situation of the limitation of available data.

For the assessment of flood vulnerability, MODIS 8 days composition was used to observe the water surface from 2001 to 2015 as the historical flood areas.

For earthquake vulnerability assessment, the stereo GeoEye images and Landsat time series were employed to provide the ages of buildings.

For land price estimation, the stereo GeoEye images, Landsat image, and Nighttime light data were employed to obtain the building types with commercial, industrial, and residential buildings.

For modeling urban expansion, the stereo GeoEye images were used to detect the multi-centers of the urban areas. Also, urban expansions from 1978 to 2015 were detected by using Landsat time series.

1.4 Outline of this study

For the first step, the fundamental process to support in calculating flood and earthquake risk reductions and assessments are performed as follows. Firstly, we evaluated the assessment of flood vulnerability that describes in chapter 2. Secondly, we conducted the assessment of earthquake vulnerability that accounts in chapter 3. Thirdly, we performed the estimation of land price describing in chapter 4. Fourthly, we developed the modeling of urban expansion to predict urban expansion in the future and explained the details in chapter 5.

For the next step, the integral process for flood and earthquake risks reductions were proposed. By relating the urban expansion modeling enhanced with Master plan to flood and earthquake vulnerabilities, the predicted urban expansions by reducing flood and earthquake vulnerabilities have been performed and described in chapter 6.

For the next step, the integral process for flood and earthquake risks assessments in term of economic loss relating to GRDP were introduced. To evaluate flood and earthquake risk reductions in term of economic losses relating to GRDP, we converted the predicted land covers into economic areas by using land price estimation associated with the predicted economic growth and then calculated the flood and earthquake risks in term of economic losses relating to GRDP. Then, the statistical information of flood and earthquake risks in term of economic losses with multiples scenarios are calculated and discussed in chapter 7. The framework of this research was depicted in Figure 1.1.

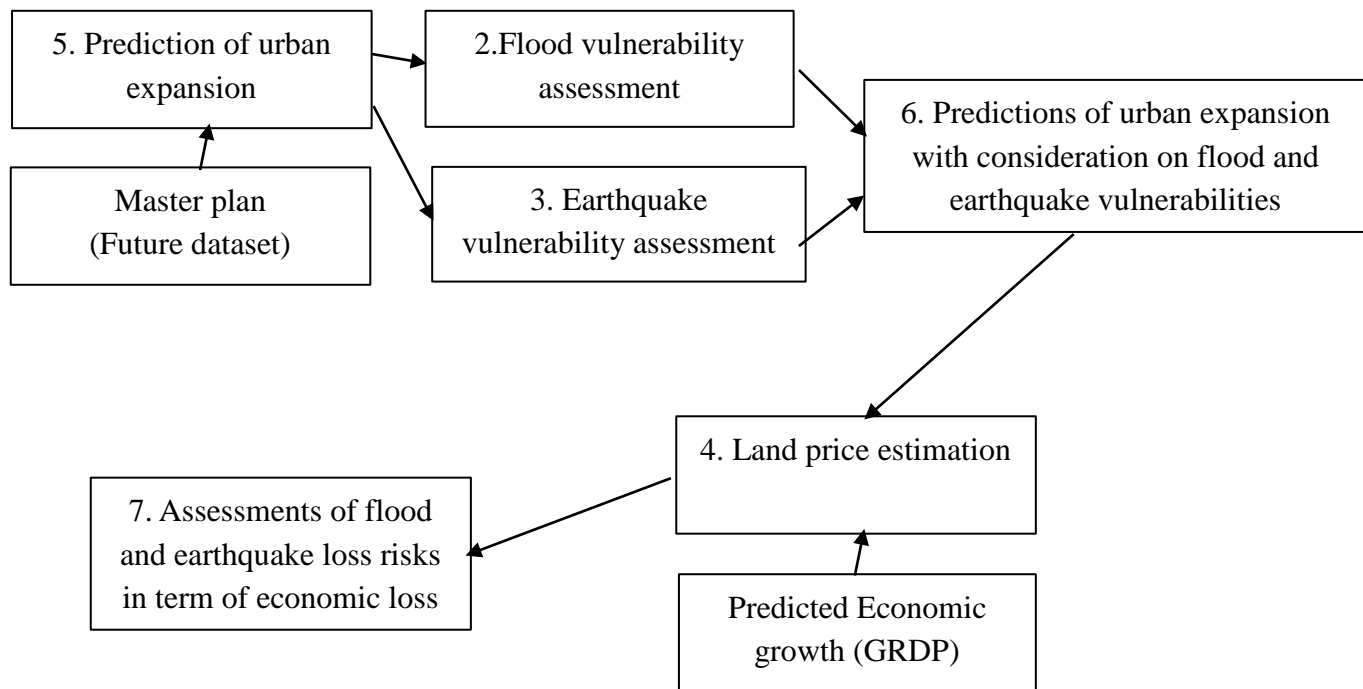


Figure 1.1 The framework of this research

In this research, the spatial resolution of the results is 30 meters. The details of remotely sensed data, GIS data, and supplement data are described in Table 1.1, 1.2, and 1.3, respectively.

Table 1.1 Remotely sensed dataset

No.	Satellite and sensor	Bands	Resolution	Acquired time
1	Landsat-3 MMS	4	60 m.	1978-11-22
2	Landsat-4 TM	7	30 m.	1990-11-12
3	Landsat-7 ETM	8	30 m.	2000-11-07
4	Landsat-5 TM	7	30 m.	2009-11-08
5	Landsat-8 OLI	11	30 m.	2015-11-25
6	GeoEye Stereo-mode RGB	3	0.5 m.	2013-11-08 2013-11-16
7	SRTM DEM v. 4.1	1	90 m.	2008
8	MODIS MOD09Q1 Surface reflectance	2	250 m.	8-days composition from 2001 to 2015
9	VIIRS DNB Nighttime light	1	460 m.	1-year composition in 2012 and in 2015
10	TRMM 3B-43 rainfall	1	28,000 m.	Monthly-data from 2001 to 2015

Table 1.2 GIS dataset

No.	Type	Source	Acquired year
1	Road	JICA	2012
2	Railway	JICA	2012
3	Soil map	Myanmar Agriculture Service	2002
4	Seismic map	Thant	2012
5	Population density	GPWv4	2015
6	Master plan	JICA	2016

Table 1.3 Supplement dataset

No.	Type	Source	Acquired year
1	Surveying elevation	NIHON KOEI Company	2012
2	Surveying building	Sritarapipat	2015
3	Land use map	JICA	2012
4	Flood vulnerability map by using HydroSHEDS	ICHARM	2016
5	Flood vulnerability map by using RRI Model	ICHARM	2016
6	Flood map (Cyclone Nargis)	UNOSAT	2008
7	Land price information	Internal Revenue Department,	2012
8	Economic growth (GRDP)	JICA	2016

Chapter2. Assessment of flood vulnerability

2.1 Background

Yangon has low hills, which are long and narrow hill range in the central area running in the N-S direction with an average height of 30m and degenerates gradually into delta plains in eastwards (JICA, 2016). Yangon City lies along the Yangon River east of the Ayeyarwaddy River (the country's largest river). Yangon has had the problem with flood almost every year. Household Interview Survey (HIS), conducted targeting around 10,000 households, results indicate there are frequent flood events in Yangon and also show that 4,200 of 10,045 households (41.8%) have flood inundation every year. The flood inundation depth at the affected area is up to the ankles or knees (92.1 %) and flood inundation duration ranges from less than half day to more than six days. The Yangon River has had a large water level difference between the low and high tides. The water level of the Yangon River increases to around 2.5-3.0 m during high tide with a full moon. There are several lowland areas below 3.0 m. in Yangon with rainwater drainage issue. Most of the lowlands are located in the suburbs of Yangon. In Yangon city, the drainage system has a problem with heavy congestion (JICA, 2013). In May 2008, Cyclone Nargis made the huge flood damage in Yangon (reliefweb.int, 2015). In flooding case of 2014, Yangon had losses of more than 8.5 million US dollars with affected 63,082 people, 18 schools, 17 miles of road, eight bridges and 56,486 acres of farmland (mmtimes.com, 2016). In the extreme case, the flood has occurred 6 to 10 times a year when heavy rainfall comes with high tides during the monsoon season (World Bank, 2017). In Yangon, there have been several conditions causing the flood problem such as harsh natural conditions, rapid urbanization, and poor capacity of drainage system (Myanmar Country Report, 2016). Therefore, the assessment of flood in term of spatial information in Yangon can

support flood risk management in order to mitigate flood damages in the future.

The estimation of flood hazard map has been proposed by using GIS data (Meja-Navarro et.al, 1994). The multi-criteria analysis using GIS data was introduced to assess flood vulnerability map (Black and Burns, 2002). The assessment of flood hazard map has been developed by using the rainfall and run-off model (Schumann et.al, 2000). The methodology based on the statistical analysis to evaluate flood vulnerability map has been done (Tehrany et.al, 2013). The multi-criteria index based on the Analytical Hierarchy Process (AHP) model with seven factors; flow accumulation, rainfall intensity, geology, land use, slope, elevation, distance from drainage network has been introduced (Kazakis et.al, 2015). In Yangon, the flood vulnerability based on Yangon river geomorphology was introduced (Lwin and Khaing, 2012). They employed the river detected from satellite images and soil data to estimate flood vulnerability.

This research introduced a methodology to assess flood vulnerability in Yangon, Myanmar based on the multi-criteria analysis with seven factors of (1) land cover types, (2) elevation, (3) slope, (4) soil types, (5) flow accumulation, (6) distance from drainage channels, (7) rainfall intensity. The empirical model was employed to link with the historical water surface. Since we used the empirical model with the historical water surface, our resultant flood vulnerability map has indicated the venerable areas in term of the frequency of water surface. The resultant flood vulnerability map was related to coastal and riverine floods since we used the observed water surface analyzed by MODIS 8 days composition can observe water surface that remains more than 4 days.

2.2 Methodology

2.2.1 Defining flood vulnerability assessment

In this research, we defined the factors of the flood vulnerability

following the work of Kazakis et.al.(, 2015) and there are seven factors with (1) land cover types, (2) elevation, (3) slope, (4) soil types, (5) flow accumulation, (6) distance from drainage channels, (7) rainfall intensity. The empirical model based on a linear function was employed to link between the defined factors and the historical water surface from 2001 to 2015. To estimate the coefficients in the model, the least square linear regression was applied. The resultant flood vulnerability map was related to coastal and riverine floods since we used the observed water surface analyzed by MODIS 8 days composition can observe water surface that remain more than 4 days and indicated the venerable areas in term of the frequency of water surface. The flowchart of our methodology to assess flood vulnerability is shown in Figure 2.1.

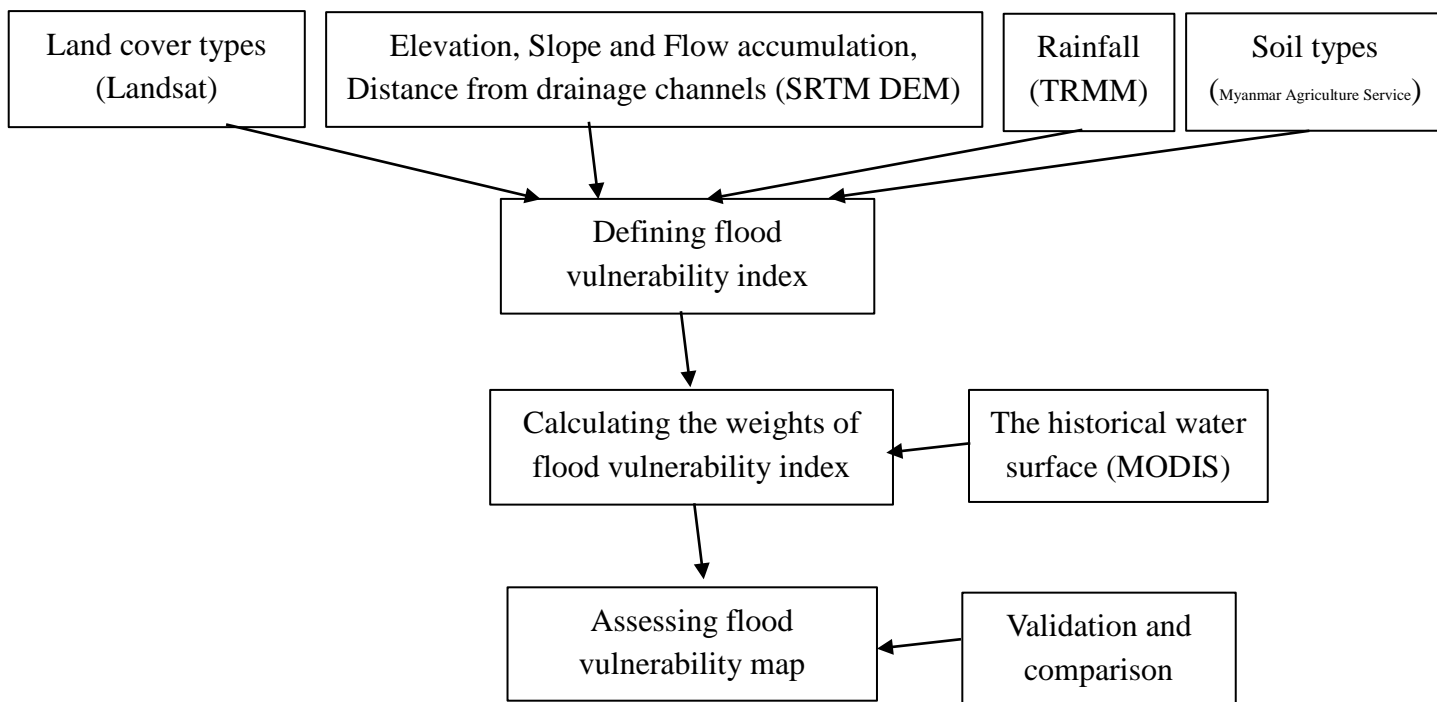


Figure 2.1 Flowchart of flood vulnerability assessment

2.2.2 Preparing data

For the defined factors, there are seven factors that were prepared. For land cover types, we used multi-spectral Landsat image in 2015 with 30 meters-resolution. We classified land cover types into five classes with urban,

cropland, forest, lake, and river by using the Mahalanobis distance (Maesschalck et.al, 2000). Mahalanobis distance is a well-known supervised classification method. It uses the mean and covariance matrix of observed data to estimate a decision boundary. The sampling points were manually selected from more than five hundred samples in each class. For elevation, we used SRTM DEM (Shuttle Radar Topography Mission digital elevation model) with 90 meters-resolution (Jarvis et.al, 2008). For slope, we calculated the slope from the SRTM DEM. For flow accumulation, we used the hydrology tool in to compute flow accumulation from the SRTM DEM. For distance from the drainage network, we calculated the Euclidean distance (M.M. Deza and E. Deza, 2009) from the drainage network from the flow accumulation. For rainfall intensity, we used TRMM (Tropical Rainfall Measuring Mission) with approximately 28 kilometers-resolution to obtain rainfall rate. For soil types, we used the soil map provided by Myanmar Agriculture Service, 2002.

For the historical flood data, we used the products of MOD09 (Surface Reflectance) with 250 meters-resolution acquired by MODIS (Moderate Resolution Imaging Spectroradiometer) from 2001 to 2015 and calculated the normalized difference vegetation index (NDVI) time-series with 8 days-composition. NDVI is a simple graphical indicator that can be used to analyze remote sensing measurements (earthobservatory.nasa.gov, 2015). Since the products were derived by 8 days-composition, they can avoid the cloud problems causing from using the optical sensors. Then, we classified the NDVI images into two classes of water coverage (low NDVI) and non-water coverage (high NDVI) by using the manual threshold. The historical water surface was calculated by the summation of water coverage with every 8 days from 2001 to 2015.

For supplement data for the validation process, we used the daily products of LSWC (land surface water coverage) with approximately 9 kilometers-resolution derived from AMSR-E (Advanced Microwave Scanning Radiometer-EOS) and AMSR-2 from 2001 to 2015 (Xi and Takeuchi, 2016) to compare with the historical flood result derived from the NDVI time-series. Also, we selected the big flood event by cyclone Nargis in 2008 to compare with

the NDVI time-series.

2.2.3 Defining flood vulnerability index

We defined the flood vulnerability in term of the index with a range from 0.0 (the lowest vulnerability) to 1.0 (the highest vulnerability). We assumed that the relationship between flood vulnerability and the defined factors as a linear function (following the work of Kazakis et.al., 2015). The equation of flood vulnerability index is expressed with the defined factors and the weights as the below equation.

$$FVI = w_f \cdot F + w_i \cdot I + w_g \cdot G + w_u \cdot U + w_s \cdot S + w_e \cdot E + w_d \cdot D \quad (2.1)$$

Where FVI = Flood vulnerability index, F = Flow accumulation, I = rainfall intensity, G = soil types, U = land cover types, S = slope, E = elevation, D = distance from drainage network. w_f = the weight of flow accumulation, w_i = the weight of rainfall intensity, w_g = the weight of soil types, w_u = the weight of land cover types, w_s = the weight of slope, w_e = the weight of elevation, w_d = the weight of distance from drainage network.

For defining the parameters of flood vulnerability index, we used the K-means method to group the data values for ranking of the index values. K-Means is an unsupervised-classification method and popular for cluster analysis (Hartigan and Wong, 1979). We assigned the parameters of flood vulnerability index in Table 2.1.

Table 2.1 The defined parameters of flood vulnerability index

Parameters	Class	Index value
Flow acc. (F)	600,000-2,000,000	1.0
	60,000-600,000	0.8
	10,000-60,000	0.6
	400-10,000	0.4
	0-400	0.2
Distance. from drainage (D)	0-270	1.0
	271-540	0.8
	541-810	0.6
	811-1350	0.4
	1350-3510	0.2
Elevation (E)	0-3	1.0
	4-7	0.8
	8-10	0.6
	11-17	0.4
	18-68	0.2
Land cover (U)	Urban	1.0
	Vegetation	0.67
	Forest	0.33
Rainfall rate (I)	0.29	0.5
Slope (%) (S)	0-0.20	1.0
	0.21-0.62	0.8
	0.63-1.19	0.6
	1.20-2.62	0.4
	2.63-14.18	0.2
Soil types (G)	Rocks	0.8
	Alluvial	0.2

2.2.4 Estimating the weights of flood vulnerability index

We estimated the seven weights of flood vulnerability index by linking between the flood water surface and the defined factors. We defined that the FVI of 0.0 is the lowest summation of water surface (every 8 days) from 2001 to 2015 and the FVI of 1.0 is the highest summation of water surface. To calculate the seven weights of flood vulnerability index, we applied the least square regression method with Equation 2.1. A least squares regression is a standard

method in regression analysis to the approximate solution of the set of equation (Lawson and Hanson, 1974). After computing the least square regression, the estimated weights are expressed as below.

Table 2.2 The weights of flood vulnerability index based on the empirical model

W_f	W_i	W_g	W_u	W_s	W_e	W_d
-10.2	29.0	5.01	-0.06	4.37	59.9	3.9

In addition, the weights of flood vulnerability index based on AHP by expert opinions [5] are shown in the below table.

Table 2.3 The weights of flood vulnerability index based on AHP by expert opinions

W_f	W_i	W_g	W_u	W_s	W_e	W_d
3	1	0.3	1.2	0.5	2.1	2.1

2.3 Results and discussions

2.3.1 The assessment of flood vulnerability map

The flood vulnerability map based on the empirical model by linking between the historical surface water coverage is displayed in Figure 2.2. Then, we compared our estimated flood vulnerability map with the flood vulnerability map based on AHP by expert opinions (Kazakis et.al, 2015) (Figure 2.3). We also compare with the flood vulnerability maps based on the rainfall-runoff model with (1) flooding caused by the cyclone Nargis by using HydroSHEDS analyzed by ICHARM, 2016 (Figure 2.4) and (2) the costal flood by Cyclone Nargis with the rainfall (100-year flood) by using RRI Model analyzed by ICHARM, 2016 (Figure 2.5).

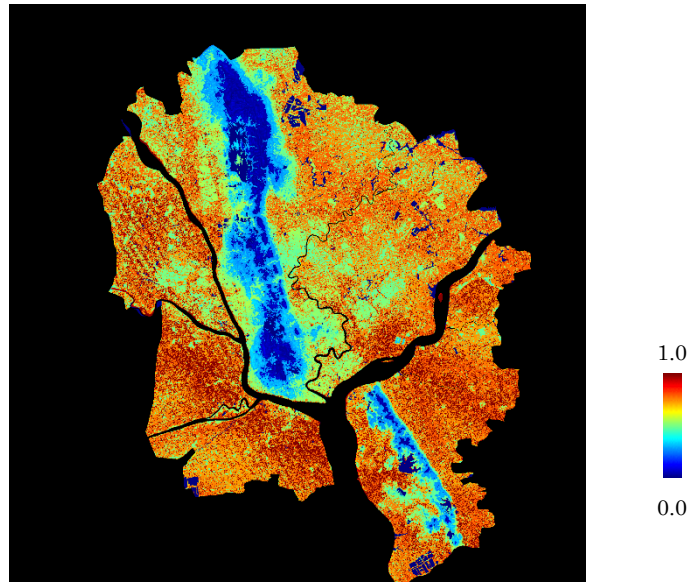


Figure 2.2 The flood vulnerability map based on the empirical model (30 meters-resolution)

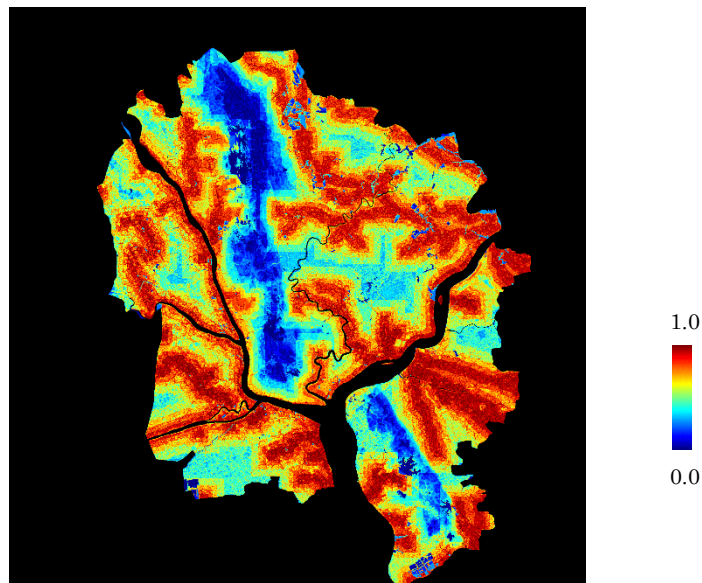


Figure 2.3 The flood vulnerability map based on AHP by expert opinions (30 meters-resolution)

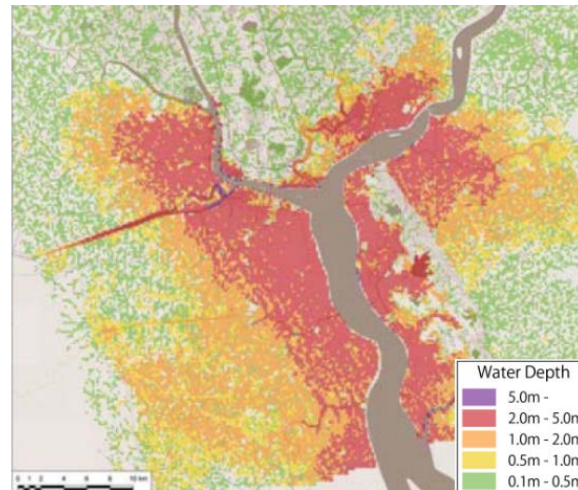


Figure 2.4 The flood vulnerability map based on flooding caused by cyclone Nargis using HydroSHEDS by ICHARM, 2016 (450 meters-resolution)

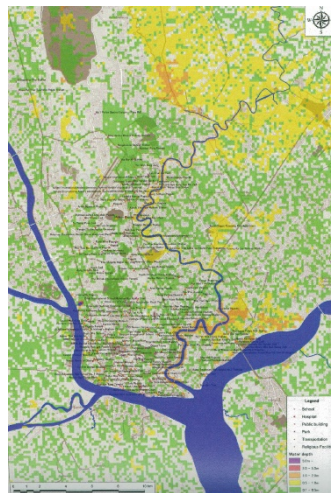


Figure 2.5 The flood vulnerability map based on the costal flood by Cyclone Nargis with the rainfall (100-year flood) by using RRI Model by ICHARM, 2016 (450 meters-resolution)

By comparing with the flood vulnerability map based on flooding caused by cyclone Nargis using HydroSHEDS by ICHARM (Figure 2.4), we found that our flood vulnerability map based on the empirical model (Figure 2.2) has more similarity to the flood vulnerability map based on flooding by cyclone than the flood vulnerability map based on AHP model (Figure 2.3). However, when comparing our flood vulnerability map (Figure 2.2) with flood vulnerability map based on the costal flood by Cyclone Nargis with the rainfall (100-year

flood) by using RRI Model by ICHARM (Figure 2.5), our result looks over estimation.

By using the empirical model linking with the historical water surface, it can help to estimate the impacts of the defined factors in flood vulnerability assessment, whereas the AHP method followed the suggestion by the expert opinions. As a result, by using the methodology based on AHP, it is suitable for general cases or in the case of unknown flood historical data. However, since the regional area has own characteristic and the different features, the weights of flood vulnerability should be specific by following the observed flood historical data. Since we used the empirical model with the historical water surface, our resultant flood vulnerability map has indicated the venerable areas in term of the frequency of water surface. While the flood vulnerability maps by ICHARM has indicated the venerable areas in term of water depth by using rainfall and runoff model. By considering in term of the water depth of the simulated flood in Yangon, by using RRI model, the water depth of the flood has varied from 50 centimeters to 1 meter.

We investigated that by using the empirical model, the elevation has the highest impacts, whereas by using AHP model, the flow accumulation has the highest impact. By using empirical model, the impacts of flow accumulation and drainage network could not be detected since the estimation relies on the historical flood surface analyzed by MODIS NDVI 8-days composition. MODIS NDVI 8-days composition can only detect water surface that remains more than 4 days.

2.3.2 The validation of historical water surface

Since we did not use the actual flood historical map, the estimated flood historical map (Figure 2.6) is necessary to be validated. In this research, we used LSWC derived from AMSR-E and AMSR-2 in the validation process since the LSWC products were derived from the microwave sensing that has the potential to penetrate clouds. The averaged LSWC map from 2001 to 2015 is

depicted in Figure 2.7. We found that the estimated flood historical map by NDVI time series has a high relationship with LSWC.

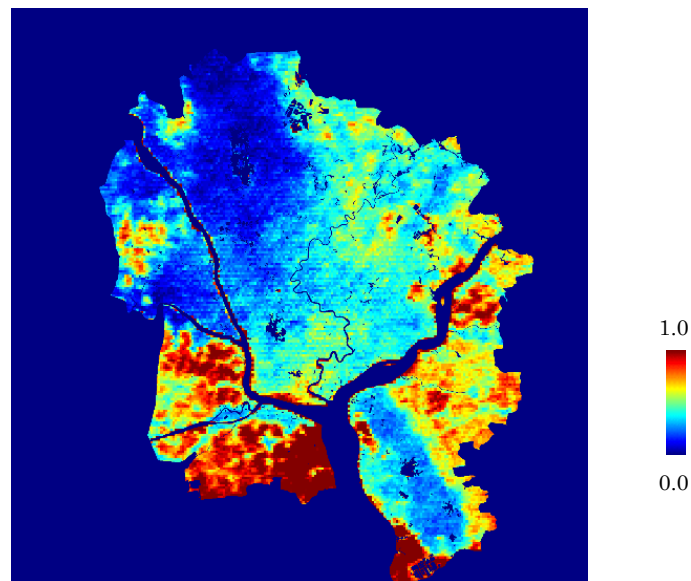


Figure 2.6 The historical water surface map using NDVI-time series from 2001 to 2015 (250 meters-resolution)

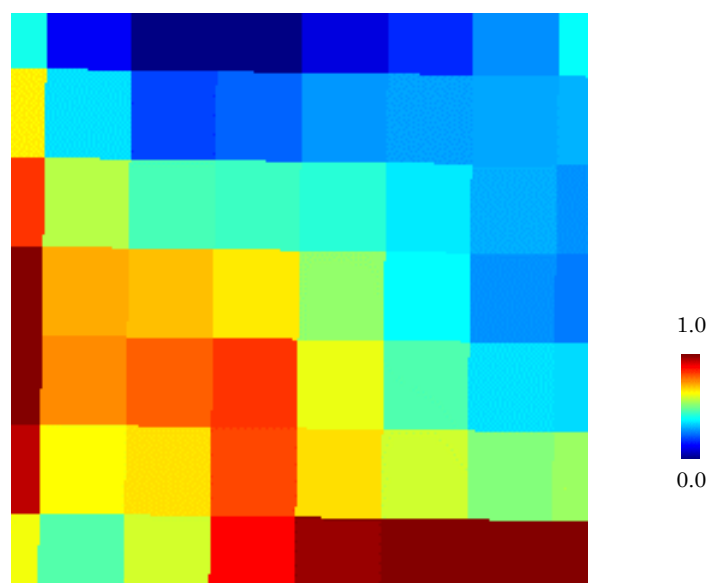


Figure 2.7 The averaged LSWC map using AMSR-E and AMSR-2 from 2001 to 2015 (9 kilometers-resolution)

In addition, the big flood event in 2008 was selected to compare the MODIS NDVI time series. MODIS NDVI 8 days composition image during the flood event in 2008 is displayed in Figure 2.8 and the actual flooded areas on May 5, 2008, that was analyzed by UNOSAT (unitar.org, 2015) is shown in

Figure 2.9 and also the estimated flooded areas by using the MODIS NDVI 8 days composition image is shown in Figure 2.10.

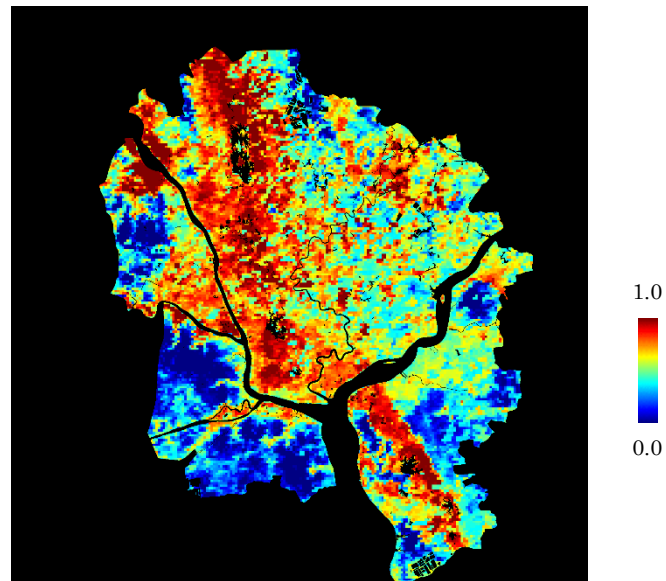


Figure 2.8 MODIS NDVI 8 days composition image during the flood event in 2008 (250 meters-resolution)

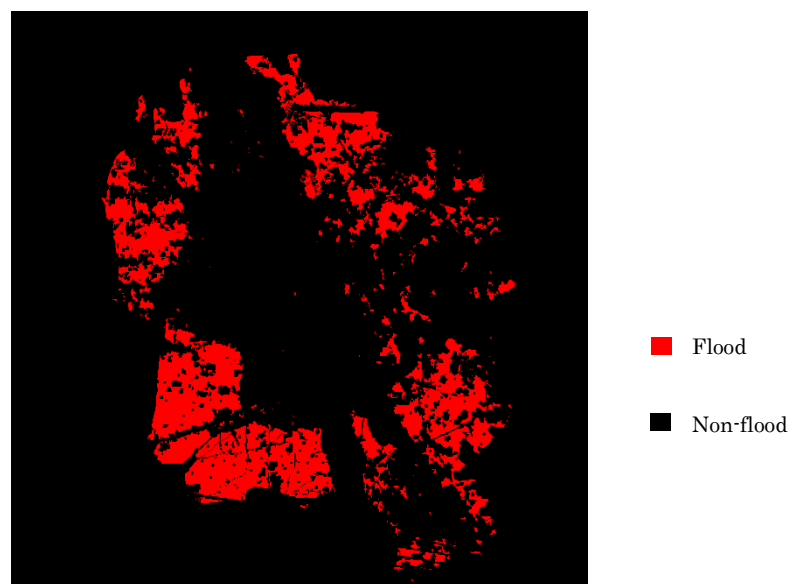


Figure 2.9 The actual flooded areas map in the flood event in 2008 by UNOSAT

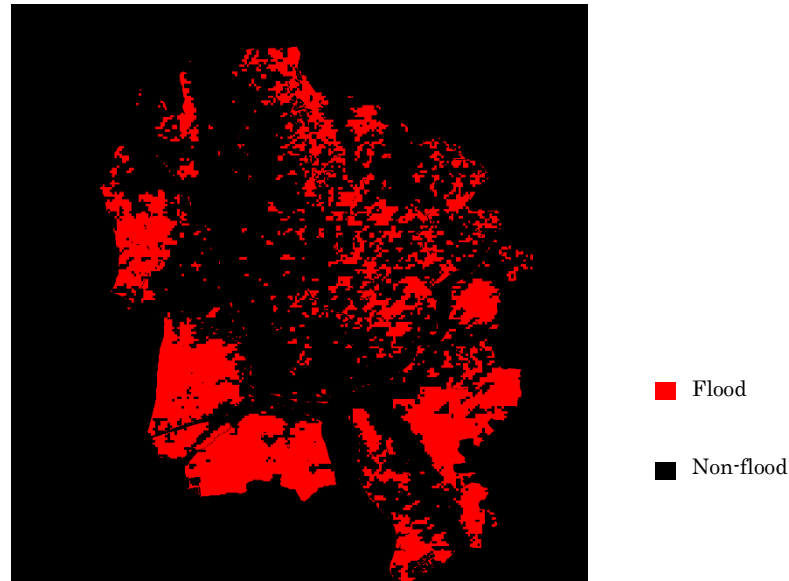


Figure 2.10 The estimated flooded areas map in the flood event in 2008 by MODIS NDVI 8 days composition image

According to the figure 2.09 and 2.10, the accuracy of the estimated flooded areas in 2008 by using MODIS NDVI 8 days composition image versus actual flooded areas in 2008 is 74.77% with true positive rate (TPR) of 73.01% and true negative rate (TNR) of 75.44%. This compared result confirmed that NDVI MODIS could observe water surface with the efficiency.

2.3.3 The validation of land cover image and SRTM DEM

Since we used the land cover image and SRTM DEM as the defined factors, they are needed to be validated to confirm the reliability of the input data. For the land cover image, we compared the land cover image in 2015 (Figure A.1) with the land use map in 2012 by JICA Study Team (Figure A.2). The accuracy of the land cover image in 2015 is 79.32% with the Kappa coefficients 0.72% (Table A.1). For SRTM DEM, we compared the elevation from SRTM DEM with the surveying elevation data with 98 locations in 2012 by NIHON KOEI Company, The RMSE (Root Mean Square Error) of the elevation from SRTM DEM is 6.20 meters. The validated results confirmed that the land cover image and SRTM DEM are reliable to be used as the input data.

2.4 Remarks

This study introduced a methodology to assess flood vulnerability in Yangon, Myanmar based on the empirical model by using Remote Sensing technology and GIS data.

In the experiment, we found that the assessment of flood vulnerability map based on the empirical model has a higher relationship with the flood vulnerability map based on flooding caused by cyclone Nargis using HydroSHEDS than based on the AHP model. However, when comparing our flood vulnerability map with flood vulnerability map based on the coastal flood by cyclone Nargis with the rainfall by using RRI Model, our result looks over estimation.

By using the empirical model, it can help to estimate the weights of the assessment of flood vulnerability. We investigated that by using the empirical model, the elevation has the highest impacts, whereas by using AHP model, the flow accumulation has the highest impact. By using empirical model, the impacts of flow accumulation and drainage network could not be detected since the estimation relies on the historical water surface analyzed by MODIS NDVI 8 days composition that can only detect water surface areas that remain more than 4 days. Our resultant flood vulnerability map has been related to coastal and riverine floods and indicated the venerable areas in term of the frequency of water surface. Our proposed model takes the advantage of using the observed water surface with the constantly long-term observation, whereas the rainfall runoff model takes employment of the flood simulation.

In addition, by comparing with LSWC derived from AMSR-E and AMSR-2 (microwave remote sensing) with MODIS NDVI time series, the historical water surface by the MODIS NDVI time series looks similar to the observed water surface by the LSWC. When comparing the estimated flooded areas by the NDVI 8 days composition in 2008 and the actual flooded areas, the accuracy is 74.77%. As a result, MODIS NDVI 8 days composition can observe the historical flood data with the efficiency.

Chapter3. Assessment of earthquake vulnerability

3.1 Background

In Myanmar, based on the statistics of seismically active areas, it indicates that Myanmar is an earthquake prone area since it lies on the Alpide Belt (Thein and Swe, 2008). According to the seismicity and the records of the previous magnitude earthquakes, Yangon can be regarded as the low to medium seismicity region (Thant, 2012). Moreover, tectonically the region is surrounded by the subduction zone between the Indian Plate and Burma Plate to the west and the right lateral Sagaing fault to the east. In the past, the most significant earthquake event that affected around Yangon is the earthquake event in Bago on 5th May 1930 with the magnitude of 7.3. This earthquake caused 500 deaths and huge destruction in Bago. In Yangon, there were considerable damage and 50 deaths in this event. This earthquake was originated from the Sagaing fault. Until now, a large earthquake has not appeared more than 80 years (JICA, 2013). Obviously, Yangon can be expected as a potential risk of the earthquake disaster in the future. Hence, in Yangon, earthquake risk assessment is needed to support earthquake risk management and its reduction.

The assessment of earthquake risk for the United States by the Federal Emergency Management Agency (FEMA) was introduced (FEMA, 2012). It evaluated physical damages such as damaged buildings and social damage such as casualties based on damage functions and census tract areas. Cinicioglu et al.(, 2007) presented an integrated damage-causing model including (1) ground shaking as a major effect, (2) landslide, liquefaction and seismic bearing capacity as minor effects. This method considered each effective phenomenon separately and in combination for two districts; Bakırköy and Ömerli, in Istanbul city. Assessment of earthquake risk in Tabriz, Iran was

introduced (Karimzadeh et.al, 2014). They used GIS information including soil's type and ground water. Assessment of earthquake-induced landslides was proposed (Song et. al, 2012). They focused on Beichuan, China and used the Bayesian network with GIS data to estimate earthquake risk area. Probabilistic hazard assessment for Yangon region was proposed by Thant (, 2012). The seismic hazard analysis is performed by applying the probabilistic way. The analysis of the earthquake fragility curve of the damaged buildings in Yangon was conducted (Gadagamma et.al, 2014). Damage states were idealized based on the performance level of building from pushover analysis.

In this research, we proposed the assessment of earthquake vulnerability based on the multi-criteria analysis modeling with six factors of the seismic intensity, soil types, slope, height, material and age of a building.

3.2 Methodology

3.2.1 Defining earthquake vulnerability assessment

We defined that the factors of earthquake risk are related to (1) the seismic wave, (2) soil type (3) slope (4) the height of a building, and (5) the age of the building. Firstly, for the seismic wave map, the area, which is the higher PGA (Peak ground acceleration), is a higher risk to be damaged by the earthquake. Secondly, the area which is located in alluvial areas (soft areas) has a high risk. Thirdly, the area which is located in the high slope area is a high risk to happen land slide during an earthquake, on the other hand, the area which is located in low slope (flat area) is more secure. Fourthly, high-rise buildings have a higher damage when earthquake occurring than low-rise buildings. Fifthly, the ages of the buildings, the old buildings are easier to collapse while the new buildings are lowly risky to fall down. We followed the work of Karimzadeh (, et.al, 2014). Firstly, we used the soil types and slope as the linear function to calculate the seismic amplitude map (Microzonation map). Then, we computed the ground shaking map by multiplying between the simulated seismic intensity (Thant, 2012) and the seismic amplitude map.

Next, we simulated the building damage map by calculating the fragility function with reinforce concrete (RC) material (Gadagamma et.al, 2014) from the ground shaking map and the heights of buildings. We integrated the damaged buildings and the ages of buildings to calculate the building vulnerability map. The flowchart of our methodology to assess earthquake vulnerability is depicted in Figure 3.1.

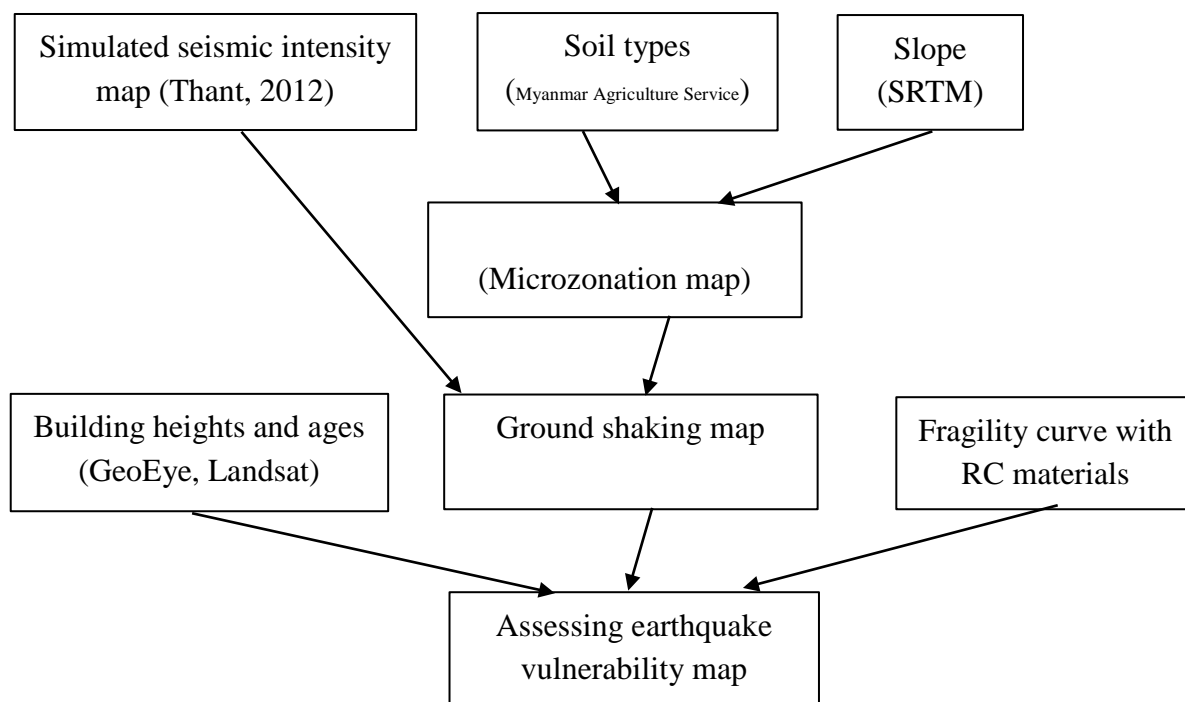


Figure 3.1 Flowchart of earthquake vulnerability assessment

3.2.2 Preparing data

Firstly, the slope was calculated from SRTM DEM with the length of 100 meters. For the ages of buildings, it is very hard to directly observe the age of buildings. Therefore, we used the ages of urban areas to indicate the ages of the building. We classified the Landsat images with 30 meters-resolution in 1978, 1990, 2000, 2009 and 2015 into land cover images from 1978 to 2015 with two classes of urban and non-urban (cropland, forest, lake, and river) by using

the Mahalanobis distance method (Supervised-classification). After that, the indirect age of building was able to be obtained. Then, by using stereo GeoEye images with 0.5 meters-resolution in 2013, we extracted DSM (Digital Surface Model) and DTM (Digital Terrain Model). By subtracting DSM by DTM, DBM (Digital Building Model) are provided. By combining with urban areas from the land cover image in 2015, the building heights are provided without the effects of trees.

For GIS data, for the seismic map, we used the simulated seismic map in term of PGA at the probabilities of 2% and 10% by Thant (, 2012). For soil types, we used the soil map provided by Myanmar Agriculture Service, 2002.

3.2.3 Calculating ground shaking map

We calculated the ground shaking map following the work of Karimzadeh (, et.al, 2014). Firstly, we calculated the seismic amplitude map. Next, we used the simulated seismic intensity from the work of Thant, 2012). Then, we computed the ground shaking map by multiplying between the simulated seismic intensity and the seismic amplitude map.

Firstly, for the earthquake amplitude map or microzonation map, earthquake amplitude was defined in term of the index with a range from 0.0 (the lowest amplitude) to 1.0 (the highest amplitude). The earthquake amplitude index was defined as the linear function with the defined factors of (1) soil types and (2) slope. The equation of the earthquake amplitude index is expressed as the below equation.

$$EA = w_G \cdot G + w_S \cdot S + C \quad (3.1)$$

Where EA = Earthquake amplitude, G = Soil types, S = Slope, H = Height of building, C = Constant value (Bias value)

For defining the values of the parameters of earthquake amplitude index, we used the K-means method to help to group the data values and then we ranked the values of group data as a linear function with an equal step. We

assigned the parameters of earthquake amplitude index as the below table.

Table 3.1 The defined parameters of earthquake amplitude index

Parameters	Class	Index value
Soil types	Alluvial	1.0
(G)	Lateritic soil (Rock)	0.5
Slope (degree)	Mean of 2.68	1.0
(S)	Mean of 1.38	0.75
	Mean of 0.57	0.50
	Mean of 0.55	.025

For the weights of the earthquake amplitude index, we followed the expert opinion from the work of Karimzadeh (, et.al, 2014). The weight of soil type (w_G) is 0.3 and the weight of slope (w_S) is 0.1. In the work of Karimzadeh, they used the factors of soil type, slope, alluvial thickness, water table, and predominant period. However, in this research, we had the defined factors of soil types and slope and we did not have an alluvial thickness, water table, and predominant period. As a result, the bias (C) will be 0.6 since it is expressed in term of unobserved parameters of alluvial thickness (the weight of 0.25), water table (the weight of 0.25), and predominant period (the weight of 0.1). The earthquake amplitude map is depicted in figure 3.2.

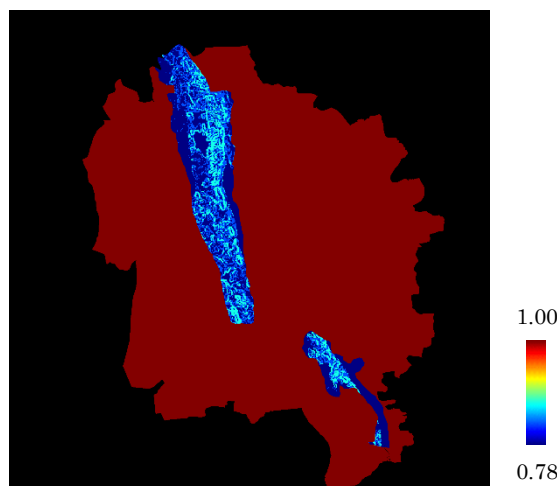


Figure 3.2 The earthquake amplitude map

Next, for the seismic intensity map, we used the seismic intensity map from the work of Thant (, 2012). The seismic hazard analysis is simulated by applying the probabilistic way. In this research, we used the seismic intensity map in term of PGA (Peak Ground Acceleration) with the probabilities of 2% and 10%. The seismic intensity maps with the probabilities of 2% and 10% are illustrated in the figure 3.3 a and b, respectively.

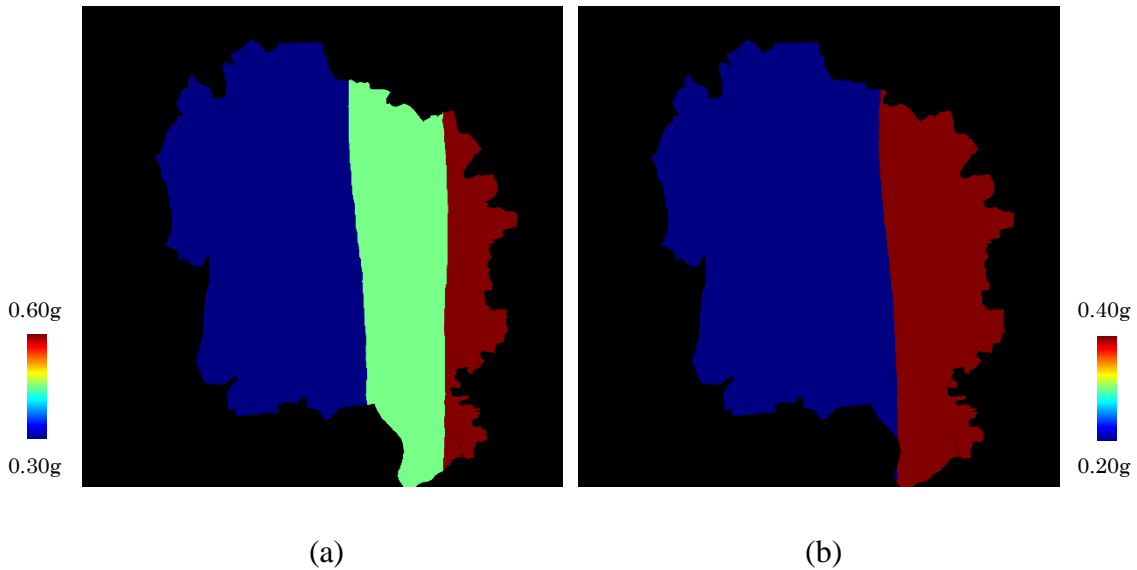


Figure 3.3 The seismic intensity maps in term of PGA with the earthquake probabilities of (a) 2% and (b) 10%

Then, for the ground shaking map, the earthquake amplitude map and the seismic intensity map are integrated to compute the ground shaking map. The equation of the ground shaking in term of PGA is expressed as the below equation.

$$GS = EA \cdot EI \quad (3.2)$$

Where GS = Ground shaking, EA = Earthquake amplitude, EI = Earthquake intensity

The ground shaking map with the probabilities of 2% and 10% are shown in figure 3.4 a and b, respectively.

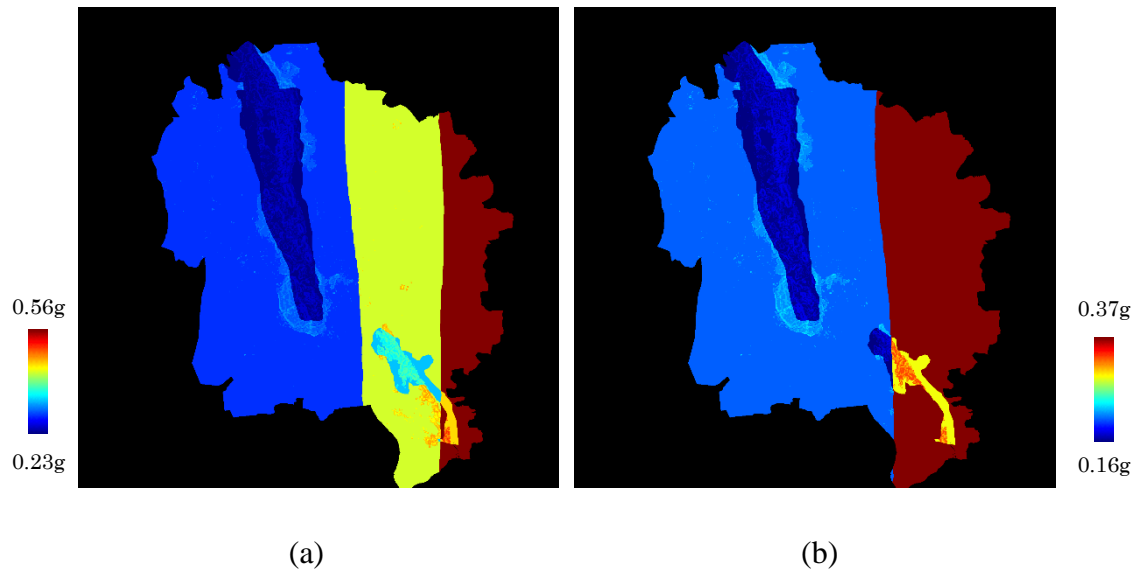


Figure 3.4 The ground shaking maps in term of PGA with the earthquake probabilities of (a) 2% and (b) 10%

3.2.4 Computing earthquake building vulnerability map

We simulated the building damage from the ground shaking map and the building heights with the fragility curve (Gadagamma et.al, 2014). Then, we integrated the damaged buildings and the ages of buildings to calculate the building vulnerability map.

For simulating the building damage, we used the fragility curve from the work of Gadagamma (, et.al, 2014) with the heights and materials of buildings and the ground shaking map to simulate the building damage. The fragility curve was calculated by using the non-linear static pushover analysis. A building survey group called SATREPS visited Yangon in 2015 and found that that 95% of the buildings are reinforced concrete (RC) buildings and the other buildings are steel buildings and brick-nogging buildings. As a result, RC buildings are applied as the main material for the simulation. In this research, there are two types of the materials with RC 2500psi and RC 1250psi and there are two types of building heights with low-rise building (1-3 floors) and high-rise building (4-6 floors). The fragility curves with (1) low-rise building with RC 2500psi, (2) high-rise building with RC 2500psi (3) low-rise building

with RC 1250psi, (4) high-rise building with RC 1250psi were calculated and are depicted as below.

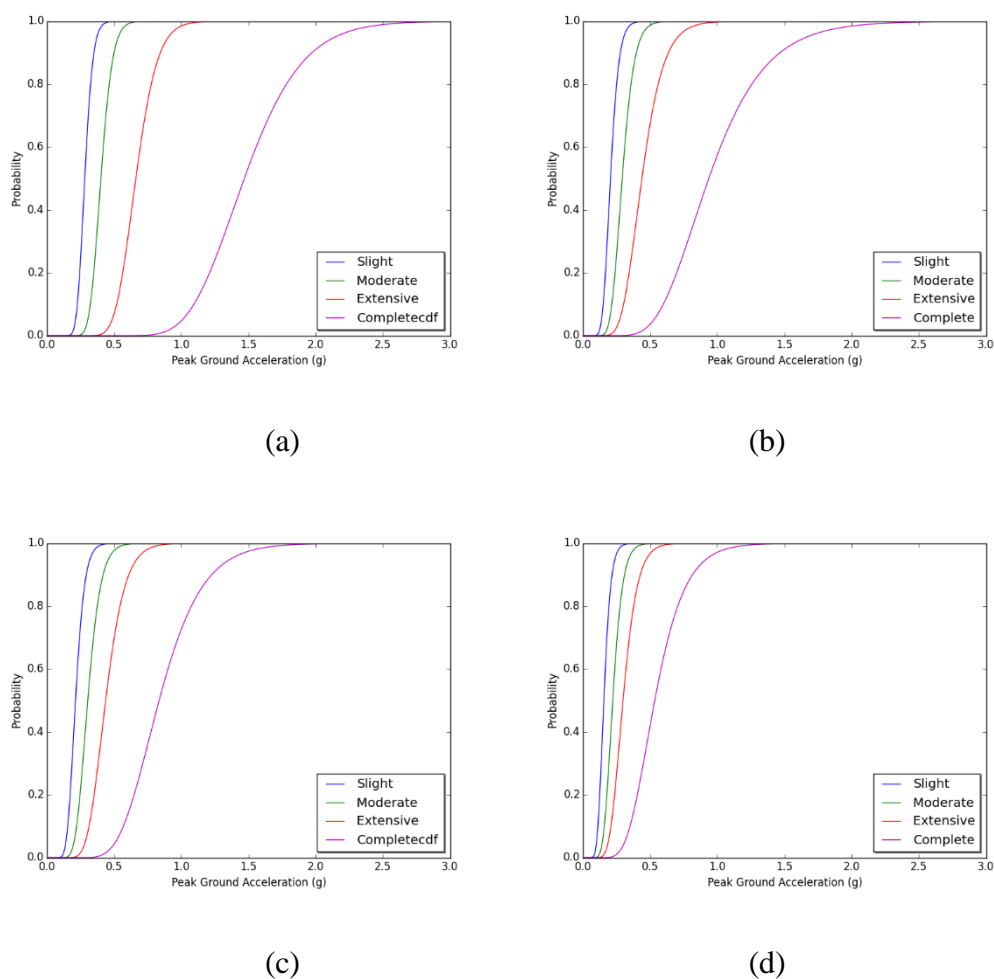


Figure 3.5 The fragility curves with (1) low-rise building with RC 2500psi, (2) high-rise building with RC 2500psi (3) low-rise building with RC 1250psi, (4) high-rise building with RC 1250psi

In this research, we have the ground shaking maps with the probabilities of 2% and 10% and the two materials of RC 2500psi and RC 1250psi. Therefore, we have the four cases of the simulated building damage in Table 3.2.

Table 3.2 The cases of the simulated building damage

No.	RC materials	Probability of Earthquake
Case 1	RC 2500psi	Probability of 10%
Case 2	RC 1250psi	Probability of 10%
Case 3	RC 2500psi	Probability of 2%
Case 4	RC 1250psi	Probability of 2%

For calculating the building damage state with the fragility curve, we defined that if the building has the value of the fragility curve is more than 30% at the damage state, the building will have that damage state. After the simulations of the building damages with the fragility curves, the simulated building damages with four cases are illustrated in Figure 3.6.

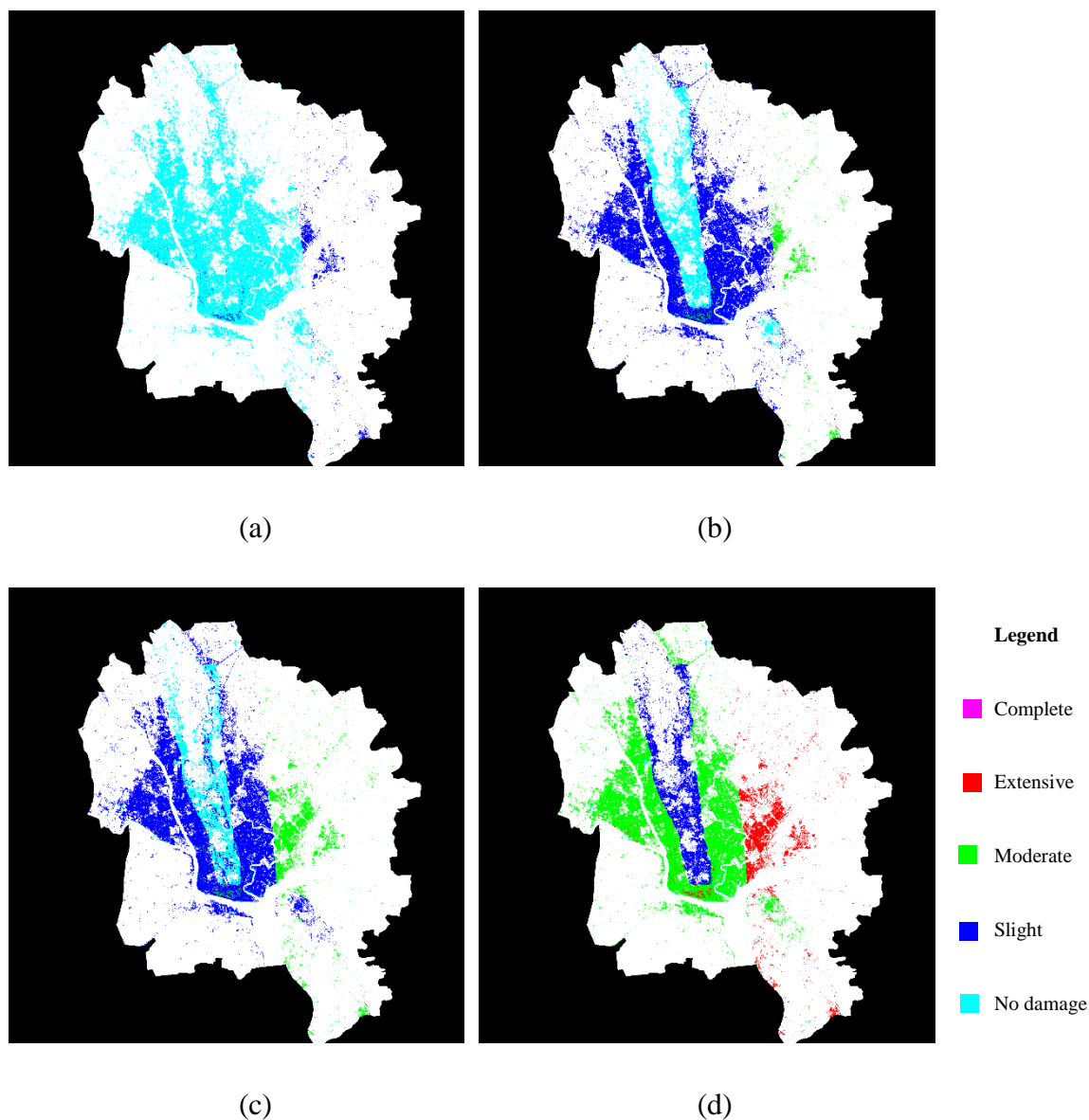


Figure 3.6 The simulated building damages with (a) the probability of 10% and RC 2500psi, (b) the probability of 10% and RC 1250psi, (c) the probability of 2% and RC 2500psi, (d) the probability of 2% and RC 1250psi

Then, we integrated the simulated building damage and the age of the building to calculate the earthquake building vulnerability index. the earthquake building vulnerability index was defined in term of the index with a range from 0.0 (the lowest vulnerability) to 1.0 (the highest vulnerability). The earthquake vulnerability index was defined as the linear function with the defined factors of the building damage and the ages of the buildings. The equation of the earthquake vulnerability index is expressed as the below equation.

$$EVI = w_D \cdot D + w_A \cdot A \quad (3.3)$$

Where EVI = Earthquake building vulnerability index, D = Building damage, A = Age of building

For defining the values of the parameters of earthquake building vulnerability index, we ranked the values as linear function with equal step. We assigned the parameters of earthquake building vulnerability index as the below table.

Table 3.3 The defined parameters of earthquake building vulnerability index

Parameters	Class	Index value
Damage of building (D)	Complete	1.0
	Extensive	0.75
	Moderate	0.50
	Slight	0.25
Age of building (A)	1978	1.0
	1990	0.75
	2000	0.50
	2009	0.25

For the weights of the earthquake building vulnerability index, we assumed that the simulated building damage as the major factor with the weight of 0.8 and the age of the building as minor factor with the weight of 0.2.

3.3 Results and discussions

3.3.1 The results of earthquake building vulnerability maps

The assessment of earthquake building vulnerability map with four cases of (1) the probability of 10% and RC 2500psi, (2) the probability of 10% and RC 1250psi, (3) the probability of 2% and RC 2500psi, (4) the probability of 2% and RC 1250psi in Figure 3.7 a, b, c, and d, respectively.

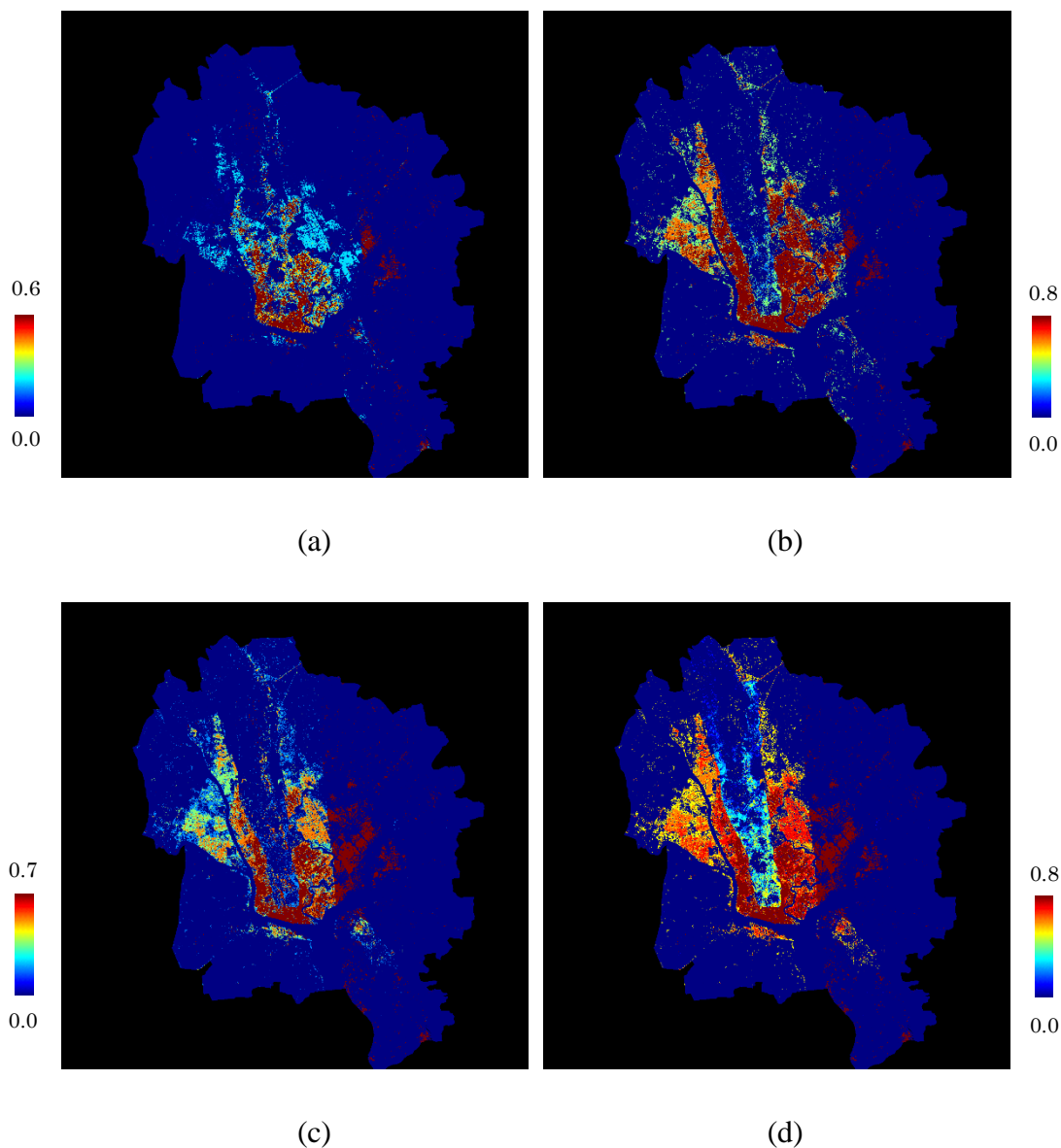


Figure 3.7 The earthquake building vulnerability map with (a) the probability of 10% and RC 2500psi, (b) the probability of 10% and RC 1250psi, (c) the probability of 2% and RC 2500psi, (d) the probability of 2% and RC 1250psi

According to the earthquake vulnerability maps with multiple cases (Figure 3.6 and 3.7), we found that when the earthquake occurs with the probability of 10% and buildings are made from the RC 2500psi, the low-rise buildings have no damages but the high-rise buildings have slight damages. Also, the buildings in the eastward have slight damages since they are located on the areas close to the faultline. Next, when the earthquake occurs with the probability of 10% and buildings are made from the RC 1250psi, the low-rise building have slight damages and high-rise buildings have moderate damages

but some buildings located on lateritic soil (one type of rock) have no damages since lateritic soil have endure the ground shaking better than alluvial soil. Also, the buildings in the eastward have moderate damages. Then, when the earthquake occurs with the probability of 2% and buildings are made from the RC 2500psi, the low-rise building have slight damages and high-rise buildings have moderate damages but some buildings located on lateritic soil have no damages. Also, the buildings in the eastward have moderate damages and the effective areas in the eastward are wider. Then, when the earthquake occurs with the probability of 2% and buildings are made from the RC 1250psi, the low-rise building have moderate damages and high-rise buildings have extensive damages but some buildings located on lateritic soil have slight damage. Also, the buildings in the eastward have extensive damages and the effective areas in the eastward are wider. In summary, In Yangon, the eastward areas have high vulnerable areas sine they are located close to faultline. Almost areas are located on alluvial areas that has also high vulnerable areas. However, few areas have high vulnerable areas from high slope. By combining with the ages of the buildings, we found that the buildings in downtown areas in Yangon are very old buildings. Thus, the downtown areas are at high risk of the damage of the earthquake since the buildings are high and very old. By using the high quality of the building materials such as RC 2500psi, it can help to protect or reduce the earthquake damage; especially in the eastern area.

3.3.2 The validation of the heights of buildings and digital surface model

Since we used the estimated heights of the buildings as the defined factor, and the estimated DSM as the information to calculate the building heights. they are needed to be validated to confirm the reliability of the remotely sensed data. For building heights, we compared the estimated building heights in 2013 (Figure A.3) with surveying building heights data with 6 regions with 59 buildings (22 residential buildings, 22 commercial buildings, 15 industrial buildings) in 2015 (Figure A.4). The comparison of the estimated heights and surveying heights of the buildings indicated there is a high correlation (Table

A.2). For the DSM, we compared the estimated DSM from with the surveying elevation data with 98 locations in 2012 by NIHON KOEI Company, The RMSE of the estimated DSM is 1.62 meters. The validated results confirmed that estimated building heights and the estimated DSM are reliable to be employed.

3.4 Remarks

We proposed the earthquake vulnerability map by using the seismic intensity, soil type, slope, building height, building material and building age. The earthquake vulnerability map with multiple-cases were proposed by varying the earthquake probabilities and building materials.

In the experiment, we found that in the safest case with the earthquake probability of 10% and RC 2500psi, the low-rise buildings have no damages but the high-rise buildings have slight damages. Also, the buildings in the eastward have slight damages since they are located on the areas close to the faultline. In the worst case with the earthquake probability of 2% and RC 1250psi, the low-rise building have moderate damages and high-rise buildings have extensive damages but some buildings located on lateritic soil have slight damage. Also, the buildings in the eastward have extensive damages and the effective areas in the eastward are wider. As a result, In Yangon, the eastward areas have high vulnerable areas sine they are located close to faultline. Almost areas are located on alluvial areas that has also high vulnerable areas. However, few areas have high vulnerable areas from high slope. We also found that the downtown area in Yangon is very risky for the earthquake vulnerability causing from high-rise buildings and very old buildings. By using the high quality of the materials such as RC 2500psi, it can help to protect or reduce the earthquake damage.

In the validations of the estimated building heights and the estimated DSM, The validated results confirmed that they are reliable to be used.

However, the other factors such as ground water and alluvial thickness should be considered to improve the assessment of earthquake vulnerability.

Chapter4. Estimation of land price

4.1 Background

The industrial structure in Myanmar was composed of the agriculture, livestock, fishery, and forestry sector (36%); the trade sector (20%); the process and manufacturing sector (20%); and the services sector (18%). In Yangon, the industrial structure was composed of the processing and manufacturing sector (37%); the trade sector (25%); and the services sector (24%) (JICA, 2013). Lacking well land use planning and management in the past (World Bank, 2017), Yangon has complexes areas by mixed land use areas among commercial, industrial and residential areas. Land price is the one indicator that can indicate economic areas (Nichols, 1970; Deaton, 2001). Land price does not only depend on land use areas (commercial, industrial or residential areas) but also, surrounding environments such as elevation (low or high elevations), railways (close or far from railway) etc. Estimating the land price in term of spatial information can help to find which areas are important (high value) or non-important (low value) in term of economic aspect. According to the previous chapters, Yangon has high potential risks of flood and earthquake. Therefore, land price areas can link with the flood and earthquake vulnerable areas to calculate the assessments of flood and earthquake loss risk that can be employed to support the disaster management in Yangon.

The estimations of land price have been widely conducted in various research works (Ihlanfeldt, 2007; Tsutsumi et.al, 2011). Xu and Li (, 2014) introduced the empirical model of land price in urban residential development. Geographic information system (GIS) data such as residential, commercial and industrial areas were mainly applied to estimate land price. The model of land price distribution was developed (Hu et.al, 2013). These researchers employed multifractal inverse distance weighted interpolation and the fractal filtering method with sampled land price data to assess land price distribution. Lin and

Zhu (, 2014) proposed a spatial analysis on the incremental value of land in China at the national scale. The capitalization effects of school, residential, and commercial areas were employed to estimate the undeveloped land price (Burge, 2014).

This research proposed the methodology to estimate the land price in term of spatial information in Yangon, Myanmar. Our proposed method is based on the multi-criteria analysis modeling. The empirical model was used to relate the modeling to land price information.

4.2 Methodology

4.2.1 Defining land price model

In this research, we defined that the factors to indicate land price are (1) building types with residential, commercial, and industrial buildings (2) land cover change with urban and non-urban (3) elevation (4) the distance from railways (5) the population density. The empirical model based on a linear function was employed to link between land price information and the defined factors. To estimate the coefficients in the model, the linear regression was applied. The flowchart of our methodology is shown in Figure 4.1.

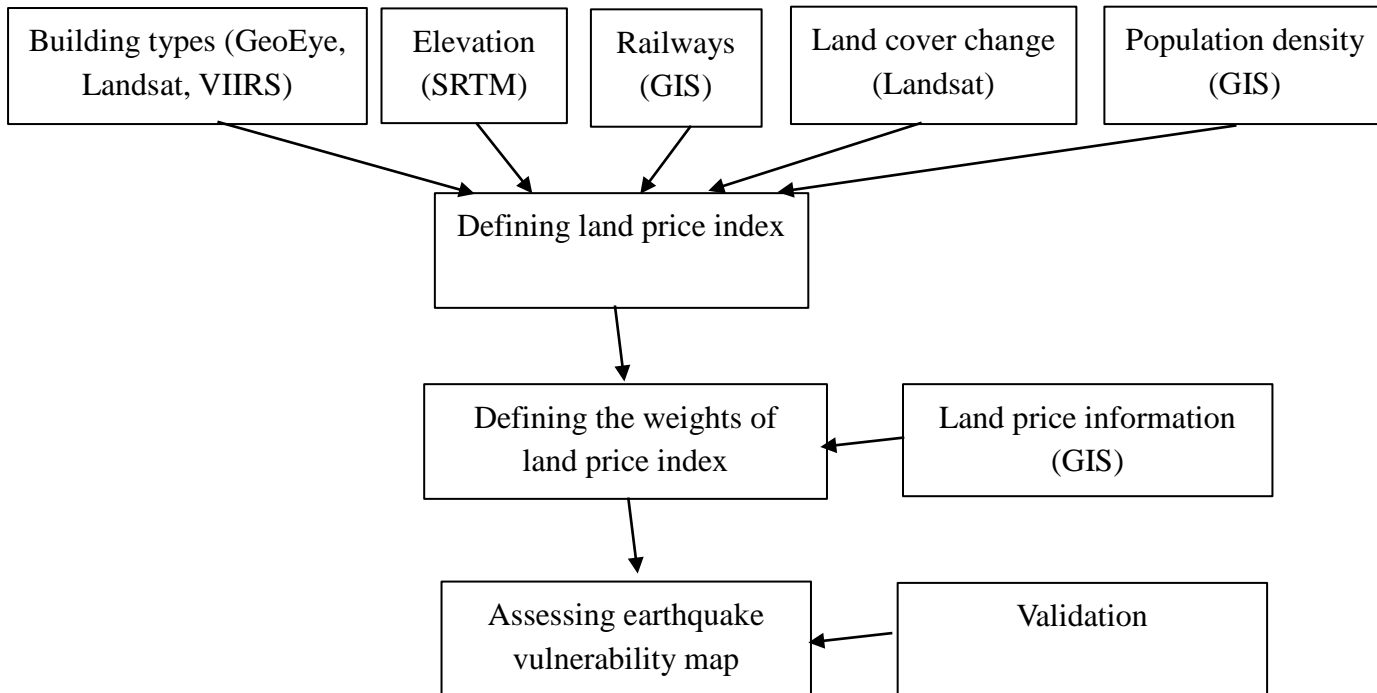


Figure 4.1 The flowchart of land price estimation

4.2.2 Preparing data

For the defined factors, four factors; (1) building types (2) land cover change (3) elevation (4) the distance from railways, and the population density were needed to be prepared.

For building types, we used stereo GeoEye images with 0.5 meters resolution in 2013 and Landsat image in 2015 with 30 meters resolution and VIIRS nighttime light data approximately 460 meters resolution in 2012. By using stereo GeoEye images, we extracted DSM (Digital Surface Model) and DTM (Digital Terrain Model). By subtracting DSM by DTM, DBM (Digital Building Model) are provided. The Landsat image was classified by Mahalanobis distance (Supervised Classification) to provide a land cover image. VIIRS nighttime light image was classified by K-means (Unsupervised Classification) to provide the different nighttime light activities. By using the hierarchy classification with the DBM, land cover image and the different nighttime light activities, the building types with (1) residential building (2) commercial

building (3) industrial building are provided (Sritarapipat and Takeuchi, 2017a).

For land cover changes, we employed multispectral Landsat image with 30 meters resolution in 1978, 1990, 2000, 2009 and 2015. We classified land cover types into two classes with (1) urban, (2) non-urban (vegetation, forest, river, and lake) by using the Mahalanobis distance. After classifying the Landsat images, land cover time series from 1978 to 2015 were provided.

For elevation, we used the SRTM DEM as the estimated elevation. Then, we separated the elevation into five groups from low to high elevations by using K-means.

For the distance from railways, we calculated the Euclidean distance from railways that were provided by JICA. Next, we separated the distance from railways into five groups from near to far distances by using K-means method.

For the density of population, we used the population density map in 2015 of The Gridded Population of the World Version 4 (GPWv4). GPW models the distribution of the human population (counts and densities) on a continuous global surface. The GPW data was modeled census information may be analyzed in conjunction with other data sets such as land cover without concern for endogeneity, or double counting (GPWv4).

For land price information, we employed the land price information that provided from the Internal Revenue Department, Ministry of Finance, Myanmar for calculating tax payment. We used the land price information in term of the index at the township scale.

4.2.3 Defining land price index

We defined the land price in term of the index with a range from 0.0 (the lowest land price) to 1.0 (the highest land price).

According to Sharif (and Esa, 2014) and O' Conner (and Conlon, 1993) works, the forest is a very low land price, and cropland is low land price, while the

urban has a varying land price from a low to high land price. Hence, we defined that the index of land price with land cover as the below table.

Table 4.1 The land price index of urban, cropland, and forest

Parameters	Class	Index value
LPI	Urban	1.0-0.3
(land price index)	Cropland	0.2
	Forest	0.1

We assumed that the relationship between the land price for urban areas and the defined factors is a linear function. The equation of land price index is expressed as the equation below.

$$\text{LPI} = w_B \cdot B + w_E \cdot E + w_R \cdot R + w_L \cdot L + w_P \cdot P + c \quad (4.1)$$

Where LPI = land price index, B = Building types, E = Elevation, R = the distance from railways, L = land cover changes, w_B = the weight of building types, w_E = the weight of elevation, w_R = the weight of the distance from railways, w_L = the weight of land cover changes, w_P = the weight of population density, c = Constant value.

For defining the parameters of building types and land cover change for the land price index, we assigned the parameters in Table 4.2.

Table 4.2 The defined parameters of land price index

Parameters	Class	Index value
Building types (B)	Commercial building	1.0
	Industrial building	0.5
	Residential building	0.25
Land cover change (L)	Urban from 1978	1.0
	Urban from 1990	0.75
	Urban from 2000	0.5
	Urban from 2009	0.25
Elevation (E)	Highest elevation	1.0
	Lowest elevation	0.0
Distance from railways (R)	Closest from railway	1.0
	Furthest from railway	0.0
Population density (P)	High population density	1.0
	Low population density	0.0

4.2.4 Estimating the weights of land price index

We estimated the five weights of land price index by linking between the land price information and the defined factors. We defined that the LPI of 0.0 is the lowest land price in 2012 and the LPI of 1 is the highest land price in 2012. To calculate the seven weights of the land price index, we applied the least square regression method with Equation 4.1. After computing the least square regression, the estimated weights are expressed as the below table.

Table 4.3 The weights of land price index based on the empirical model

WB	WE	WR	WL	WP	C
0.188	0.726	0.001	0.110	0.315	-0.060

4.3 Results and Discussions

4.3.1 The estimation of land price index

The estimated land price map based on the empirical model by linking between the land price information and the defined factors is displayed in figure 4.2.

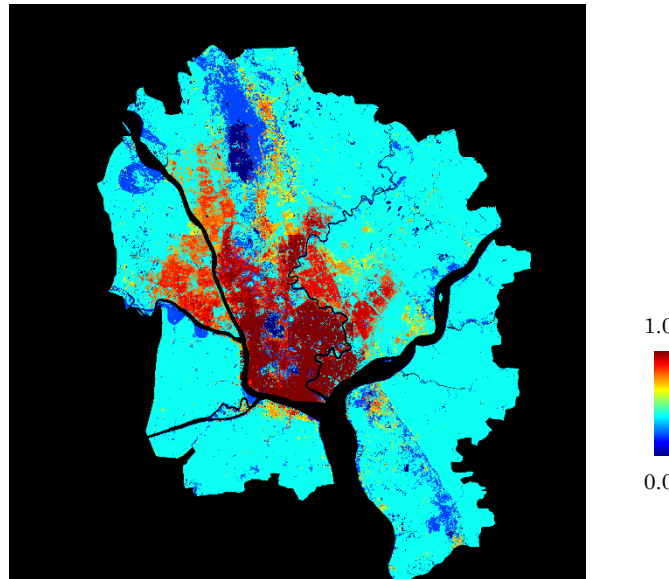


Figure 4.2 The estimation of land price in Yangon

According to the experiments, we found that the elevation, building types and population density have high impacts to the estimation, and land cover change has a medium impact, and railways have a very low impact. For each factor affected to land price, we investigated that for the building types, commercial buildings have high land prices but industrial and residential buildings have low land prices. For elevation, the areas that are located on higher elevations have higher land prices. For railways, the areas that are located closer to railways have higher land prices. For land cover changes, the areas that were urban in the past have higher land prices. For the population density, the areas that have a high population density is a higher land price.

4.3.2 The validation of land price index

The estimated land price map at the township scale is depicted in Figure 4.3 and the actual land price map in township scale is depicted in Figure 4.4. The comparison between estimated and actual land prices in each township in term of plotting lines is shown in Figure 4.5. The mean absolute error at the township scale is shown in Figure 4.6. The average of mean absolute error at the township scale is 0.147.

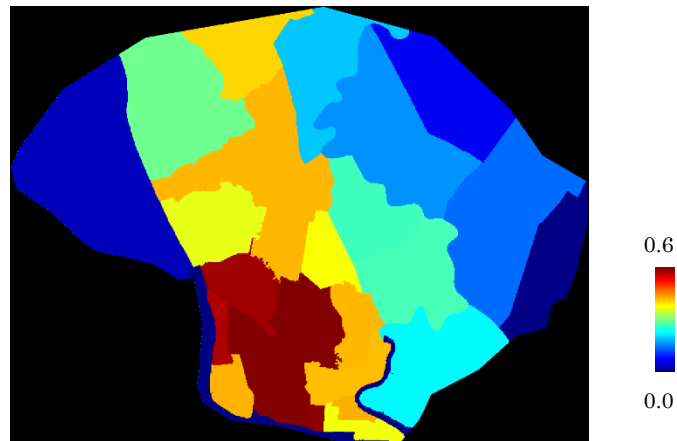


Figure 4.3 The estimated land price map at the township scale in 2012

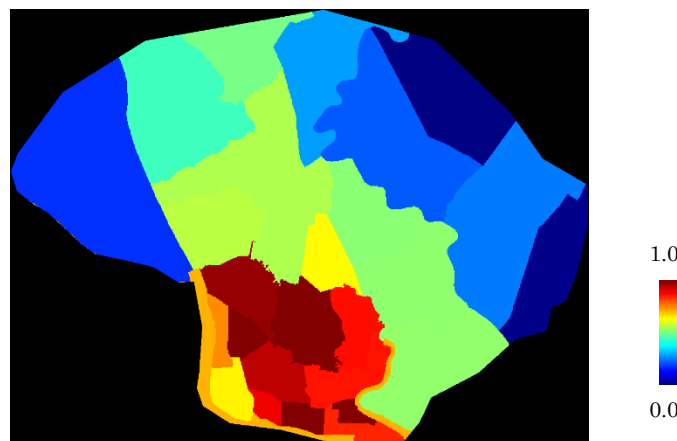


Figure 4.4 The actual land price map at the township scale in 2012

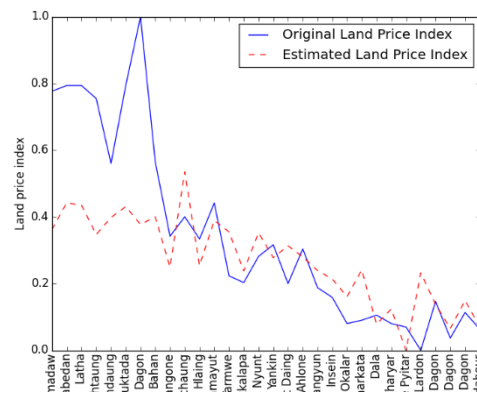


Figure 4.5 The comparison between the estimated and actual land prices in 2012 at the township scale

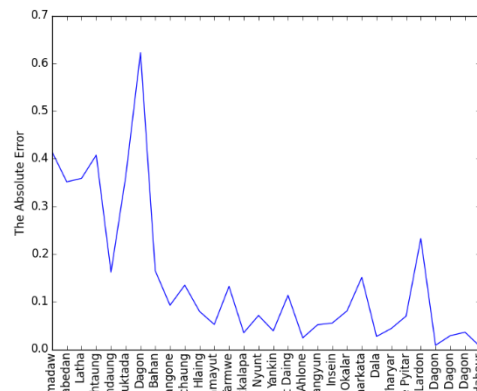


Figure 4.6 The mean absolute error of the estimated and actual land prices in 2012 at the township scale

According to the comparing results between the estimated and actual land price in Yangon at the township scale, the estimated land prices of almost townships look very close to the actual land prices. However, some of the estimated land prices look quite different. We investigated that some townships have low buildings but have high land price since they have many tourist places (low buildings). Since our model did not include the tourist place (significant structure), our result made errors in that areas. Moreover, the tourist place can not be detected by using only remote sensing. The other information should be considering such as the people flow data that can be obtained by using call detail record (CDR) from mobile phone. Other factors such as the road types and other transportations can be applied to obtain the higher accuracy as well. For assigning parameters, in this research, we

assigned the parameter values as a linear function. To improve the accuracy of the land price estimation, we might assign the parameter indexes as an exponential function instead of linear function. To obtain the land price at the higher resolution, the higher spatial information of actual land price should be used such as in the road scale or in the household scale.

4.3.3 The validation of the building classification

Since we used the estimated building uses as the defined factor, it is required to be validated to confirm the reliability of the land price estimation. We compared the estimated building types in 2013 (Figure A.5) (Sritarapipat and Takeuchi, 2017a) with the land use map in 2012 (Figure A.6). The accuracy of the estimated building types is 76% with the Kappa coefficient of 0.58 (Table A.3). It is confirmed that estimated building type is reliable to be used.

According to the validations of the estimated building types and elevation, they confirmed that the estimated building types and elevation can be employed in the model with the reliability.

4.4 Remarks

This research introduced a methodology to estimate land price in Yangon, Myanmar based on the empirical model by using Remote Sensing data and GIS data. We used the five factors of building type, elevation, urban areas in the past, railway, population density to indicate the land price in Yangon, Myanmar. We used actual land price to help calculating the weight of land price index.

In the experiments, we found that for building types, commercial buildings have high land prices, industrial buildings have medium land prices, and residential buildings have low land prices. For the elevation, the higher elevations have higher land prices. For the urban areas in the past, the older urban areas have higher land prices. For railways, the areas near railways have high land prices. For population density, the areas that have the higher

population are higher land prices. For validation, we compared between estimated and actual land prices. We found that the average of mean absolute error at the township scale is 0.147. The estimated land prices of almost townships look very close to the actual land prices. However, some of the estimated land prices look quite different.

To improve the accuracy of land price estimation, in the setting parameters, the parameters values can be assigned in term of an exponential function instead of a linear function. Also, the other factors such as the locations of significant structures (tourist places) can be used in the land price estimation to improve the accuracy as well.

Chapter5. Modeling urban expansion

5.1 Background

Yangon had rapidly increased population growth in the past decade. The average growth rate of population in Yangon City between 1998 (3.69 million population) and 2011 (5.14 million population) is 2.58% annually whereas, the national population growth rate of 0.9% (JICA, 2013). JICA Team estimated that the growth rate per year is around 8% with the GRDP of 17.6 billion US dollars in 2016 and the GRDP of 75.9 billion US dollars in 2035. As increasing population and economic development in Yangon, urban has rapidly increased. Urban growth is rather a complex process. Since urban expansion causes from many factors such as human behaviors, population rates, the economic states, the policies of the government and so on. Remote sensing technology provides the physical information that can directly monitor the urban areas from the past to the present. Hence, it can lead us to understand the mechanism of urban expanding or how urban expands (Bagan and Yamagata, 2012). In the other hand, by understanding the system of urban expansion, the urban expansion modeling can be created to predict urban areas in the future (Clarke and Gaydos, 1998). Since Yangon is regarded as the high risk of flood and earthquake, to support disaster risk management in Yangon, Myanmar, we need to understand the phenomena of urban expansion and create the model of urban expansion to predict urban areas in the future.

The various kinds of urban expansion models have been widely developed in order to understand the system of urban expansion and predict the urban areas in the future. Urban land-use model based on spatial interaction model was developed by Lowry (, 1964). Spatial interaction model known as the gravity model was described the spatial relations between two objects. All interactions in the system are the spatial relations between any pairs of all objects. By using the interactions, the estimated urban areas can be generated. Next, the statistical model was used for introducing urban expansion model. The model

relies on a mathematical mechanism. For the example work from Sklar and Costanza (, 1991), the statistical model was defined as a set of equations relating the population growth and the land-use change. Next, an urban growth model based on automata cellular was proposed (Batty, 1997). The automata cellular model refers to cell space with the pixel and neighboring pixels including the transition rules from land use change. Moreover, by using multi-agent-based model, the residential distribution estimation was developed (Benenson, 1998). The Multi-agent system model; including the automata cellular model with translation rules and relating to human behaviors and the environments, could be used to simulate urban areas in efficacy. The monitoring of urban expansion in Yangon was proposed by Moe (, 2009). He observed the urban growth pattern by using the collected information from Yangon City Development committee and field surveying.

We proposed the methodology to model urban expansion based on the dynamic statistical modeling by using remotely sensed data and GIS data. The seven factors of (1) the distance from the multi-centers of the urban areas, (2) the distance from the urban areas in the past, (3) the distance from roads, (4) the distance from railways, (5) land elevation, (6) the class translation, (7) the separated lands by the rivers are included in the model.

5.2 Methodology

5.2.1 Modeling urban expansion

Generally, urban expansion considers on three aspects of (1) the facilities such as department store, office, school etc., (2) the transportation such as roads, railways, (3) the environments such as river and mountain (Zhang, 2001). In this research, we defined the factors to indicate urban expansion as follows: (1) the distance from the multi-centers of the urban areas, (2) the distance from the urban areas in the past, (3) the distance from roads, (4) the distance from railways, (5) and elevation, (6) the class translation, (7) the separated lands by the rivers. In the estimation step, the maximum likelihood

estimator (Cho, 2006) was used with the observed parameters to estimate urban expansion. In the prediction step, the unknown parameters in the future were estimated from observed parameters. Using the estimator with the estimated parameters, the urban areas in the future was predicted. The flowchart of our methodology is shown in Figure 5.1.

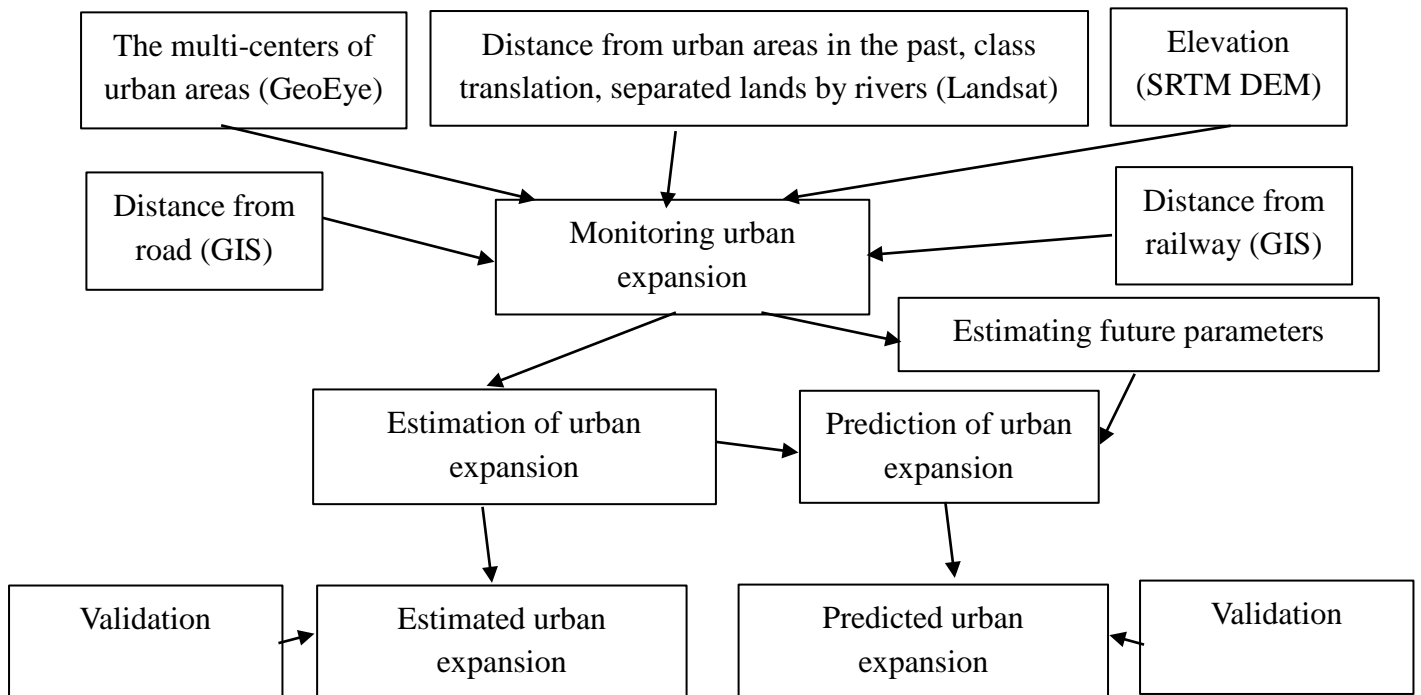


Figure 5.1 The flowchart of modeling urban expansion

5.2.2 Preparing data

For Remotely sensed data, the multispectral Landsat images with a 30 m.-resolution in 1978, 1990, 2000, 2009 and 2015 were classified into a land cover change with urban, vegetation and water from 1978 to 2015. Using the result of the land cover change, we obtained urban expansion data, urban area in the past, class translation and separated lands by the rivers. Next, stereo GeoEye images with a 0.5 meters resolution in 2013 were employed to obtain the height of the building. Using the height of the building and the separated

lands by the rivers, the multi-centers of the urban areas were extracted with 18 centers of urban areas. Then, SRTM DEM was used to obtain elevation. For GIS data, the information of roads and railways were provided by JICA.

5.2.3 Monitoring urban expansion with defined factors

We monitored urban expansion extracted from the classification results from 1978 to 2009 with the defined factors of (1) the distance from the multi-centers of urban areas, (2) the distance from urban areas in the past, (3) the distance from roads, (4) the distance from railways, (5) elevation, (6) the class translation, (7) the separated lands by the rivers. In this research, urban expansion refers to non-urban areas that changed to urban areas.

Firstly, for monitoring urban expansion relating to the distance from the multi-centers of the urban areas, we calculated the Euclidean distances of non-urban pixels that changed to urban from the pixels to the nearest center of the urban areas in each region. The 18 regions of the multi-centers of urban areas are shown in Figure 5.2. The means and variances of the Euclidean distance from the multi-centers of the urban areas in each region from 1978 to 2009 are shown in Table 5.1, and Figure 5.3 displayed the means of the Euclidean distances from the multi-centers of urban areas in term of bar graphs. The examples of the histograms of the Euclidean distances from the multi-centers of the urban areas in the region of the center #1 with time variation are depicted in Figure 5.4.

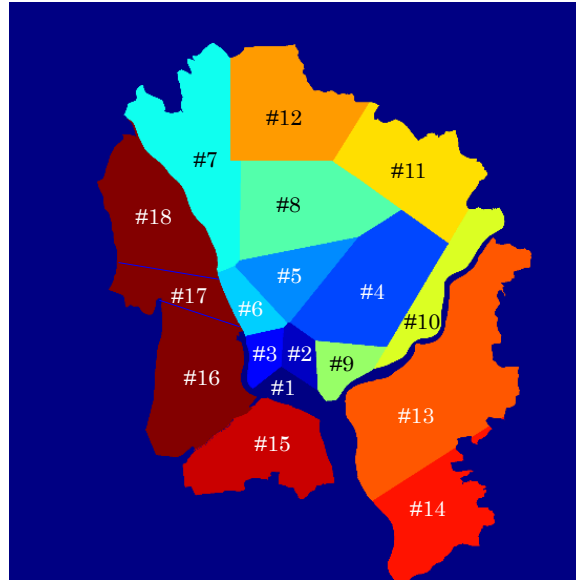


Figure 5.2 The 18 regions of the multi-centers of urban areas

Table 5.1 The means and variances of the Euclidean distance from the multi-centers of urban areas in each region from 1978 to 2009 (Pixels)

Region	1978→1990		1990→2000		2000→2009	
	Mean	Variance	Mean	Variance	Mean	Variance
Center #1	62.23	646.15	68.90	512.30	73.21	654.69
Center #2	72.62	970.60	69.70	799.90	62.35	669.71
Center #3	62.47	491.98	63.56	352.34	62.66	389.74
Center #4	70.68	2946.32	121.89	3639.07	147.92	6854.92
Center #5	79.14	1307.11	107.93	2320.64	105.01	2782.65
Center #6	69.58	1302.25	79.97	1446.33	79.70	1599.41
Center #7	104.70	1424.57	114.55	2794.73	107.85	6332.89
Center #8	93.17	1522.07	112.43	3386.76	124.07	4978.58
Center #9	63.46	722.15	64.39	842.24	79.58	1474.87
Center #10	136.00	12978.11	65.60	939.53	120.84	14464.76
Center #11	55.36	304.66	64.09	4144.84	113.98	6191.45
Center #12	64.66	3702.80	75.68	3227.24	94.52	3960.43
Center #13	97.51	5310.95	85.21	5734.63	119.77	13005.83
Center #14	236.71	3861.06	117.61	17848.36	105.01	11565.94
Center #15	35.18	677.55	66.76	1324.71	69.45	2024.03
Center #16	62.73	2841.02	99.04	3042.08	109.50	5082.64
Center #17	88.44	1702.25	48.13	991.30	63.20	1442.22
Center #18	31.19	343.80	94.26	2767.35	115.10	4463.16

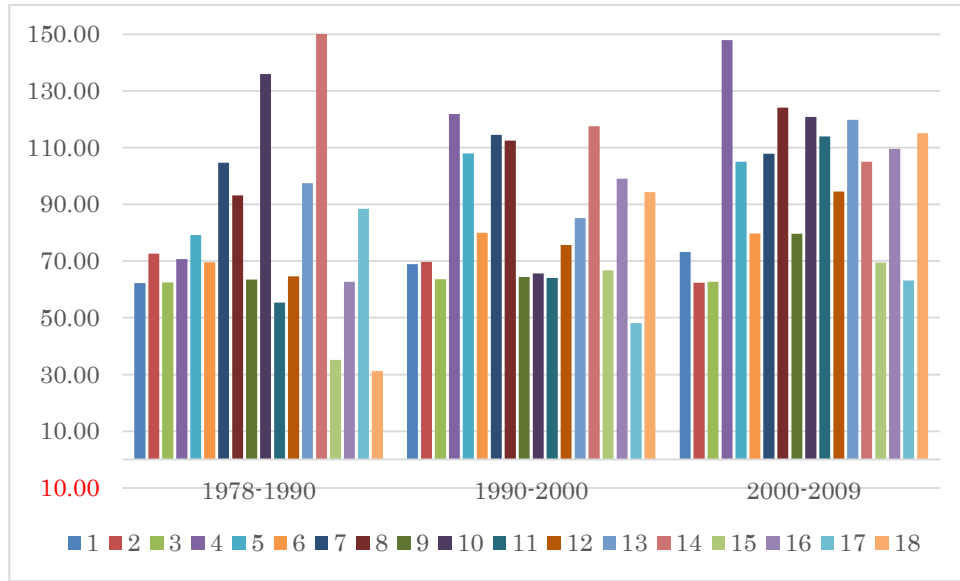


Figure 5.3 The bar graphs of the means of the Euclidean distance from the multi-centers of urban areas in each region from 1978 to 2009 (Pixels)

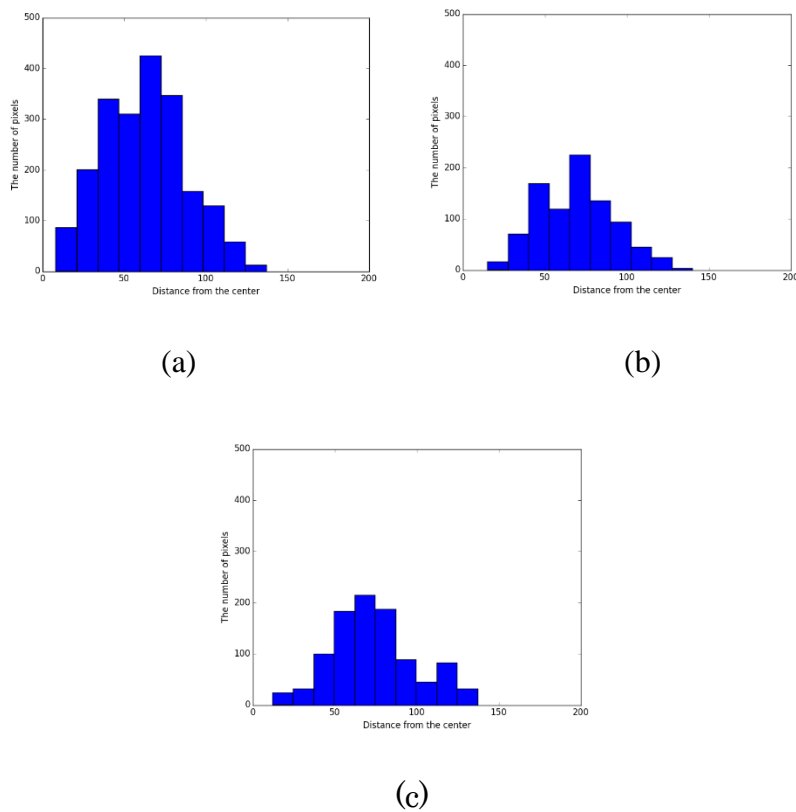


Figure 5.4 The histograms of the Euclidean distance from the multi-centers of urban areas in the region of the center #1 in the years of (a) 1978→1990, (b) 1990→2000, (c) 2000→2009 (Pixels)

According to the increasing values of the means of the Euclidean distance from the multi-centers of urban areas from 1978 to 2009 in the almost regions (Figure 5.3), we investigated that the urban expanded from the near distance from the multi-centers of the urban area to the far distance. The distributions of the histograms seem as the Gaussian distributions (Figure 5.4).

Secondly, for monitoring urban expansion to the distance from the urban areas in the past from 1978 to 2009, we calculated the Euclidean distances of non-urban pixels that changed to urban from the pixels to the nearest urban areas in the past. The mean and variance of the Euclidean distance from the urban areas in the past from 1978 to 2009 are described in Table 5.2 and Figure 5.5.

Table 5.2 The means and variances of the Euclidean distance from the urban areas in the past from 1978 to 2009 (Pixels)

	1978-1990	1990-2000	2000-2009
Mean	2.30	6.06	3.66
Variance	12.03	66.71	46.90

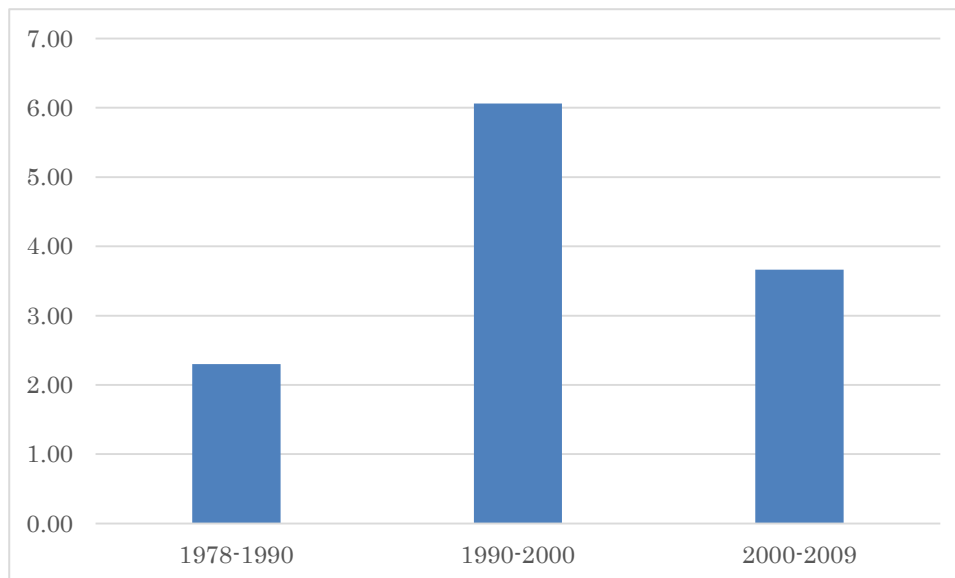


Figure 5.5 The bar graphs of the means of the Euclidean distance from the urban areas in the past from 1978 to 2009 (Pixels)

According to Table 5.2 and Figure 5.5, we found that the urban areas grew

up near the urban area in the past.

Thirdly, for monitoring urban expansion to the distance from the roads, we calculated the Euclidean distances of non-urban pixels that changed to urban from the pixels to the nearest roads. The mean and variance of the Euclidean distance from the roads are 1.42 and 4.34, respectively. The histogram of the Euclidean distances from the roads is shown in Figure 5.6.

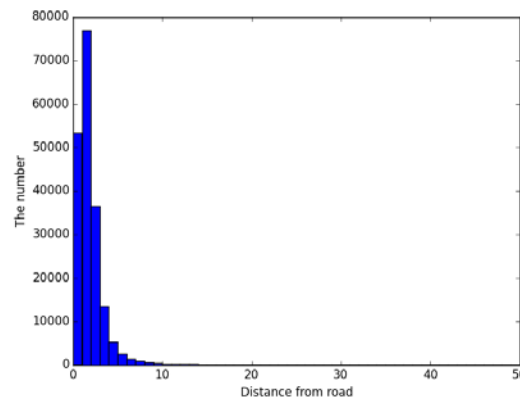


Figure 5.6 The histogram of the Euclidean distances from the roads (Pixels)

We found that the urban grew up along the roads, and the distribution appears as the Gamma distribution (Figure 5.6).

Fourthly, for monitoring urban expansion to the distance from the railways from 1978 to 2009, we calculated the Euclidean distances of non-urban pixels that changed to urban from the pixels to the nearest railway. The mean and variance of the Euclidean distance from the railways from 1978 to 2009 are described in Table 5.3 and Figure 5.7.

Table 5.3 The means and variances of the Euclidean distance from the railways from 1978 to 2009 (Pixels)

	1978-1990	1990-2000	2000-2009
Mean	30.25	53.50	70.87
Variance	571.27	2302.61	4055.56

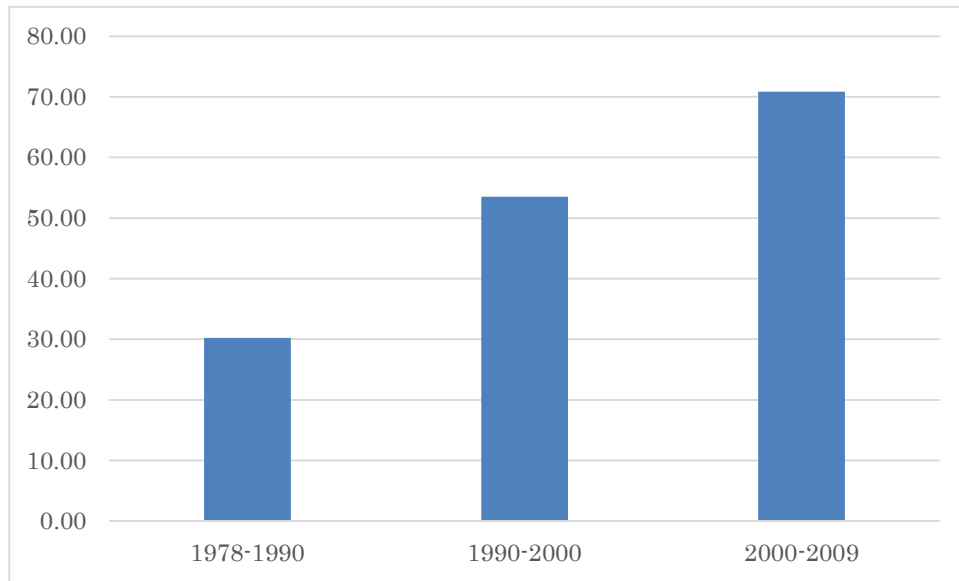


Figure 5.7 The bar graphs of the means of the Euclidean distance from the railways from 1978 to 2009 (Pixels)

According to Table 5.3 and Figure 5.7, we investigated that the urban areas grew up close to railways

Fifthly, for monitoring urban expansion to the elevation from 1978 to 2009, we observed the elevation of non-urban pixels that changed to urban. The mean and variance of the elevation from 1978 to 2009 are described in Table 5.4 and Figure 5.8.

Table 5.4 The means and variances of the elevation from 1978 to 2009 (Pixels)

	1978-1990	1990-2000	2000-2009
Mean	14.71	12.46	11.45
Variance	67.11	63.31	69.57

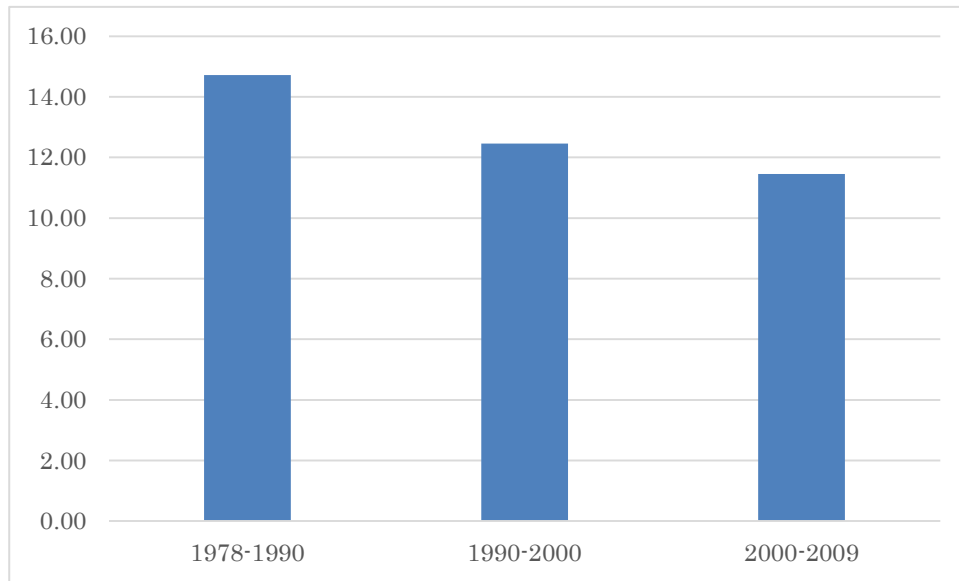


Figure 5.8 The bar graphs of the means of the elevation from 1978 to 2009 (Pixels)

According to Table 5.4 and Figure 5.8, we found that the urban areas grew up from the high to low elevations.

Sixthly, for monitoring urban expansion relating to the class translation, we observed the number of vegetation and water (non-urban) turn into urban from the land cover change from 1978 to 2009. The examples of the class translation in the region of the center #1 with time variation are illustrated in Table 5.5 and Figure 5.9 in term of a line graph.

Table 5.5 The class translation in the region of the center #1 from 1978 to 2009 (Pixels).

	1978-1990	1990-2000	2000-2009
urban→urban	8,410	10,942	12,780
vegetation→urban	2,123	1,774	2,208
water→urban	409	64	69

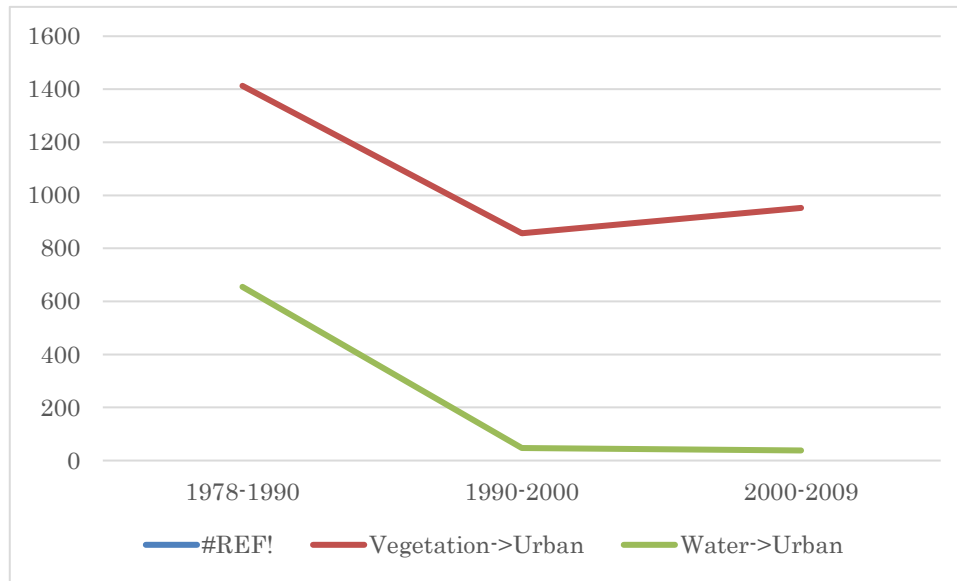


Figure 5.9 The class translation in the region of the center #1 from 1978 to 2009 (Pixels)

We found that the urban grew up from vegetation more than from water. In this research, we defined that urban always change to urban. Also, the urban expansion refers to non-urban (vegetation and water) that changed to urban. Therefore, the class translation from urban to urban was not included in our model.

5.2.4 Estimation of urban expansion

We used the maximum likelihood estimator (Cho et.al, 2006) with the dynamic statistical modeling to estimate urban expansion (Sritarapipat and Takeuchi, 2017b). By using the estimator, the probabilities with the defined factors by observing urban expansion are maximized to calculate the locations of urban expansion. The equation of estimating urban expansion is expressed in equation 1.

Maximizing The probability of class translation + The probability of the distance from the multi-centers of the urban areas + The probability of the distance from urban areas in the past + The probability of the distance from

roads + The probability of the distance from railways + The probability of land elevation (5.1)

The probabilities of class translation with the multi-centers with the separated lands by rivers was defined as Markov chain. The probabilities of the distance from the multi-centers of the urban areas, the distance from urban areas in the past, the distance from roads, the distance from railways, and land elevation were assumed as Gaussian distribution. By consideration of the independent terms, Equation 5.1 can be separated into two equations with Equation 5.2 and equation 5.3.

Maximizing The probability of class translation (5.2)

Maximizing The probability of the distance from the multi-centers of the urban areas + The probability of the distance from urban areas in the past + The probability of the distance from roads + The probability of the distance from railways + The probability of land elevation (5.3)

Equation 5.2 can be expressed with the more details as the below equation.

$$\sum_{i=1, j=1}^{m, n} \text{vegetation}(i, j, t) \rightarrow \text{urban}(i, j, t+1) = N_{\text{vegetation}(t) \rightarrow \text{urban}(t+1)} \quad \text{and}$$

$$\sum_{i=1, j=1}^{m, n} \text{water}(i, j, t) \rightarrow \text{urban}(i, j, t+1) = N_{\text{water}(t) \rightarrow \text{urban}(t+1)} \quad (5.4)$$

Equation 5.3 can be explained with the more details as below

$$\text{Minimizing } \sum_{i=1, j=1}^{m,n} \left[\beta_1 \frac{(x_1(i, j, t+1) - \mu_1(t \rightarrow t+1, c))^2}{\sigma_1(t \rightarrow t+1, c)^2} + \beta_2 \frac{(x_2(i, j, t+1) - \mu_2(t \rightarrow t+1))^2}{\sigma_2(t \rightarrow t+1)^2} + \beta_3 \frac{(x_3(i, j, t+1) - \mu_3)^2}{\sigma_3^2} + \beta_4 \frac{(x_4(i, j, t+1) - \mu_4(t \rightarrow t+1))^2}{\sigma_4(t \rightarrow t+1)^2} + \beta_5 \frac{(x_5(i, j, t+1) - \mu_5(t \rightarrow t+1))^2}{\sigma_5(t \rightarrow t+1)^2} \right] \quad (5.5)$$

Where $\beta_1, \beta_2, \beta_3, \beta_4, \beta_5$ are the precision parameters that are manually assigned. From the experiments, we assigned the precision parameters as $\beta_1 = 0.2, \beta_2 = 0.2, \beta_3 = 0.7, \beta_4 = 0.3, \beta_5 = 0.1$.

Then, in order to estimate urban expansion, Equation 5.4 and Equation 5.5 are simultaneously calculated.

The land cover image in 1978 in preparing data step was set as the initial land cover image. We used the initial land cover image with observed parameters as input for the estimator to estimate land cover image in 1990. Next, we used the estimated land cover in 1990 with observed parameters to estimate land cover image in 2000. We repeated the same step to estimate land cover image in 2009.

6.2.5 Prediction of urban expansion

Since the parameters in the future could not be observed, they are required to estimate. For the amount of urban areas in the future, there are two steps for prediction. Firstly, we calculated the relationship between urban areas and population data (United Nations, 2015). We found there is a high relationship between urban areas and population data with an R-squared value of 0.98. Secondly, we used the relationship with the predicted population data in the future (Hoornweg, 2014) to predict the amount of the urban areas in the future. For predicting the locations of urban expansion in the future, we used the previous parameters with the polynomial regression to calculate the parameters used for prediction in the future. The polynomial regression is a form of linear regression, which is commonly used for trend analysis (Greenland, 1995).

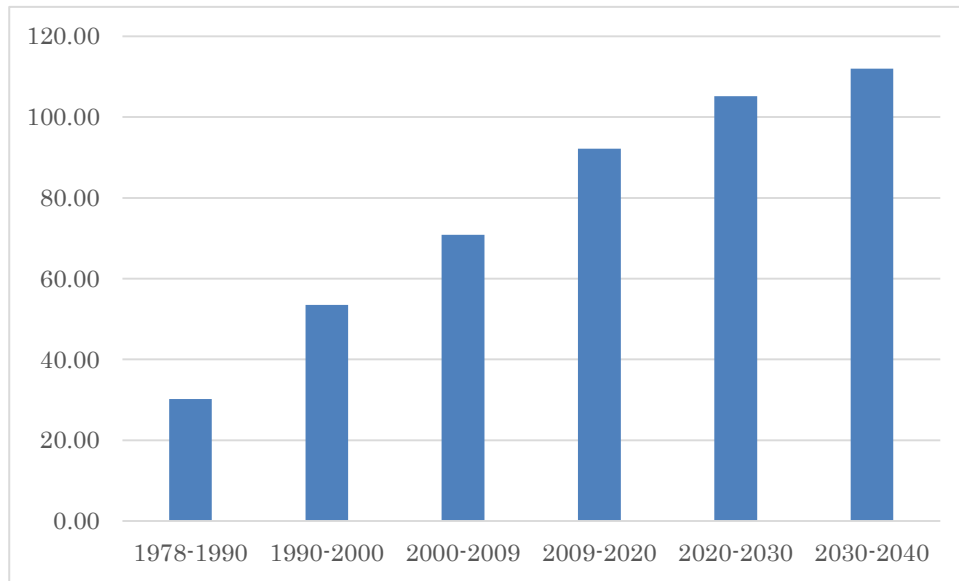


Figure 5.10 The estimated Euclidean distance from the railways from 2020 to 2040 (Pixels)

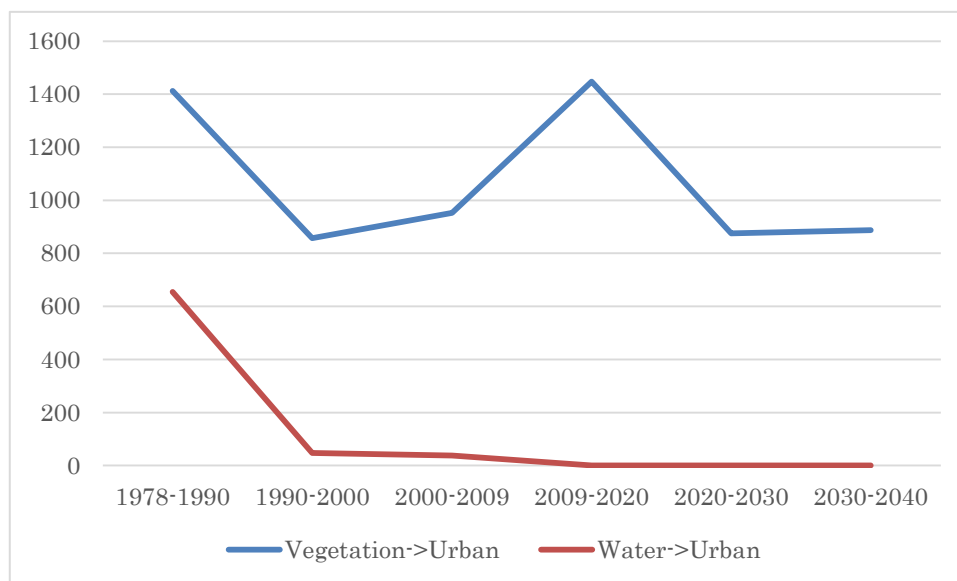


Figure 5.11 The estimated class translation in the region of the center #1 from 2020 to 2040 (Pixels)

In this research, we predicted the urban areas in 2020, 2030, 2040. We used the estimated land cover in 2009 with the estimated parameters as input for the estimator to predict land cover image in 2020. Then, we used the predicted land cover in 2020 with the estimated parameters to predict land cover image in 2030. We repeated the same step to predict land cover image in

2040. The examples of estimated parameters in the future with the estimated distance from the railways and the estimated class translation are shown in Figure 5.10 and 5.11, respectively.

5.3 Results and discussion

For estimation of urban expansion, the classification results in preparing data step were defined as referenced land cover images (Figure 5.12 a, b, c). Then, we compared the estimated land cover images by using our model (Figure 5.12 d, e, f) with the referenced land cover images. For comparison, we only used two classes with urban and non-urban (vegetation and water) to calculate the resultant accuracy.

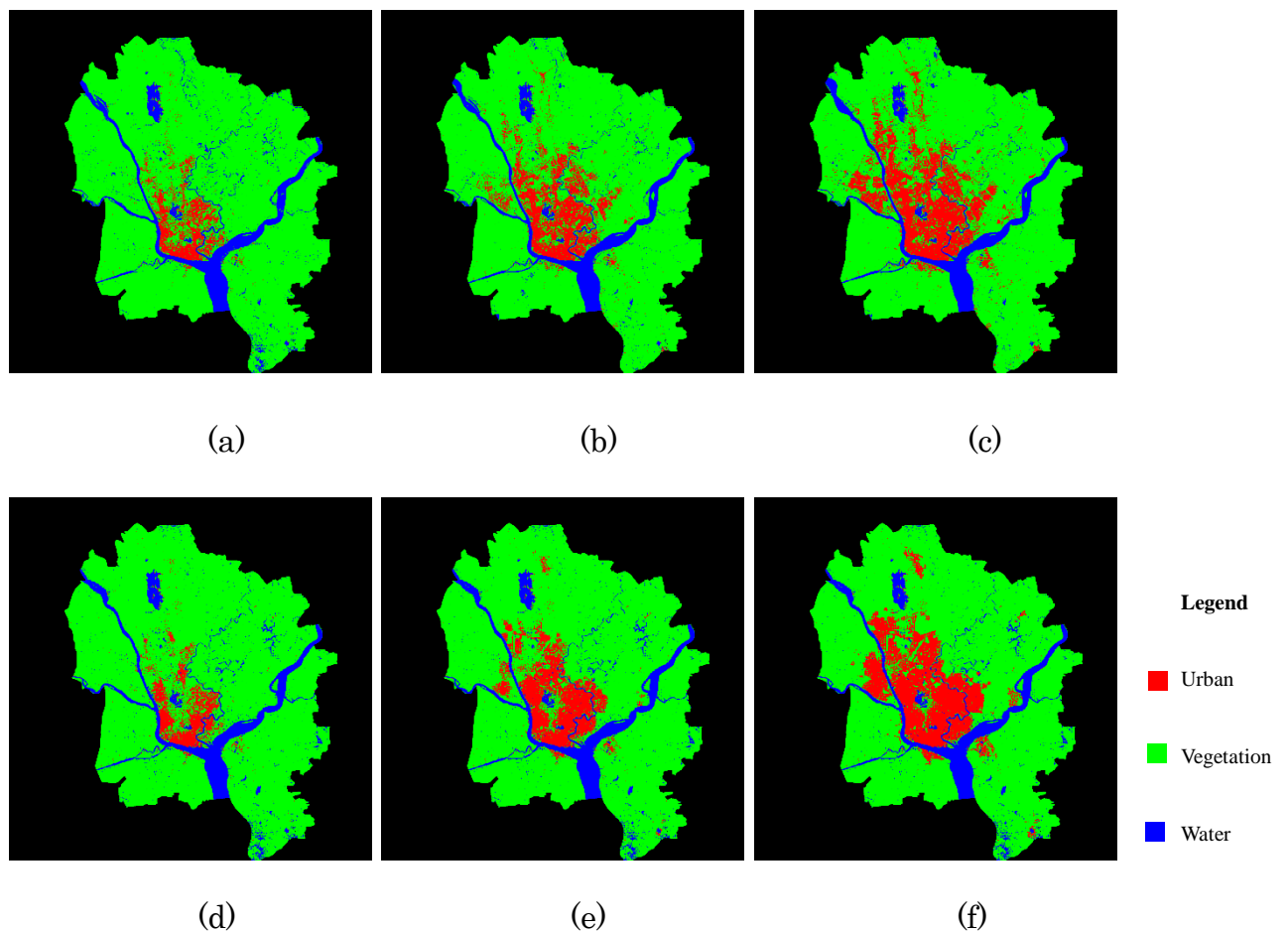


Figure 5.12 (a) Referenced land cover image in 1990, (b) Referenced land cover image in 2000, (c) Referenced land cover image in 2009, (d) Estimated land

cover image in 1990, (e) Estimated land cover image in 2000, (f) Estimated land cover image in 2009

For prediction of urban expansion, there are three predicted images in 2020, 2030, 2040 (Figure 5.13 b, c, d). For validation, the Landsat image on November 25, 2015, was selected and classified to be a land cover image as an unseen land cover image (Figure 5.13 a).

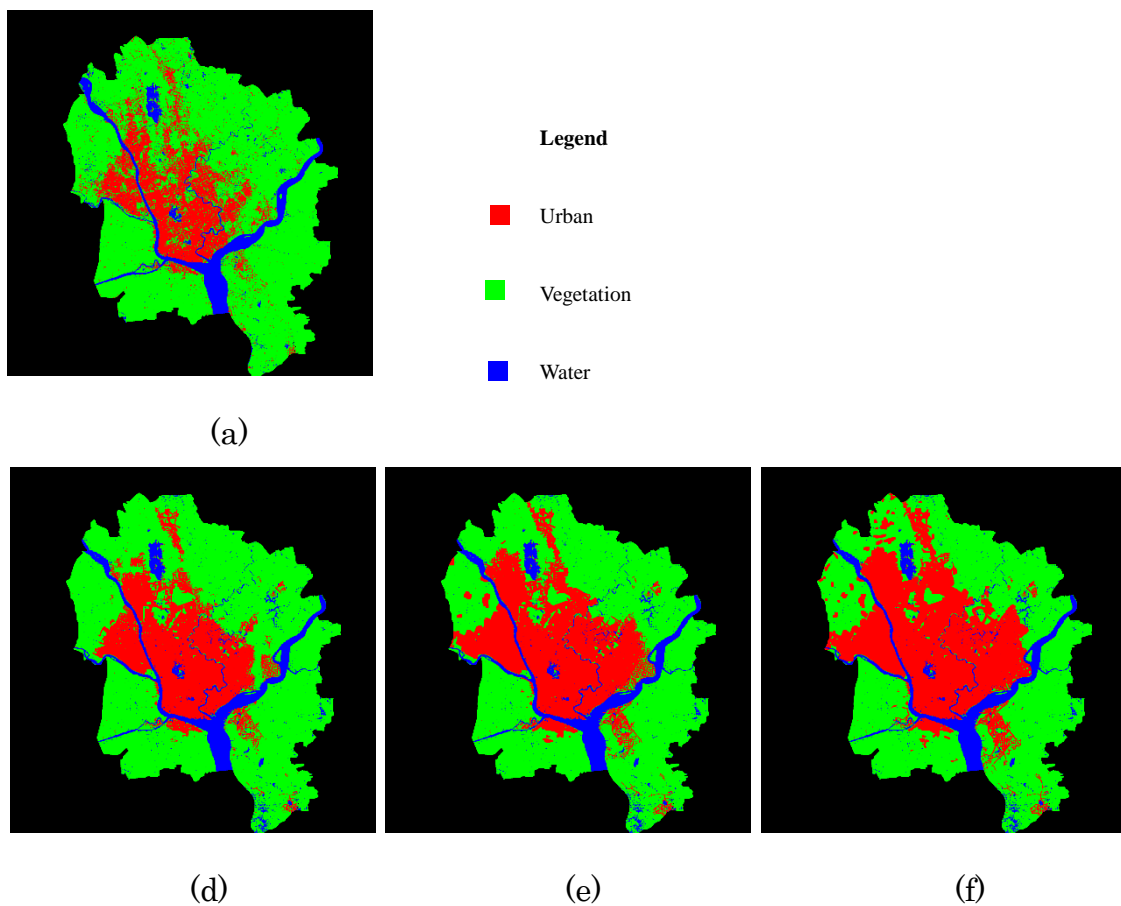


Figure 5.13 (a) The unseen land cover image in 2015, (b) Predicted land cover image in 2020, (c) Predicted land cover image in 2030, (d) Predicted land cover image in 2040

The accuracies with true positive rate (TPR) and true negative rate (TNR) of referenced versus estimated land cover images in 1990, 2000, and 2009, 2020 are expressed in Table 5.6.

Table 5.6 The accuracies of the estimation of urban expansion

Year	Accuracy (%)	True positive rate (TPR) (%)	True negative rate (TNR) (%)
1990	98.01	77.39	99.03
2000	93.63	64.10	96.55
2009	91.39	68.76	95.06
2020	88.43	82.97	89.64
Average	92.88	73.31	95.07

According to Figure 5.12 and 5.13, and Table 5.6, our proposed methodology of urban expansion modeling can estimate the urban expansion from 1990 to 2020 with the average accuracy of 92.88% with the average TPR of 73.31% and the average TNR of 95.07%.

We found that in Yangon, Myanmar, the almost urban areas grow up as follows. Urban areas grow up close to the multi-centers of urban areas. Urban areas grow up close urban areas from the past. Urban areas grow up along roads. Urban areas grow up close to railways. Urban areas grow up from high to low elevations.

By using the dynamic statistical values such as mean and variance, it can help to control the impacts of the defined factors in the estimation of the urban expansion.

In the prediction of the urban expansion from 2020 to 2040, we found that the predicted urban areas look very low distribution. The dataset in the future can be changed or added.

Since our model relies on the defined factors, especially the distance from the multi-centers of the urban areas, the almost estimated urban areas grow up near the multi-centers of the urban area. However, In particular, some urban areas grow up far from the multi-centers of the urban areas. As a result,

our method cannot estimate the urban areas that grow up far from the multi-centers of the urban areas with an accuracy.

5.4 Remarks

This research introduced a methodology to model urban expansion based on the dynamic statistical model in Yangon, Myanmar. We defined that urban expansion is related to the seven factors of (1) the distance from the multi-centers of the urban areas, (2) the distance from the urban areas in the past, (3) the distance from roads, (4) the distance from railways, (5) and elevation, (6) the class translation, (7) the separated lands by the rivers.

We found that in Yangon, urban areas grow up close to the multi-centers of urban area, near the past urban area, close to the road, near the railway, and from high to low elevations.

In the experimental results, our method estimated urban areas from 1990 to 2020 with the averaged accuracy of 93% with the averaged TPR of 73% and the averaged TNR of 95%.

By using the dynamic statistical values such as mean and variance, it can help to control the impacts of the defined factors in the estimation of the urban expansion.

In the prediction of the urban expansion from 2020 to 2040, we found that the predicted urban areas look very low distribution. The dataset in the future can be changed or added.

Chapter6. Prediction urban expansion with consideration on flood and earthquake vulnerabilities

6.1 Reviews

For the disaster risk reduction, the disaster risk reduction can be expressed in term of reducing the terms of (1) hazard, (2) vulnerability and (3) value. In this research, we focus on the disaster risk reduction expressed in term of reducing the terms of vulnerability and value. The equation of the disaster risk assessment can be shown as the below equation.

$$\text{Disaster risk reduction} = \text{Reducing Vulnerability} * \text{Value} \quad (6.1)$$

In this research, we focus on urban areas escaping from the high disaster vulnerable areas as the disaster risk reduction in the term of reducing vulnerability and value. An urban area is the very important areas comparing with surrounding areas such as vegetation, forest, water since it has characteristics of the highest population density, various human built feature, and highest important human activities. When an urban area has the impact from the disaster, it might make a huge loss and might spread the impacts to the city or the country. As a result, we tried to allocate urban areas in the future on the low venerable areas or safe areas to reduce the losses causing by disasters.

In this research, the disaster risk reduction for urban expansion in the future can be expressed in term of urban areas growing up by escaping from high disaster vulnerable areas. Thus, the prediction of urban expansion can be calculated with the disaster vulnerability in order to provide the predicted urban areas escaping from the high vulnerable areas. The flowchart of our methodology to consider flood and earthquake vulnerability is depicted in Figure 6.1.

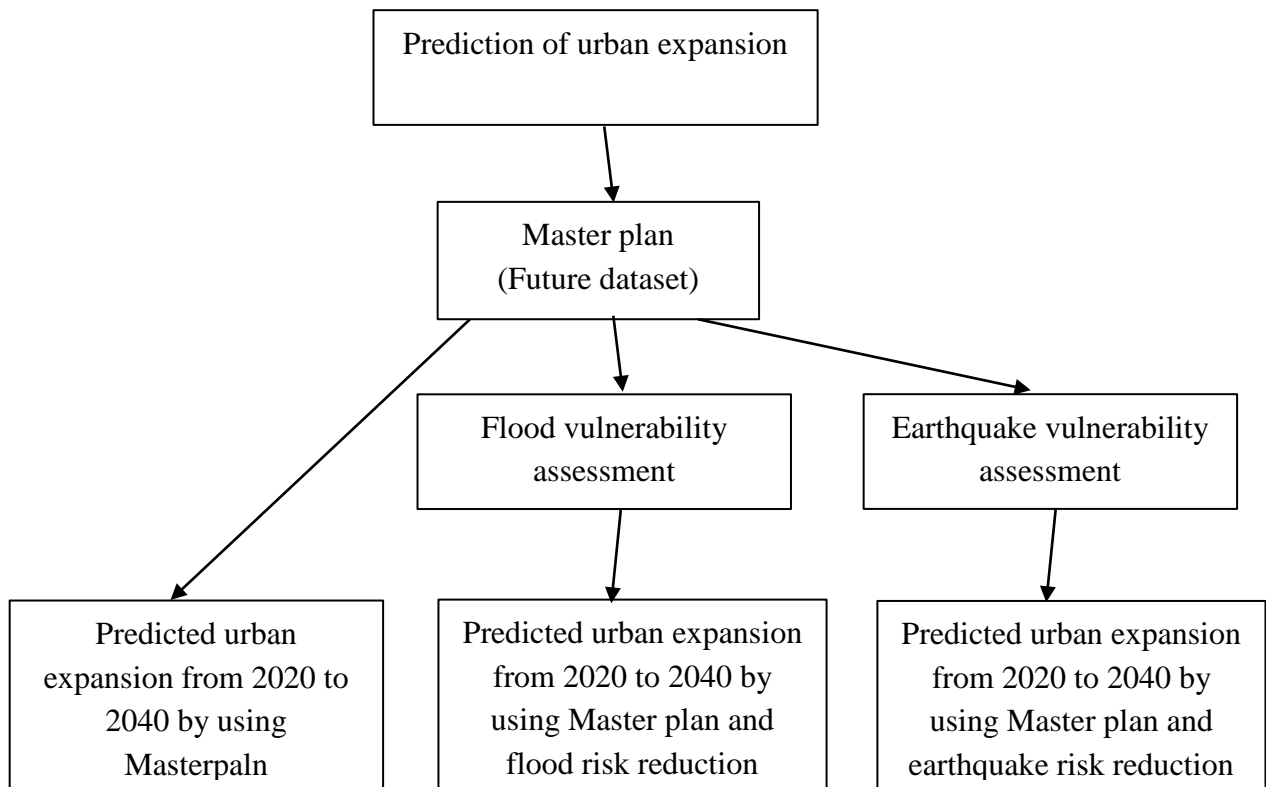


Figure 6.1 The flowchart of prediction of urban expansion considering on flood and earthquake vulnerabilities

6.2 Prediction of urban expansion with master plan

To get more reliability of the prediction of urban expansion in the future, the master plan can be used as the future dataset for the prediction model. The master plan for Yangon, Myanmar was analyzed in many aspects of urban growth by many experts and was provided by JICA Team (JICA, 2016). In the master plan, there are many features including the new town core, sub center, industrial, transportation, built-up areas in 2025, and built-up areas in 2040 (Figure 6.2).

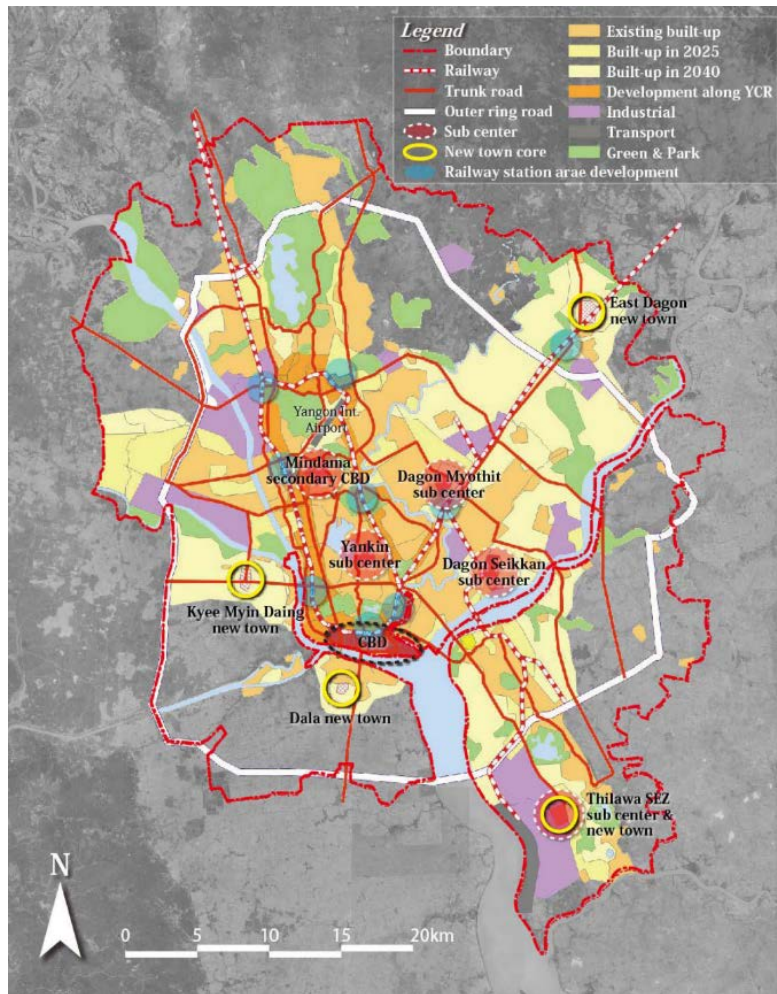


Figure 6.2 The master plan in Yangon, Myanmar by JICA Team, 2016

Those features can be used to extract new centers of urban areas, new roads and new railways as the dataset in the future for the prediction model. To get the more accuracy of the prediction of the urban expansion as much as possible, we used the land cover image in 2015 as the initial image with the urban expansion estimation to predict the urban expansion in 2020, 2030, and 2040. The predicted urban expansion images in 2020, 2030 and 2040 by using the master plan are shown in Figure 6.3 a, b, c, respectively.

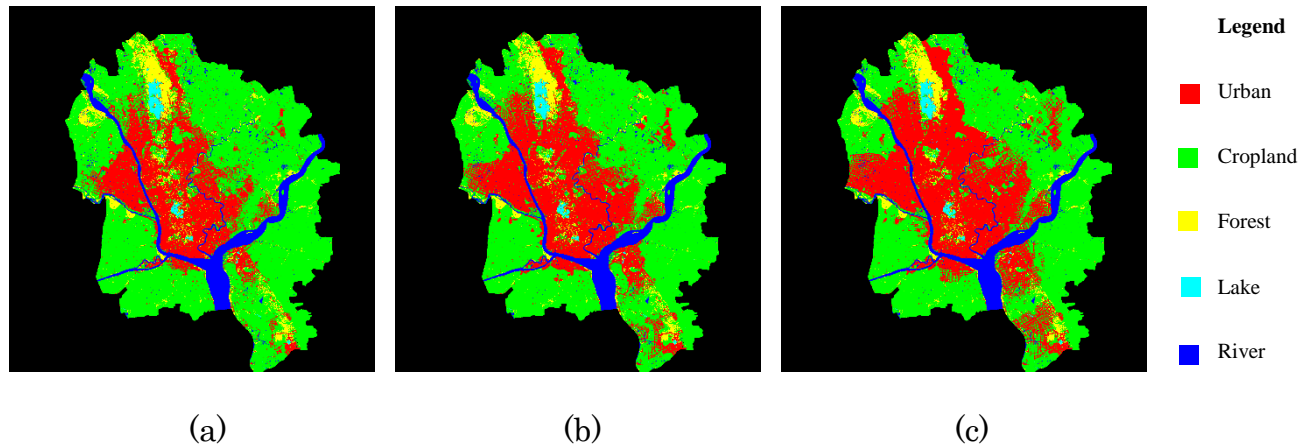


Figure 6.3 (a) Predicted land cover image in 2020 with the master plan, (b) Predicted land cover image in 2030 with the master plan, (c) Predicted land cover image in 2040 with the master plan.

By using the master plan with the prediction of the urban expansion, we can get the more reliability of the predicted urban expansion in the future. We found that resultant urban expansion in the future by using the master plan has more distribution than without using the master plan.

6.3 Prediction of urban expansion with consideration on flood vulnerability

In the prediction of urban expansion with considering flood vulnerability, we used the prediction of urban expansion with the master plan for the more reliability of the urban expansion in the future. In this research, the flood vulnerability map in Figure 2.2 was used as the one factor in the prediction model. By using the flood vulnerability map with the prediction of urban expansion, the predicted urban areas will try to escape from the high vulnerable areas. The predicted urban expansion images in 2020, 2030 and 2040 by using the master plan with the flood vulnerability map are shown in Figure 6.4 a, b, c, respectively.

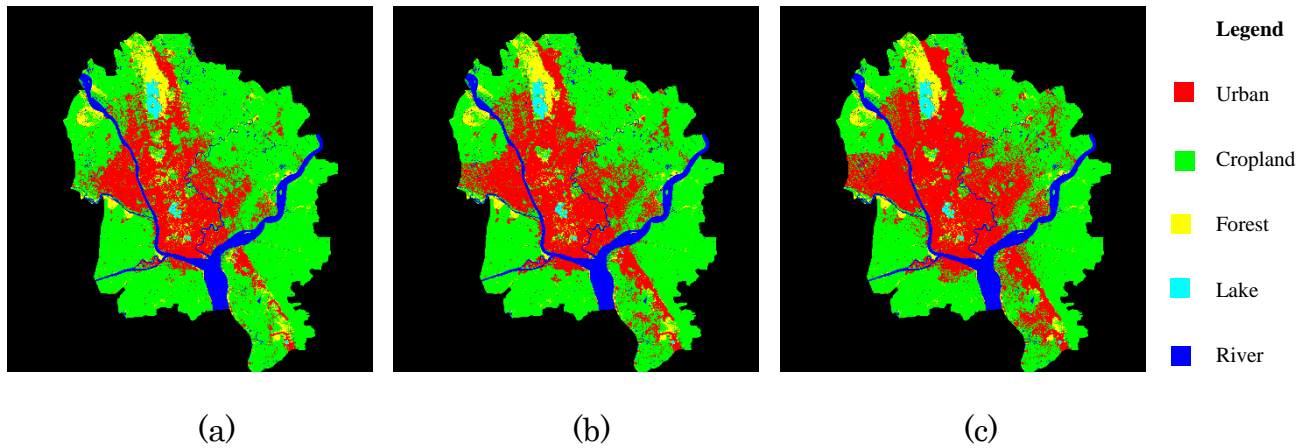


Figure 6.4 (a) Predicted land cover image in 2020 with the master plan and flood vulnerability map, (b) Predicted land cover image in 2030 with the master plan and flood vulnerability map, (c) Predicted land cover image in 2040 with the master plan and flood vulnerability map.

To evaluate the results of the predicted urban areas between using master plan, and using master plan and flood risk reduction, we used the total flood loss in term of the area. We defined that the total flood loss in term of the area as the below.

$$\text{Total_FLA}_{LC}(t) = \sum [LC(i, j, t) \times FVI(i, j)] \quad (6.2)$$

Where $\text{Total_FLA}_{LC}(t)$ = Total flood loss in term of the area at time t , $LC(i, j, t)$ = Land cover at pixel (i, j) at time t (urban, cropland, forest), $FVI(i, j)$ = Flood vulnerability index at pixel (i, j) .

The statistics of total flood loss in term of the area on urban, cropland, forest between using master plan, and using master plan and flood risk reduction in Yangon from 2020 to 2040 are described in Table 6.1.

Table 6.1 The total flood losses in term of the area between using master plan, and using master plan and flood risk reduction in Yangon from 2020 to 2040 (km²)

Using master plan			
	2020	2030	2040
Urban	231.18	297.15	364.77
Cropland	784.23	723.23	659.23
Forest	50.21	45.25	41.62
Using master plan and flood risk reduction			
	2020	2030	2040
Urban	222.39	280.53	346.56
Cropland	793.71	742.10	680.21
Forest	49.53	42.99	38.85

The comparing graphs of total flood loss in term of the area on urban between using master plan, and using master plan and flood risk reduction in Yangon from 2020 to 2040 are shown in Figure 6.5.

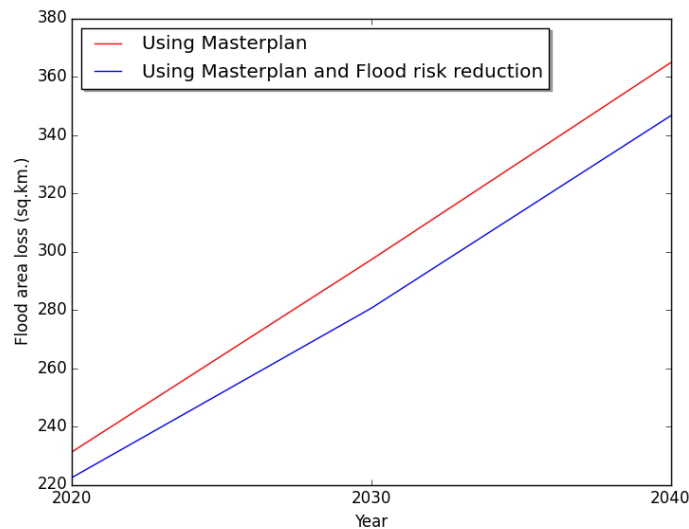


Figure 6.5 Comparing total flood loss in term of the area on urban between using master plan, and using master plan and flood risk reduction in Yangon from 2020 to 2040.

According to Table 6.1, we investigated that the total flood loss in term of the area on cropland is the highest. By considering from 202 to 2040, the total flood loss in term of the area on urban has increased since the urban

areas have grown up, but the total flood loss in term of the area on cropland has decreased because the cropland areas have shrunk, whereas the total flood loss in term of area on forest looks stable.

We found that by using the master plan with the prediction, some of the predicted urban areas are still located on the high vulnerable areas. By using master plan and flood vulnerability map with the prediction, the predicted urban areas can escape from the high vulnerable areas effectively. The statistics of the total flood loss in term of the area on urban (Figure 6.5) confirmed that the values of total flood losses in term of the area on urban from 2020 to 2040 by integrating with flood risk reduction are less than without using flood risk reduction around 3.80% for 2020, 5.60% for 2030, and 5.00% for 2040.

However, we investigated that the decreasing values of the flood area losses by using flood risk reduction and without using flood risk reduction is not so high with the different values of 3.80-5.60% since the master plan has included the consideration of flood risk.

6.4 Prediction of urban expansion with consideration on earthquake vulnerability

In the prediction of urban expansion with considering earthquake vulnerability, we also used the prediction of urban expansion with the master plan for the more reliability of the urban expansion in the future. In this research, the ground shaking map in term of PGA with the earthquake probabilities of 2% (Figure 3.4 a) was applied as the earthquake vulnerability map with the range from 0.0 (the lowest earthquake vulnerability) to 1.0 (the highest earthquake vulnerability) by using the linear transformation. The earthquake vulnerability map was used as the one factor in the prediction model. By using the earthquake vulnerability map with the prediction of urban expansion, the predicted urban areas will try to escape from the high earthquake-vulnerable areas. The predicted urban expansion images in 2020, 2030 and 2040 by using the master plan with the earthquake vulnerability map are shown in Figure 6.6 a, b, c, respectively.

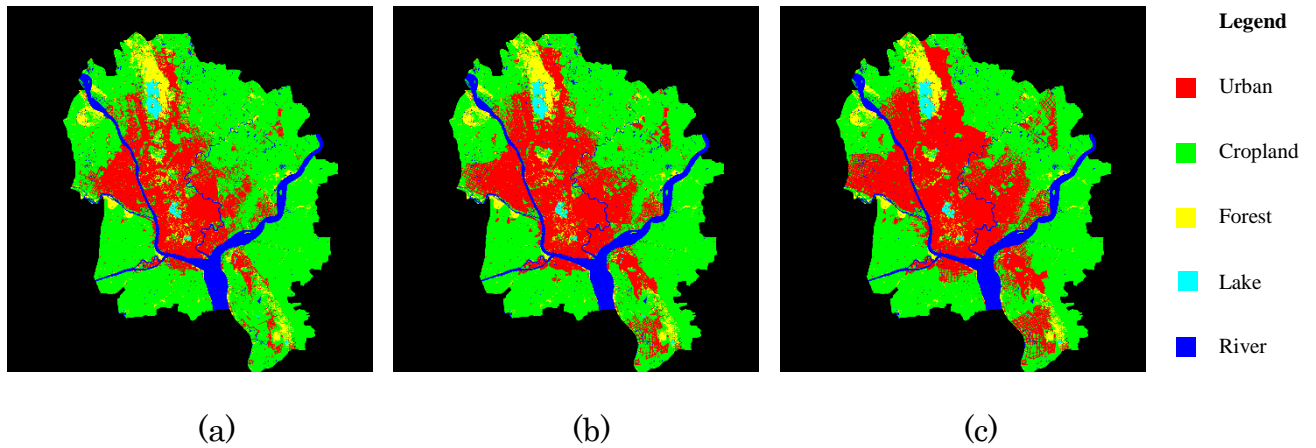


Figure 6.6 (a) Predicted land cover image in 2020 with the master plan and earthquake vulnerability map, (b) Predicted land cover image in 2030 with the master plan and earthquake vulnerability map, (c) Predicted land cover image in 2040 with the master plan and earthquake vulnerability map

To evaluate the results of the predicted urban areas between using master plan, and using master plan and earthquake risk reduction, we used the total earthquake loss in term of area. We defined that the total earthquake loss in term of area as the below equation.

$$\text{Total_ELA}_{LC}(t) = \sum [LC(i, j, t) \times EVI(i, j)] \quad (6.3)$$

Where $\text{Total_ELA}_{LC}(t)$ = Total earthquake loss in term of area at time t, $LC(i, j, t)$ = Land cover at pixel (i,j) at time t (urban, cropland, forest), $EVI(i, j)$ = Earthquake vulnerability index at pixel (i,j).

The statistics of the total earthquake loss in term of the area on urban, cropland, forest between using master plan, and using master plan and earthquake risk reduction in Yangon from 2020 to 2040 are depicted as in Table 6.2.

Table 6.2 The total earthquake losses in term of the area between using master plan, and using master plan and earthquake risk reduction in Yangon from 2020 to 2040 (km²).

Using master plan			
	2020	2030	2040
Urban	62.89	85.32	111.58
Cropland	347.23	326.32	301.23
Forest	16.80	15.28	14.12
Using master plan and earthquake risk reduction			
	2020	2030	2040
Urban	59.73	81.67	106.18
Cropland	349.29	328.99	305.64
Forest	17.90	16.26	15.10

The comparing graphs of total earthquake loss in term of the area on urban areas between using master plan, and using master plan and earthquake risk reduction in Yangon from 2020 to 2040 are shown in Figure 6.7.

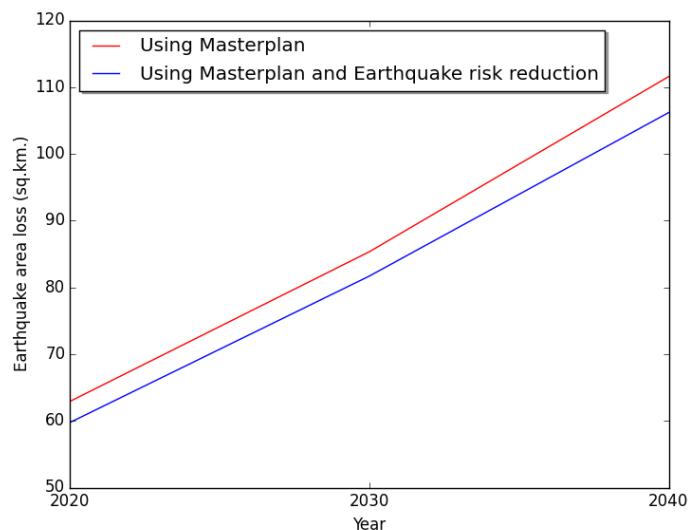


Figure 6.7 Comparing total earthquake loss in term of the area on urban between using master plan, and using master plan and earthquake risk reduction in Yangon from 2020 to 2040.

According to Table 6.2, we found that the total earthquake loss in term of the area on cropland is the highest. By considering with time variation from

2020 to 2040, the total earthquake loss in term of the area in urban areas has increased, but the total earthquake loss in term of the area on cropland areas has decreased, whereas the total earthquake loss in term of the area on forest looks stable.

We found that by using the master plan with the prediction, some of the predicted urban areas are still located on the high vulnerable areas. By using master plan and earthquake vulnerability map with the prediction, the predicted urban areas can escape from the high vulnerable areas effectively. The graphs of the total earthquake loss in term of the area (Figure 6.7) confirmed that the values of total earthquake losses in term of the area from 2020 to 2040 by using earthquake risk reduction are less than without using earthquake risk reduction. The decreasing values of earthquake losses in term of the area by using earthquake risk reduction and without using earthquake risk reduction is not so high with the different values of 5.02% for 2020, 4.28% for 2030, and 4.84% for 2040.

6.5 Remarks

By using the master plan with the prediction of urban expansion, the predicted urban expansion is more reliability since the master plan can provide many features including the new town core, sub center, industrial, transportation, built-up areas in 2025, and built-up areas in 2040 and we can use them as the future dataset.

We found that the predicted urban expansion by using the master plan has more distribution than without the master plan. Unfortunately, by using the master plan, we found that some of predicted urban areas are located on the high venerable areas. By integrating flood and earthquake risk reductions with the prediction of urban expansion, the predicted urban areas can escape from the high flood and earthquake vulnerable areas effectively. By comparing the total flood and earthquake losses in term of an area between master plan and flood and earthquake risk reductions, it confirmed that the values of total flood and earthquake area losses on the urban area by using flood and earthquake risk reduction are less than by using with only master plan.

By using the different features with the prediction model, multi-scenarios of predicted urban areas can be available to support for decision-making or policy for reducing disaster risk.

Chapter7. Assessments of flood and earthquake risks interm of economic loss

7.1 Reviews

For the disaster risk assessment, the disaster risk assessment can be expressed in term of (1) hazard, (2) vulnerability and (3) value (Kron, 2005). The equation of the disaster risk assessment can be shown as below.

$$\text{Disaster risk reduction} = \text{Hazard} * \text{Vulnerability} * \text{Value} \quad (7.1)$$

In this research, we focused on the assessment of disaster risk in term of economic loss relating to GRDP. The economic loss means changes in wealth caused by damage to structures or other physical assets. There is a direct loss (those resulting from building and infrastructure damage) and an indirect loss (those that follow on from physical damage). These can be reflected in market effects such as loss of income owing to disaster-caused destruction, and non-market effects such as loss of leisure time, longer commutes (Ahmad, 2015). According to the chapter 7, we had the land cover images from 2020 to 2040 with the multiple-scenarios with (1) using master plan (2) using master plan and flood risk reduction, and (3) using master plan and earthquake risk reduction. Then, we converted the predicted land cover images from 2020 to 2040 into land price areas from 2020 to 2040 by using land price estimation (in chapter 4). Next, we transformed land price areas from 2020 to 2040 into economic areas in term of GRDP from 2020 to 2040 by using the prediction of economic growth. Finally, we calculated the assessment of flood and earthquake risks in term of economic loss relating to GRDP from 2020 to 2040 by integrating the economic areas relating to GRDP from 2020 to 2040, and flood and earthquake vulnerabilities. The flowchart of the methodology to calculate flood and earthquake risks in term of economic loss relating to GRDP is depicted in Figure 7.1

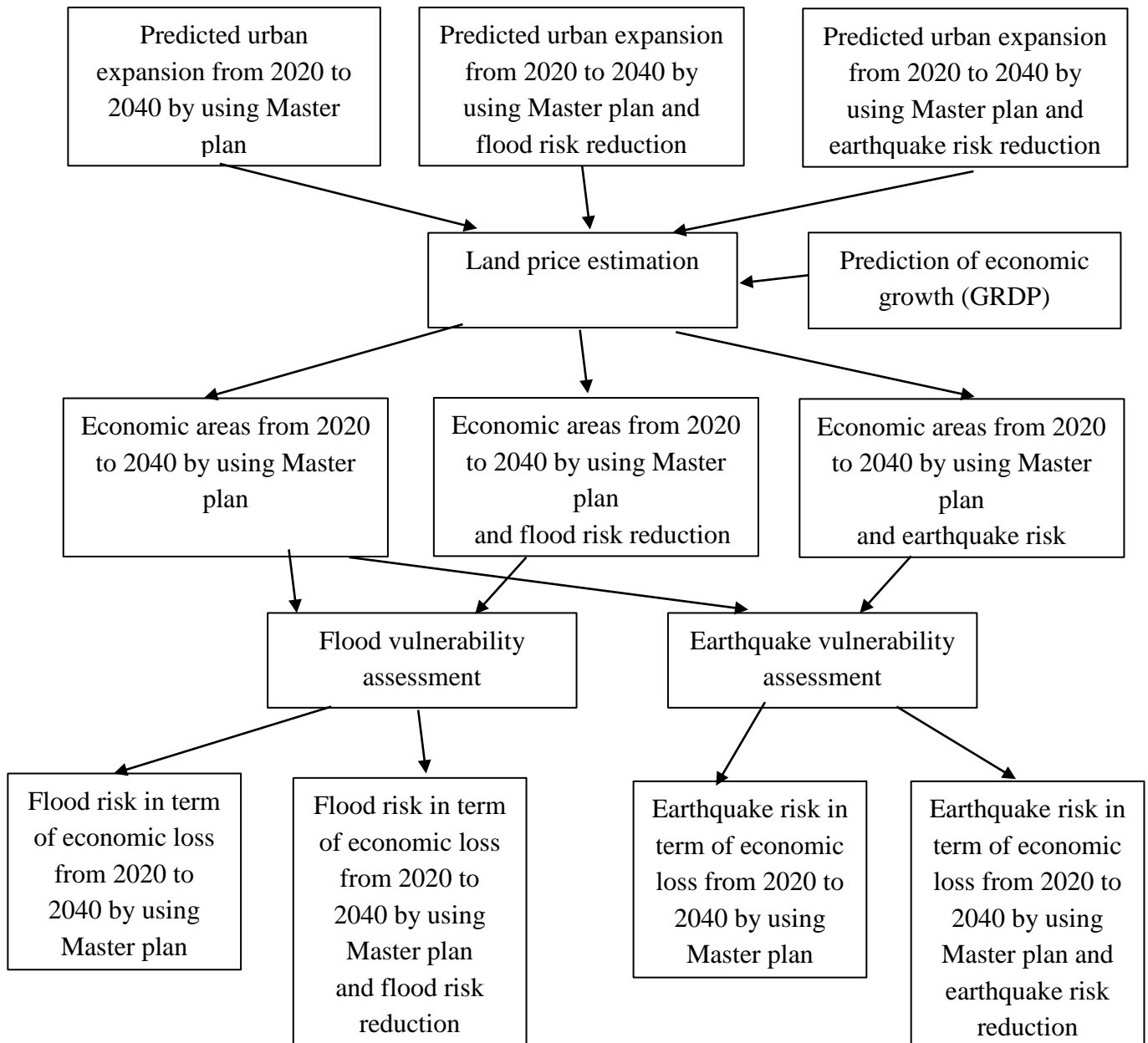


Figure 7.1 The flowchart of assessments of flood and earthquake risks in term of economic loss relating to GRDP

7.2 Converting land cover areas into economic areas

According to the chapter 7, we had the predicted land cover images with the multiple-scenarios with (1) using master plan (2) using master plan and flood risk reduction, and (3) using master plan and earthquake risk reduction from 2020 to 2040. Then, we converted the predicted land cover images from 2020 to 2040 into land price areas from 2020 to 2040 by using land price estimation (in chapter 4).

Next, we transformed land price areas from 2020 to 2040 into economic areas in terms of GRDP from 2020 to 2040 by using the prediction of economic growth. A land price has a high relationship to economic value (Nichols, 1970; Deaton, 2001). The economic value has characteristics of the dynamic value in the different time. Therefore, in this research, we employed the prediction of economic growth relating to GRDP by JICA Team (JICA, 2013) with land price areas to estimate economic value areas. The prediction of economic growth was projected as a middle case. The GRDP and GRDP per capita in Yangon would be accomplished in 2035, and after 2036 the growth rate will slow down by half of past rate. Table 7.1 shows the prediction economic growth in terms of GRDP.

Table 7.1 The prediction of economic growth relating to GRDP by JICA (US dollars)

	2020	2030	2040
Total GRDP	27,576 million	69,354 million	122,330 million
GRDP per capita	3,928	7,643	10,429

The equation to convert land price areas into economic areas was expressed in the below equation.

$$EC(i, j, t) = \frac{LPI(i, j, t)}{\sum LPI(i, j, t)} \times Total_GRDP(t) \quad (7.2)$$

Where $EC(i,j,t)$ = economic value at pixels located (i,j) at time t . $LPI(i,j,t)$ = land price index at pixels located (i,j) at time t , $Total_GRDP(t)$ = Total of Gross regional product at time t .

The estimated economic areas relating to GRDP from 2020 to 2040 are shown with the multiple scenarios with (1) using master plan in Figure 7.2, (2) using master plan and flood risk reduction in Figure 7.3, and (3) using master plan and earthquake risk reduction in Figure 7.4.

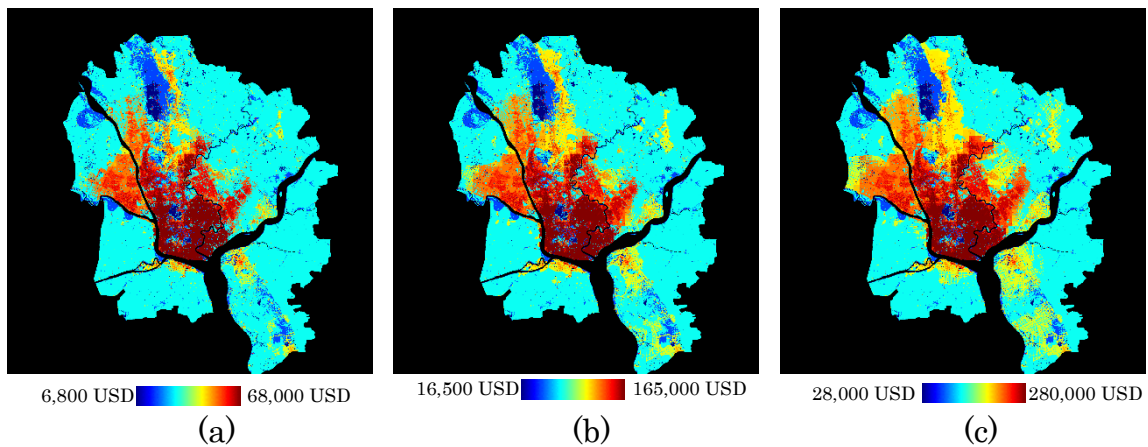


Figure 7.2 (a) economic area image in 2020, (b) economic area image in 2030
(c) economic area image in 2040 using the master plan

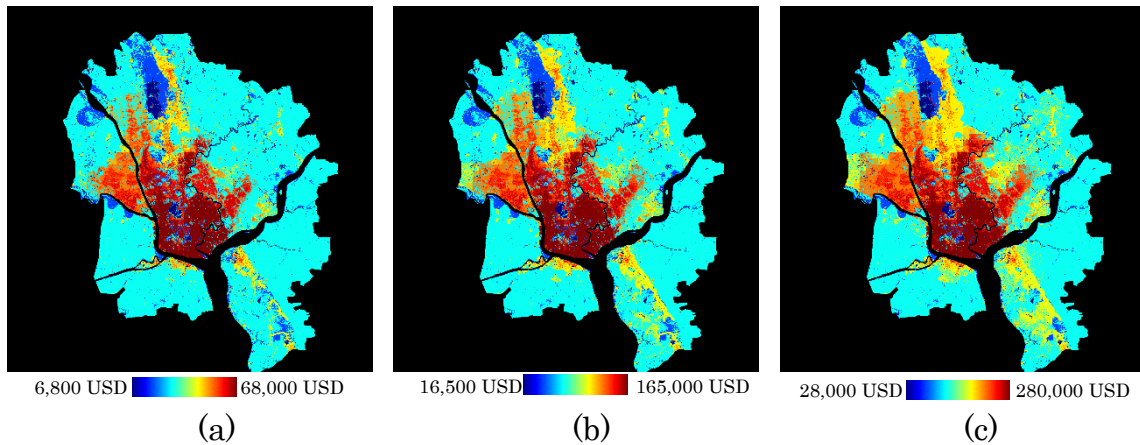


Figure 7.3 (a) economic area image in 2020, (b) economic area image in 2030
(c) economic area image in 2040 using the master plan and flood risk reduction

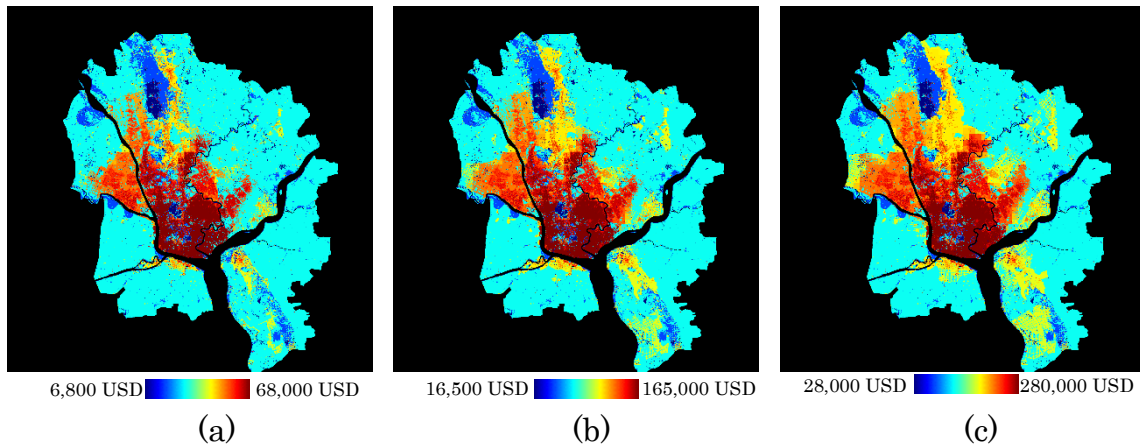


Figure 7.4 (a) economic area image in 2020, (b) economic area image in 2030 (c) economic area image in 2040 using the master plan and earthquake risk reduction

We compared the predicted economic areas from 2020 to 2040 between (1) using master plan, and (2) using master plan and flood risk reduction (Figure 7.2 and 7.3) with the flood vulnerable areas (Figure 2.2). Then, we found that the high economic value areas from 2020 to 2040 with using flood risk reduction are located on low flood vulnerable areas (safe areas) more than without using flood risk reduction.

We compared the predicted economic areas from 2020 to 2040 between (1) using master plan, and (2) using master plan and earthquake risk reduction (Figure 7.2 and 7.4) with the earthquake vulnerable areas (Figure 3.4 a). We investigated that the high economic value areas from 2020 to 2040 with using earthquake risk reduction are located on low earthquake vulnerable areas (safe areas) more than without using earthquake risk reduction.

7.3 Calculating flood and earthquake risks in term of economic loss relating to GRDP

According to equation 1, the disaster risk assessment is expressed in term of (1) hazard, (2) vulnerability and (3) value. In this research, we focused on the disaster risk assessment in term of economic loss relating to GRDP. As the work of Kron (, 2005), the disaster risk assessment can be expressed in term

of hazard, vulnerability and value. In this research, the disaster risk assessment in term of economic loss relating to GRDP is needed to calculate with three terms of hazard, vulnerability, and economic value. In term of economic value, we employed the estimated economic areas relating to GRDP as the economic value. In term of vulnerability, we used the results of flood and earthquake vulnerability assessments as the flood and earthquake vulnerabilities, respectively. In term of hazard, we applied Lloyd's City Risk Index as the hazard impacts of flood and earthquake in Yangon. Lloyd's City Risk Index is the index that indicates the potential impact on the economic output in term of GDP of 301 of the world's major cities from 18 manmade and natural threats. The risk index is based on original research by the Cambridge Centre for Risk Studies at the University of Cambridge Judge Business School. The Index shows how governments, businesses, and communities are highly exposed to systemic, catastrophic shocks and could do more to mitigate risk and improve resilience (lloyds.com, 2017).

The equation to calculate the total flood loss in term of economic relating to GRDP was defined and is expressed as below.

$$\text{Total_FLE}(t) = C_{\text{flood}} \sum [EC(i, j, t) \times FVI(i, j)] \quad (7.3)$$

Where Total_FLE(t) is Total flood loss in term of economic at time t, EC(i,j,t) = economic value at pixels located (i,j) at time t., FVI(i,j,t) = flood vulnerability index at pixels located (i,j), C_{flood} = the flood impact to economic value (3.49% for the flood impact in Yangon City).

The equation to calculate to compute the total earth risk loss in term of economic relating to GRDP was defined and is described by the below equation.

$$\text{Total_ELE}(t) = C_{\text{earthquake}} \sum [EC(i, j, t) \times EVI(i, j)] \quad (7.4)$$

Where Total_ELE(t) is Total earthquake loss in term of economic at time t, EC(i,j,t) = economic value at pixels located (i,j) at time t., EVI(i,j) = earthquake vulnerability index at pixels located (i,j), $C_{\text{earthquake}}$ = the earthquake impact to economic value (15.59% for the earthquake impact in Yangon City).

7.4 Results of flood and earthquake risks in term of economic loss relating to GRDP

7.4.1 Results of flood risk in term of economic loss relating to GRDP

We had the economic area images with the multiple-scenarios with (1) using master plan (2) using master plan and flood risk reduction, and (3) using master plan and earthquake risk reduction from 2020 to 2040. By relating to flood vulnerability assessment, the total flood losses in term of economic relating to GRDP with two scenarios with (1) using master plan and (2) using master plan and flood risk reduction in Yangon from 2020 to 2040 were computed and are shown in Figure 7.5 and Table 7.2.

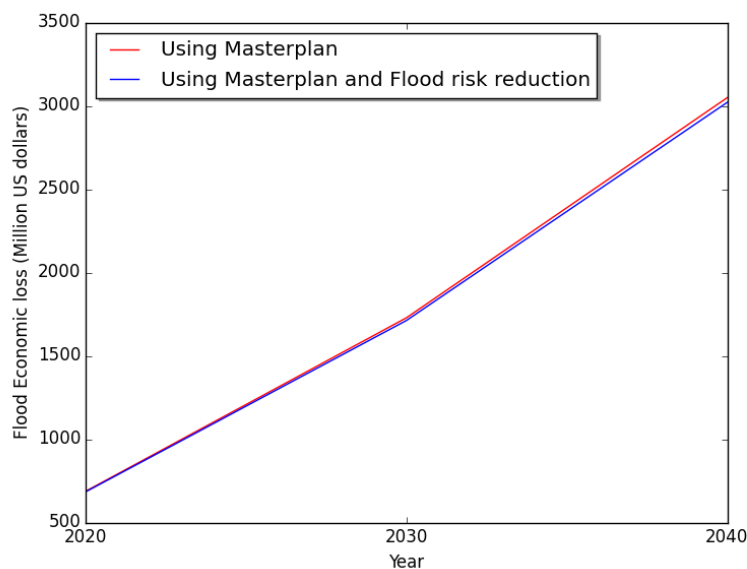


Figure 7.5 Comparing total flood losses in term of economic relating to GRDP between (1) using master plan and (2) using master plan and flood risk reduction in Yangon from 2020 to 2040 (Million US dollars)

Table 7.2 The statistics of total flood losses in term of economic relating to GRDP between (1) using master plan and (2) using master plan and flood risk reduction in Yangon from 2020 to 2040 (Million US dollars)

	2020	2030	2040
Master plan	687	1,728	3,049
Master plan and Flood risk reduction	683	1,712	3,021

According to Figure 7.5 and Table 7.2, the total flood losses in term of economic are 687 million US dollars for 2020, 1728 million US dollars for 2030, and 3,049 million US dollars for 2040. By integrating with flood risk reduction, the total flood losses in term of economic can be reduced by 4 to 28 million US dollars (4 million US dollars in 2020, 16 million US dollars in 2030, and 28 million US dollars in 2040).

Additionally, we calculated the statistics of total flood loss in term of economic relating to GRDP at the town ship scale. The statistics of total flood loss in term of economic relating to GRDP from 2020 to 2040 at the town ship scale by using master plan is shown in Figure 7.6 and by using master plan and flood risk reduction is shown in Figure 7.7. The spatial information of total flood loss in term of economic by using master plan in 2040 at the town ship scale is depicted in Figure 7.8.

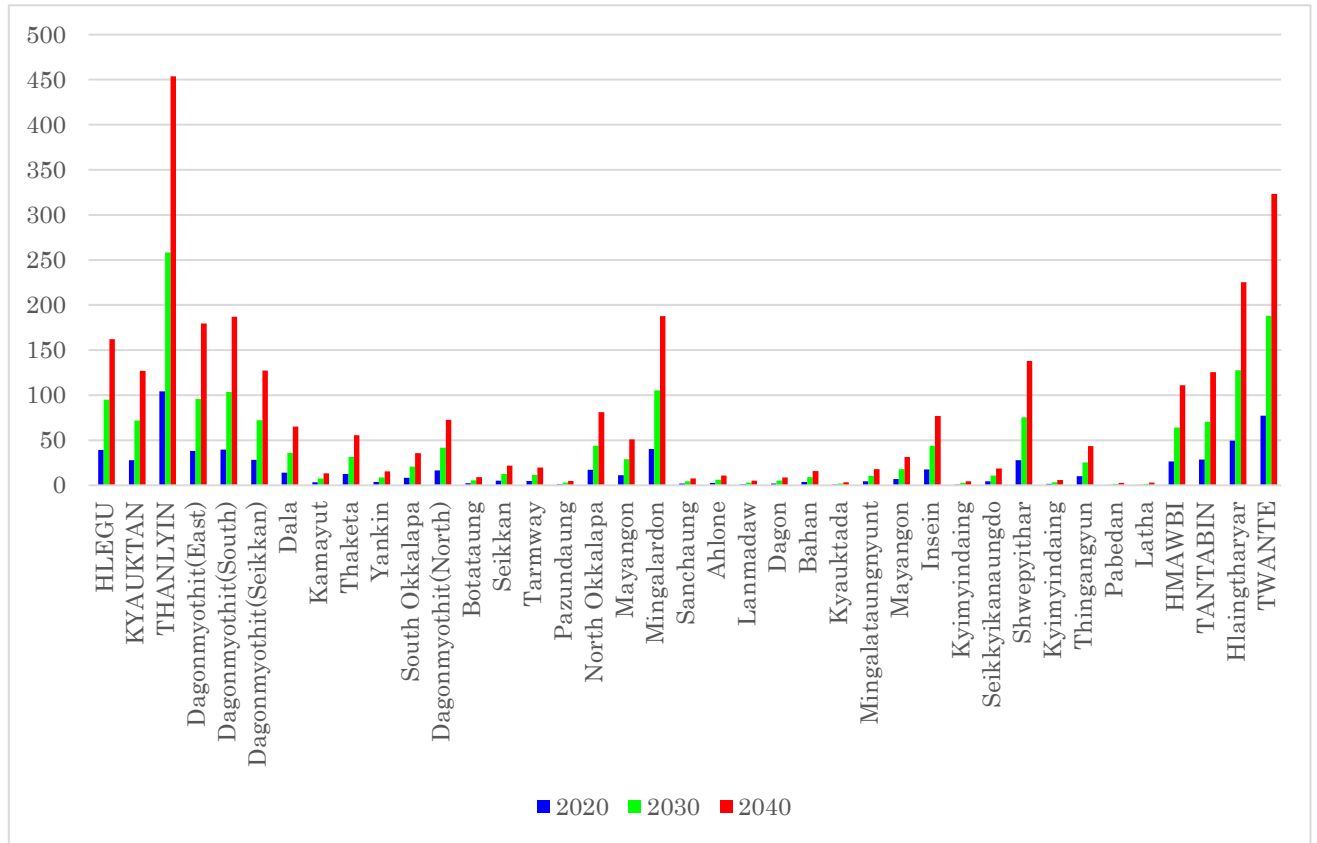


Figure 7.6 Total flood loss in term of economic relating to GRDP in Yangon from 2020 to 2040 by using master plan at the township scale (Million US dollars)

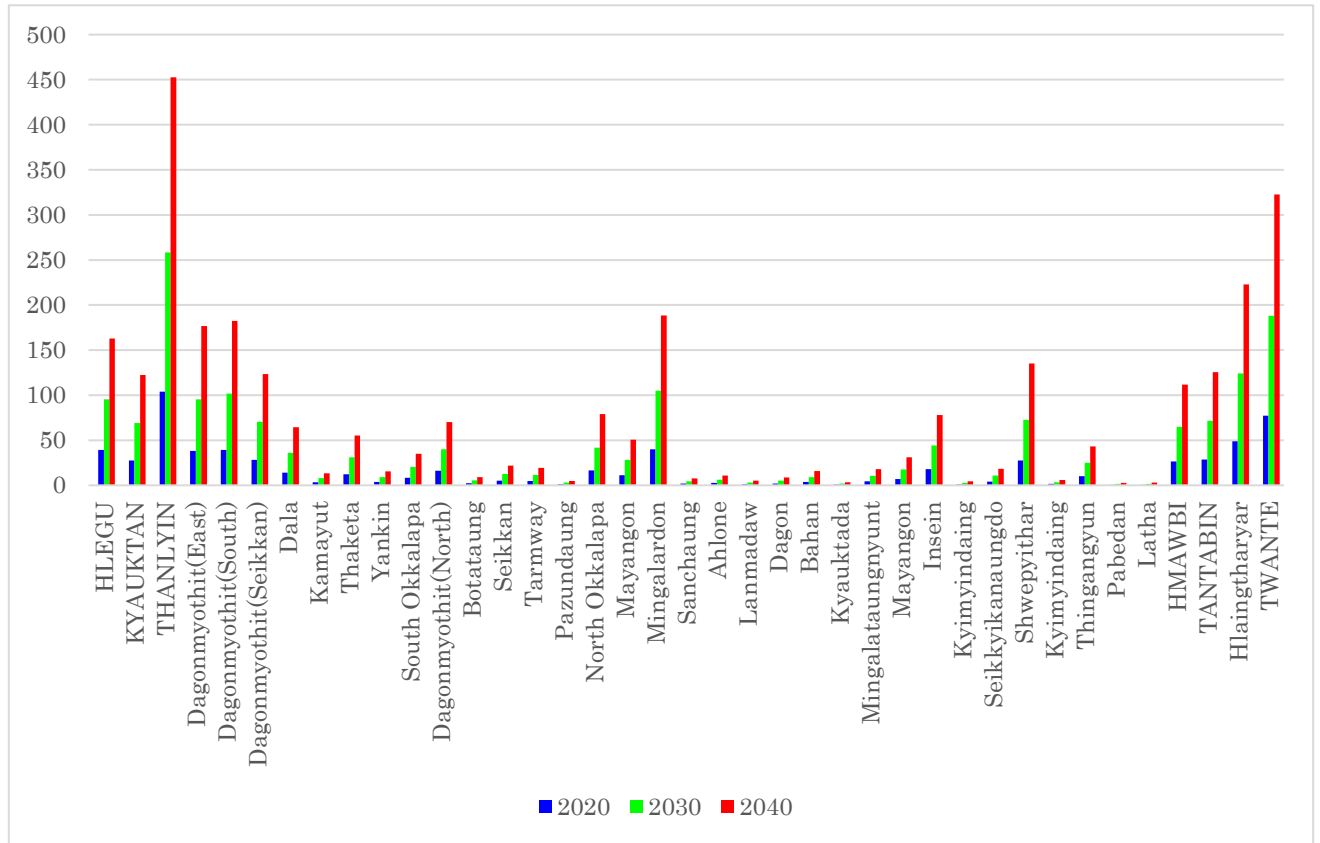


Figure 7.7 Total flood loss in term of economic relating to GRDP in Yangon from 2020 to 2040 by using master plan and flood risk reduction at the township scale (Million US dollars)

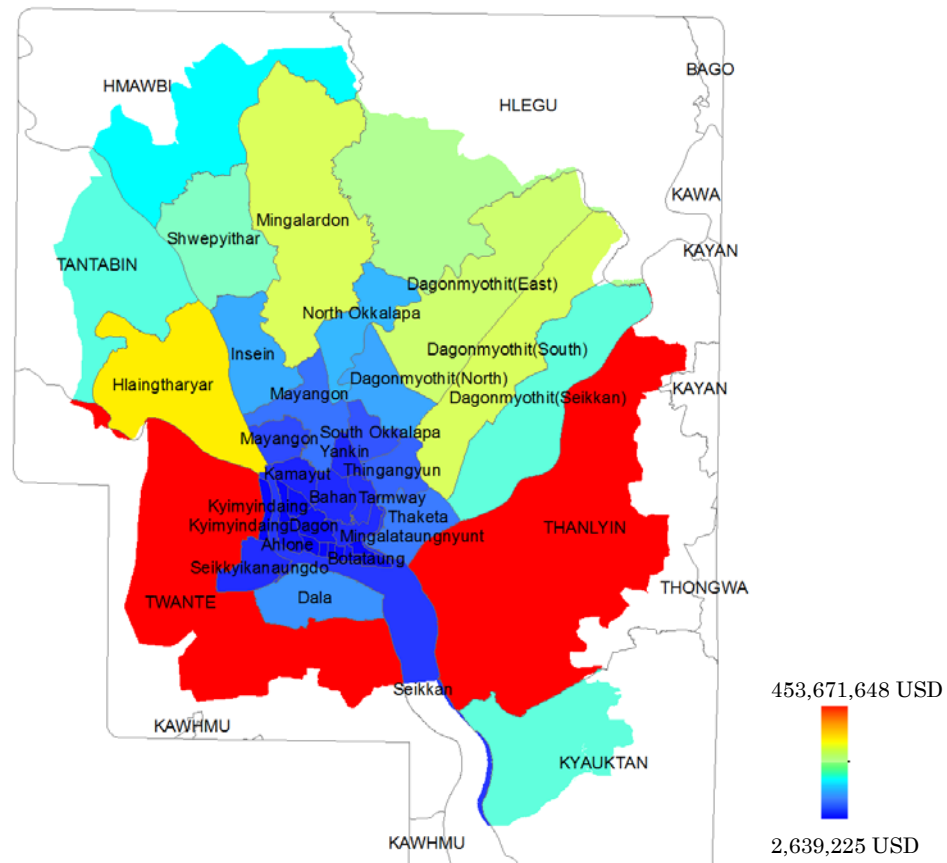


Figure 7.8 Total flood loss in term of economic relating to GRDP in Yangon in 2040 by using master plan at the township scale (US dollars)

According to Figure 7.6, 7.7 and 7.8, considering at the township, the five highest flood economic losses are Thanlyin, Twante, Haingtharyar, Mingalardon, Dagonmyothit (South). The five highest flood economic loss townships are mostly located on the low elevations.

7.4.2 Results of earthquake risk in term of economic loss relating to GRDP

For the earthquake vulnerability index, we assumed that the earthquake building vulnerability index as the earthquake vulnerability index with the range from 0.0 (the lowest vulnerability index) to 1.0 (the highest vulnerability index). We have four cases of (1) the probability of 10% and RC 2500psi, (2) the probability of 10% and RC 1250psi, (3) the probability of 2% and RC 2500psi, (4) the probability of 2% and RC 1250psi. By computing the

earthquake building vulnerability indexes with the four cases from the predict urban areas from 2020 to 2040 with (1) master plan (2) earthquake risk reduction, we have the earthquake vulnerability indexes from 2020 to 2040 with master plan and earthquake risk reduction with the four cases. Figure 7.9, 7.10, 7.11 and 7.12 show the earthquake vulnerability indexes from 2020 to 2040 with master plan and earthquake risk reduction with the four cases.

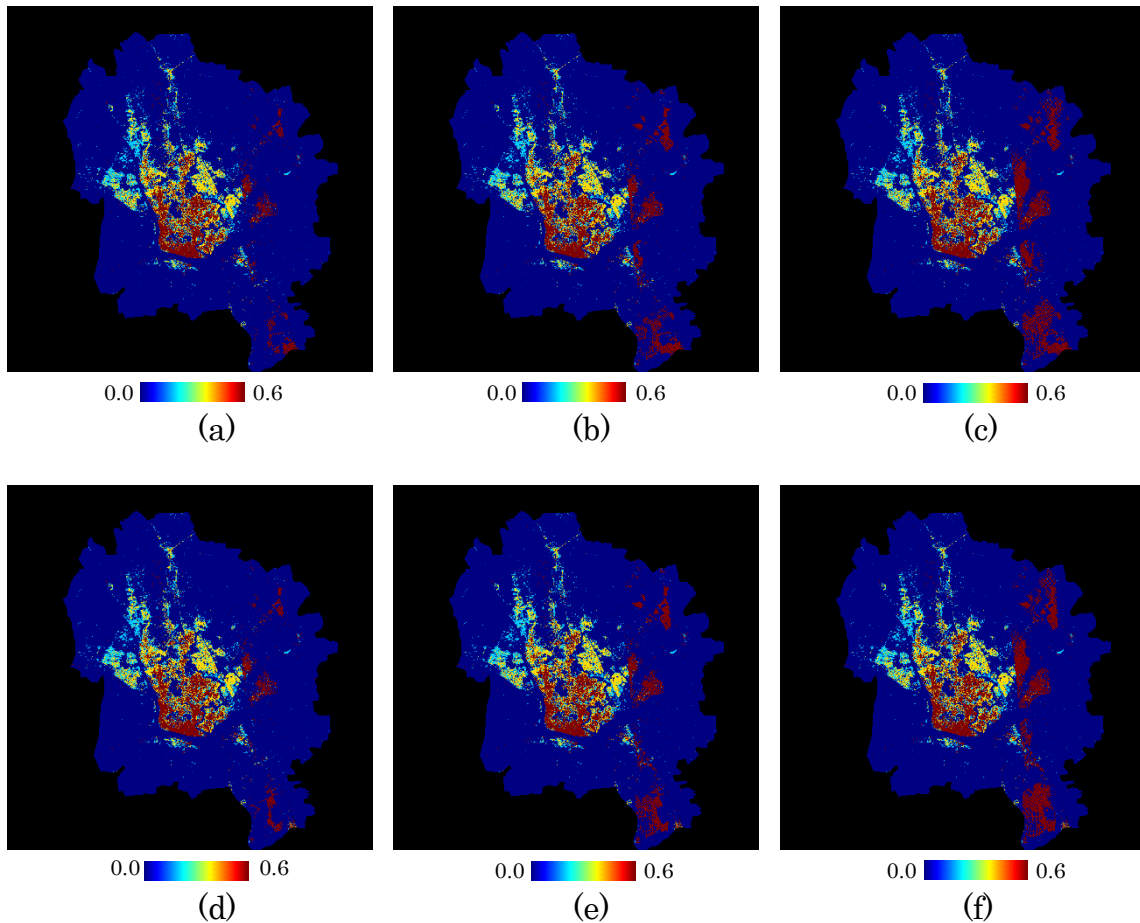


Figure 7.9 The earthquake building vulnerability indexes with master plan (a), (b), (c) in 2020, 2030, and 2040 and with earthquake risk reduction (d), (e), (f) in 2020, 2030, and 2040 with the probability of 10% and RC 2500psi

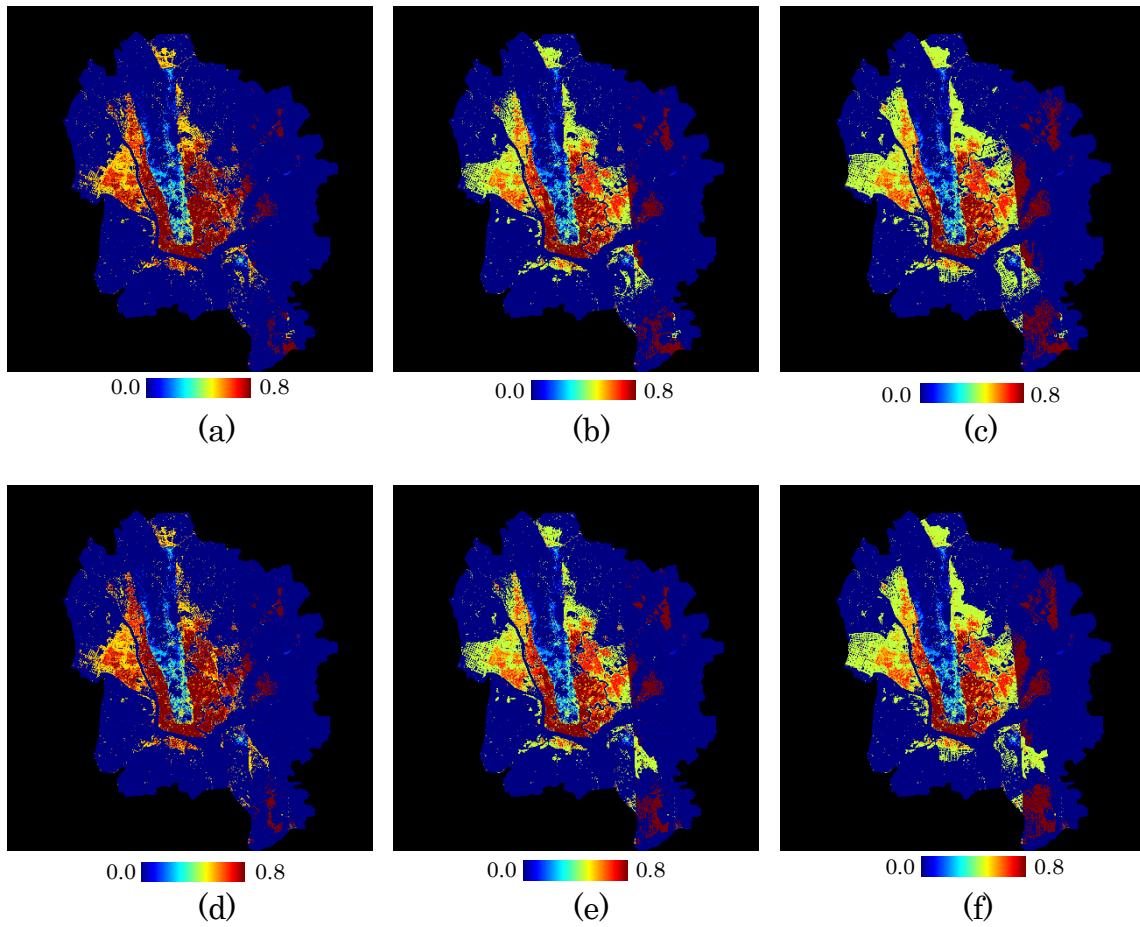


Figure 7.10 The earthquake building vulnerability indexes with master plan (a), (b), (c) in 2020, 2030, and 2040 and with earthquake risk reduction (d), (e), (f) in 2020, 2030, and 2040 with the probability of 10% and RC 1250psi

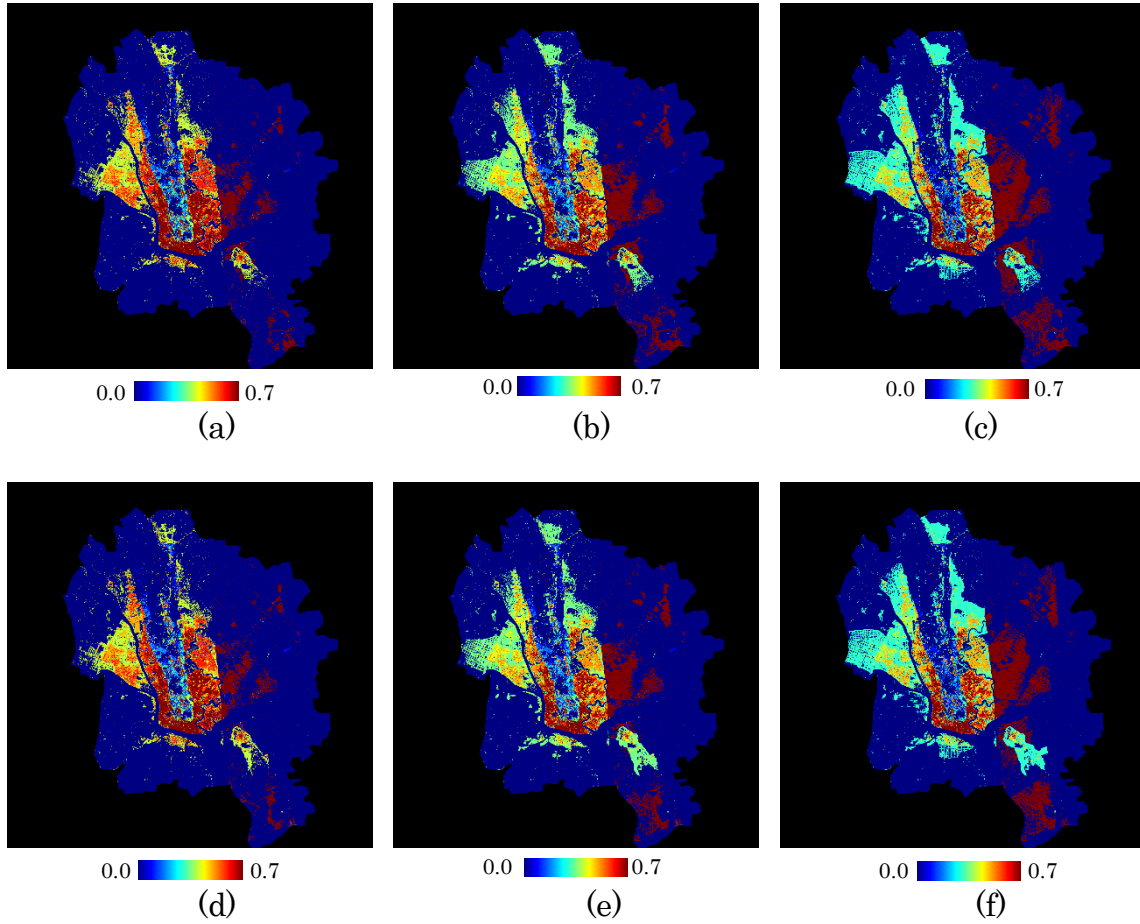


Figure 7.11 The earthquake building vulnerability indexes with master plan (a), (b), (c) in 2020, 2030, and 2040 and with earthquake risk reduction (d), (e), (f) in 2020, 2030, and 2040 with the probability of 2% and RC 2500psi

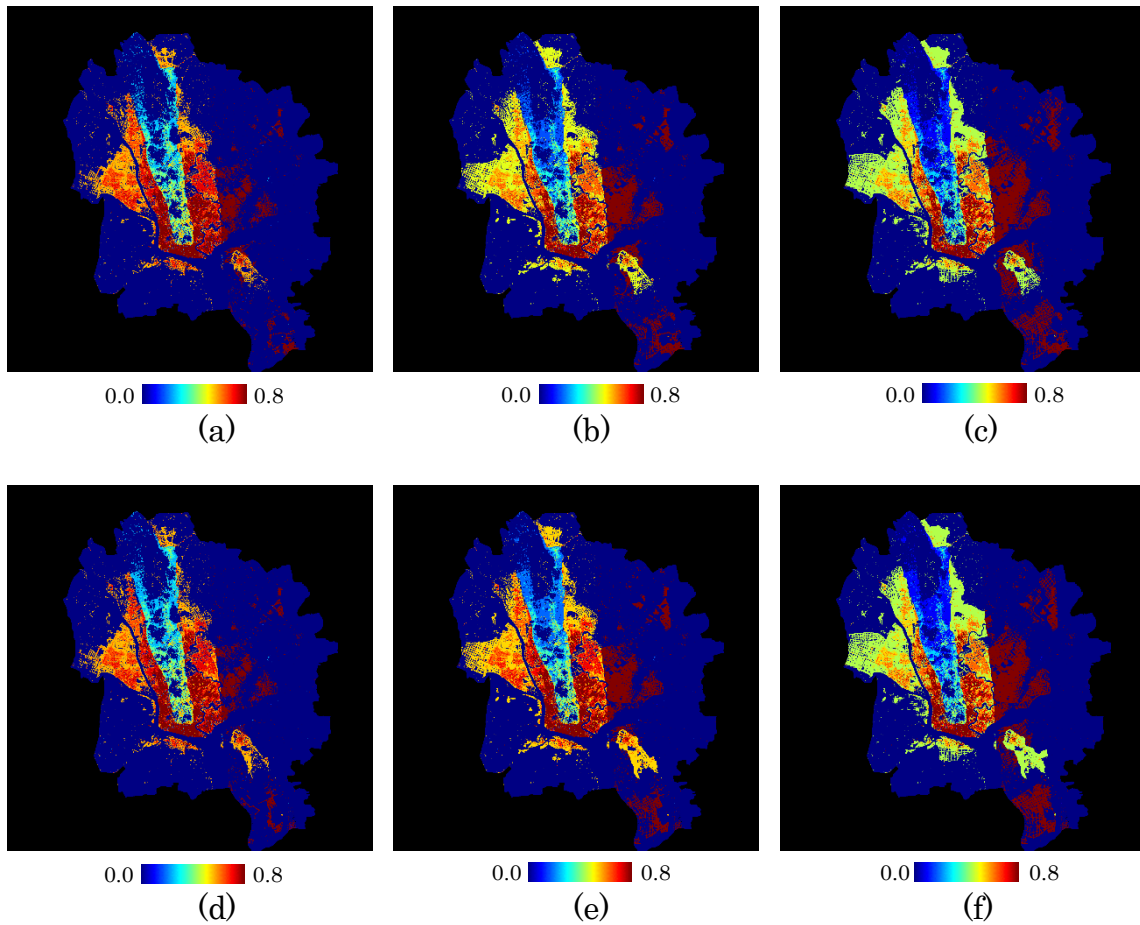


Figure 7.12 The earthquake building vulnerability indexes with master plan (a), (b), (c) in 2020, 2030, and 2040 and with earthquake risk reduction (d), (e), (f) in 2020, 2030, and 2040 with the probability of 2% and RC 1250psi

By relating to earthquake vulnerability indexes with four cases, the total earthquake losses in term of economic relating to GRDP from 2020 to 2040 with (1) using master plan and (2) using master plan and earthquake risk reduction with four cases were calculated and are shown in Figure 7.13, 7.14, 7.15 and 7.16 and Table 7.3, 7.4, 7.5, and 7.6.

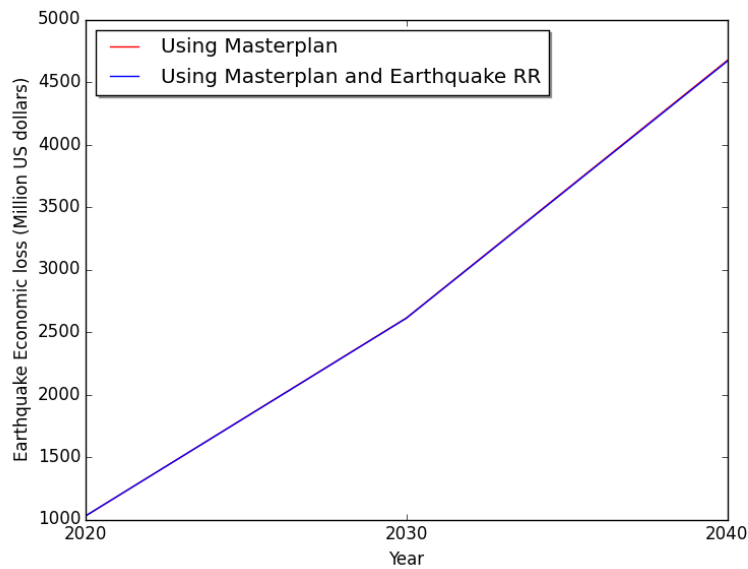


Figure 7.13 Comparing total earthquake losses in term of economic relating to GRDP between (1) using master plan and (2) using master plan and earthquake risk reduction in Yangon from 2020 to 2040 with the probability of 10% and RC 2500psi (Million US dollars)

Table 7.3 The statistics of total earthquake losses in term of economic relating to GRDP between (1) using master plan and (2) using master plan and earthquake risk reduction in Yangon from 2020 to 2040 with the probability of 10% and RC 2500psi (Million US dollars)

	2020	2030	2040
Master plan	1,029	2,613	4,673
Master plan and Earthquake risk reduction	1,028	2,610	4,666

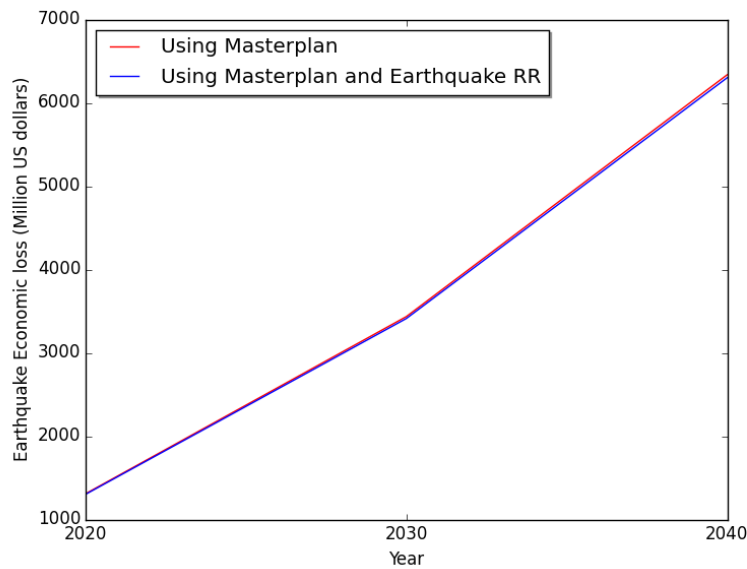


Figure 7.14 Comparing total earthquake losses in term of economic relating to GRDP between (1) using master plan and (2) using master plan and earthquake risk reduction in Yangon from 2020 to 2040 with the probability of 10% and RC 1250psi (Million US dollars)

Table 7.4 The statistics of total earthquake losses in term of economic relating to GRDP between (1) using master plan and (2) using master plan and earthquake risk reduction in Yangon from 2020 to 2040 with the probability of 10% and RC 1250psi (Million US dollars)

	2020	2030	2040
Master plan	1,309	3,435	6,337
Master plan and Earthquake risk reduction	1,302	2,412	6,302

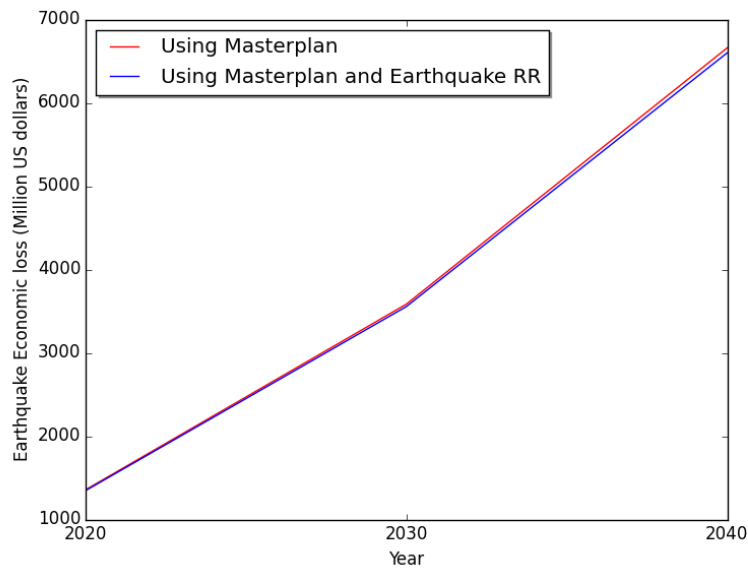


Figure 7.15 Comparing total earthquake losses in term of economic relating to GRDP between (1) using master plan and (2) using master plan and earthquake risk reduction in Yangon from 2020 to 2040 with the probability of 2% and RC 2500psi (Million US dollars)

Table 7.5 The statistics of total earthquake losses in term of economic relating to GRDP between (1) using master plan and (2) using master plan and earthquake risk reduction in Yangon from 2020 to 2040 with the probability of 2% and RC 2500psi (Million US dollars)

	2020	2030	2040
Master plan	1,356	3,584	6,660
Master plan and Earthquake risk reduction	1,346	3,555	6,600

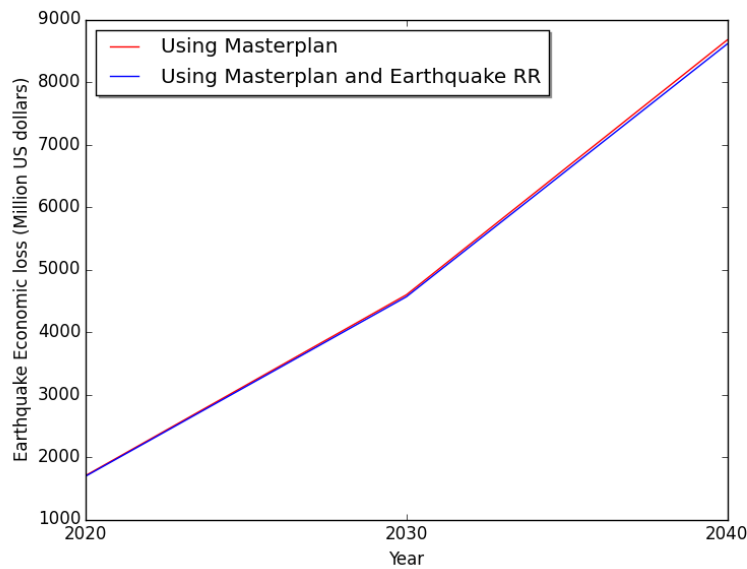


Figure 7.16 Comparing total earthquake losses in term of economic relating to GRDP between (1) using master plan and (2) using master plan and earthquake risk reduction in Yangon from 2020 to 2040 with the probability of 2% and RC 1250psi (Million US dollars)

Table 7.6 The statistics of total earthquake losses in term of economic relating to GRDP between (1) using master plan and (2) using master plan and earthquake risk reduction in Yangon from 2020 to 2040 with the probability of 2% and RC 1250psi (Million US dollars)

	2020	2030	2040
Master plan	1,702	4,595	8,673
Master plan and Earthquake risk reduction	1,692	4,563	8,609

According to Figure 7.13 and Table 7.3, the total earthquake economic losses with the probability of 10% and RC 2500psi are 1,029 million US dollars for 2020, 2,613 million US dollars for 2030, and 4,673 million US dollars for 2040. By integrating with earthquake risk reduction, the total earthquake economic losses with the probability of 10% and RC 2500psi can be reduced by 1 to 7 million US dollars (1 million US dollars in 2020, 3 million US dollars in

2030, and 7 million US dollars in 2040).

According to Figure 7.14 and Table 7.4, the total earthquake economic loss with the probability of 10% and RC 1250psi are 1,309 million US dollars for 2020, 3,435 million US dollars for 2030, and 6,337 million US dollars for 2040. By integrating with earthquake risk reduction, the total earthquake economic losses with the probability of 10% and RC 1250psi can be reduced by 7 to 35 million US dollars (7 million US dollars in 2020, 23 million US dollars in 2030, and 35 million US dollars in 2040).

According to Figure 7.15 and Table 7.5, the total earthquake economic loss with the probability of 2% and RC 2500psi are 1,356 million US dollars for 2020, 3,584 million US dollars for 2030, and 6,660 million US dollars for 2040. By integrating with earthquake risk reduction, the total earthquake economic losses with the probability of 2% and RC 2500psi can be reduced by 10 to 60 million US dollars (10 million US dollars in 2020, 29 million US dollars in 2030, and 60 million US dollars in 2040).

According to Figure 7.16 and Table 7.6, the total earthquake economic loss with the probability of 2% and RC 1250psi are 1,062 million US dollars for 2020, 2,651 million US dollars for 2030, and 4,650 million US dollars for 2040. By integrating with earthquake risk reduction, the total earthquake economic losses with the probability of 2% and RC 1250psi can be reduced by 10 to 64 million US dollars (10 million US dollars in 2020, 32 million US dollars in 2030, and 64 million US dollars in 2040).

Moreover, we calculated the statistics of total earthquake loss in term of economic relating to GRDP with the worst case of the probability of 2% and RC 1250psi at the town ship scale. The statistics of total earthquake loss in term of economic relating to GRDP from 2020 to 2040 with the probability of 2% and RC 1250psi by using master plan is shown in Figure 7.17 and by using master plan and earthquake risk reduction in Figure 7.18. The spatial information of total earthquake loss in term of economic with the probability of 2% and RC 1250psi by using master plan in 2040 at the town ship scale is depicted in Figure 7.19.

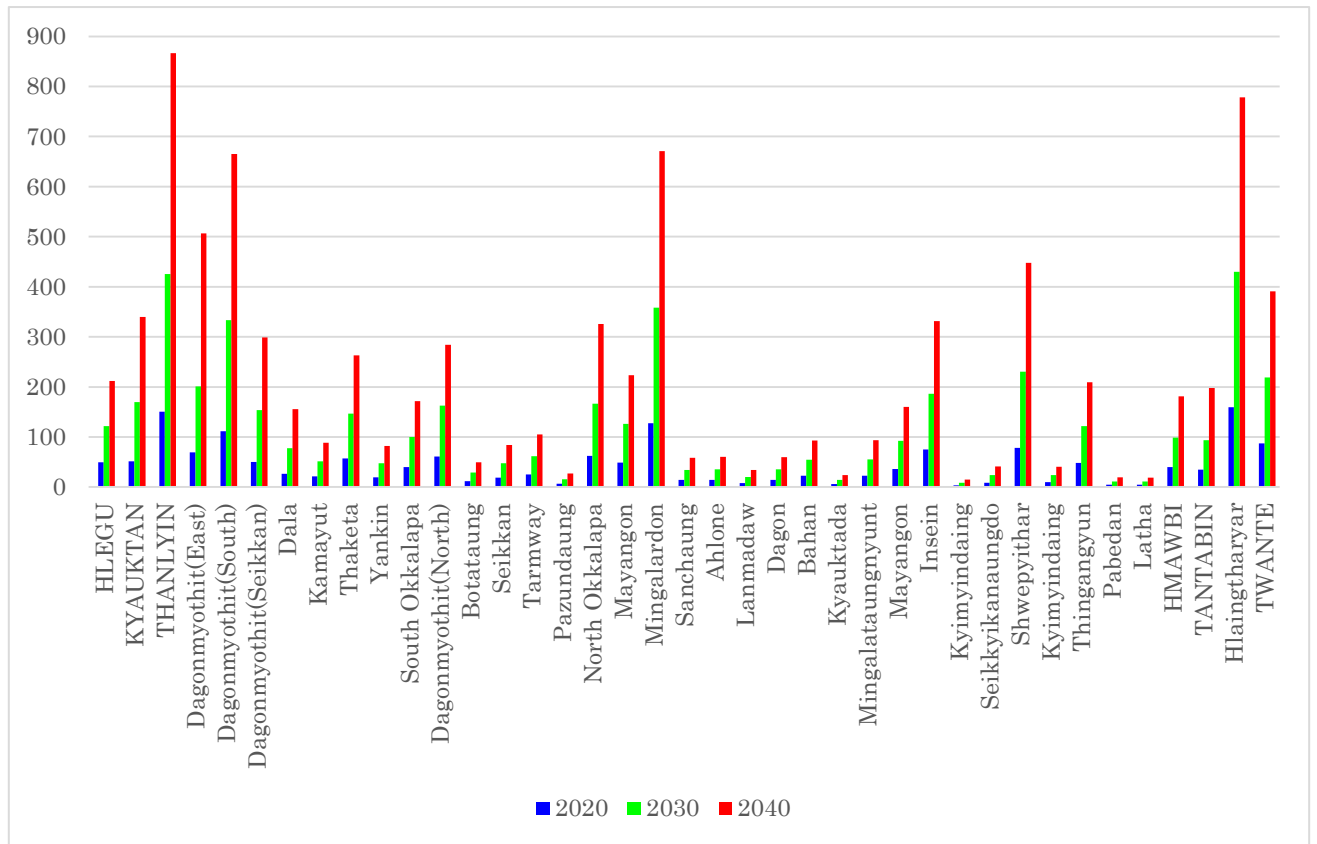


Figure 7.17 Earthquake risks in term of economic loss relating to GRDP from 2020 to 2040 with the probability of 2% and RC 1250psi by using master plan at the township scale (Million US dollars)

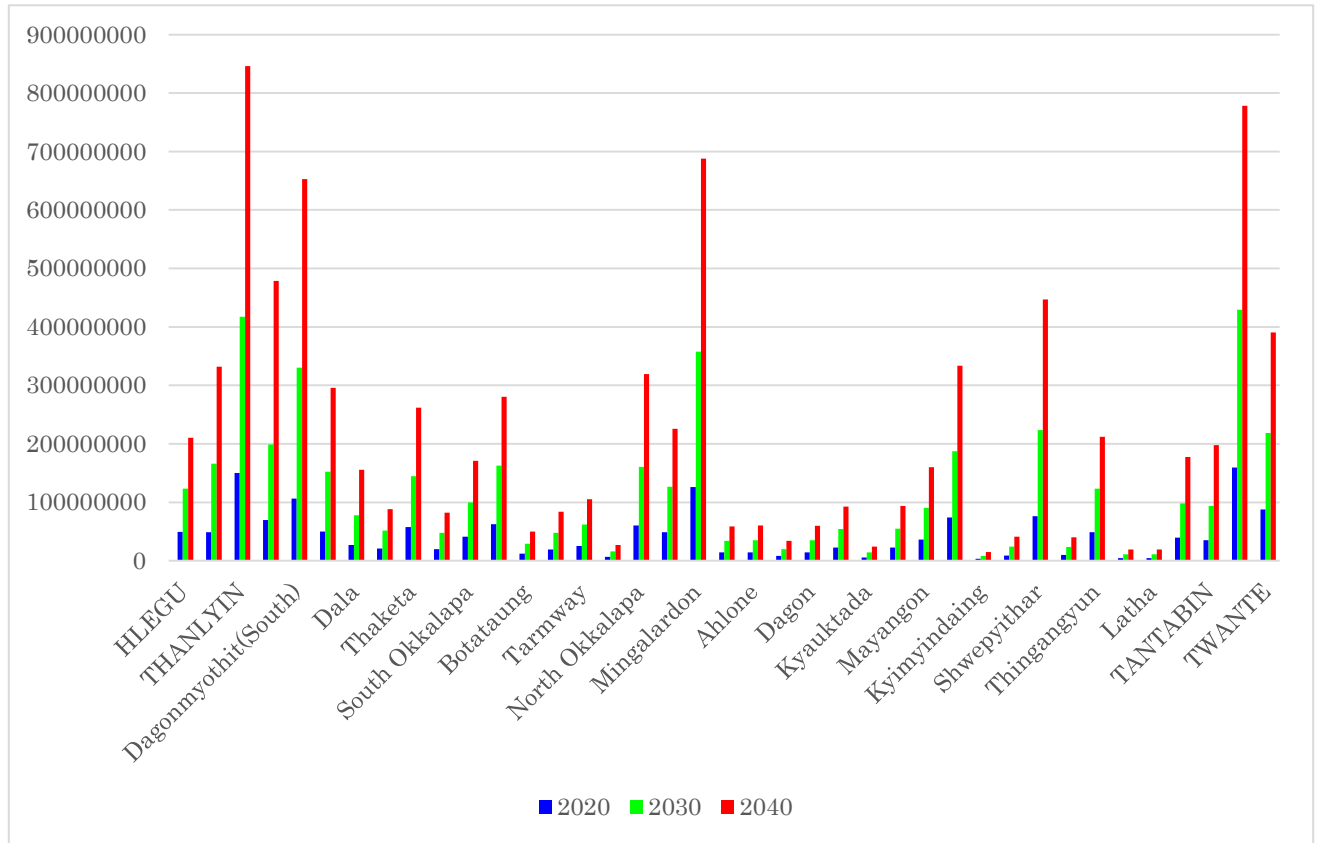


Figure 7.18 Earthquake risks in term of economic loss relating to GRDP from 2020 to 2040 with the probability of 2% and RC 1250psi by using master plan and earthquake risk reduction at the township scale (Million US dollars)

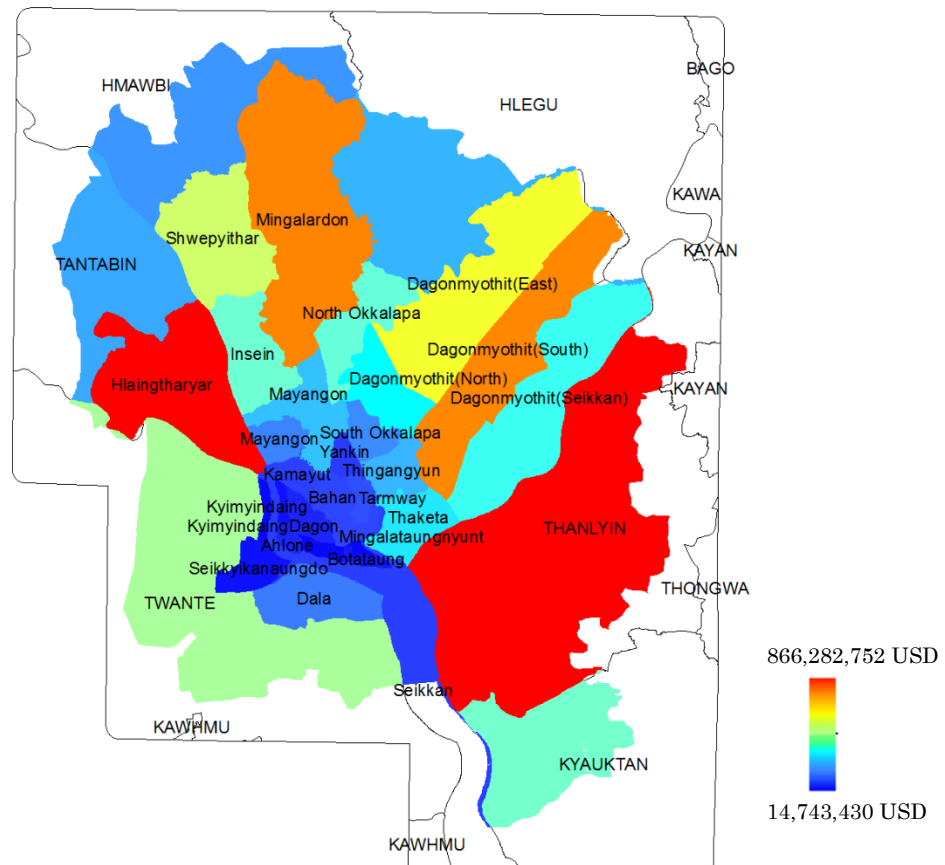


Figure 7.19 Earthquake risks in term of economic loss relating to GRDP in 2040 with the probability of 2% and RC 1250psi by using master plan at the township scale (US dollars)

According to Figure 7.17, 7.18 and 7.19, considering at the township, the five highest earthquake economic losses are Thanlyin, Hlaingtharyar, Mingalardon, Dagonmyothit (South), Dagonmyothit (East). The five highest earthquake economic loss townships are mostly located on the high ground shaking areas.

7.5 Remarks

We converted the predicted land cover images from 2020 to 2040 into predicted economic areas relating to GRDP by using land price estimation and predicted economic growth relating to GRDP. For calculating disaster risk in term of economic loss, we used the predicted economic areas, and flood and earthquake vulnerable areas, also Lloyd's City Risk Index as the impacts of disaster to economic.

The total flood economic losses in 2020, 2030, and 2040 in Yangon by using Master plan are 687 million US dollars, 1,728 million US dollars, and 3049 million US dollars, respectively. By integrating with flood risk reduction, the flood economic losses can be reduced from 4 to 28 million US dollars. At the township scale, the five highest flood economic losses are Thanlyin, Twante, Haingtharyar, Mingalardon, Dagonmyothit (South).

The earthquake economic losses with the safest case of the probability of 10% and RC 2500psi in 2020, 2030, and 2040 in Yangon are 1,029 million US dollars, 2,613 million US dollars, 4,673 million US dollars, respectively. By integrating with earthquake risk reduction, the earthquake economic losses with the safest case can be reduced from 1 to 7 million US dollars.

The earthquake economic losses with the worst case of the probability of 2% and RC 1250psi in 2020, 2030, and 2040 in Yangon are 1,702 million US dollars, 4,595 million US dollars, 8,673 million US dollars, respectively. By integrating with earthquake risk reduction, the earthquake economic losses with the worst case can be reduced from 10 to 64 million US dollars.

At the township scale, the five highest earthquake economic losses with the worst case are Thanlyin, Hlaingtharyar, Mingalardon, Dagonmyothit (South), Dagonmyothit (East).

Chapter8. Investigation of the high-rise buildings growth

8.1 Reviews

To get more reality of prediction of urban expansion, the prediction of high-rise building expansion should be considered. High-rise buildings are very important areas in term of economic value (high economic value). To improve the estimated economic value areas, the high-rise buildings expansion should be included in the land price model for more accuracy in calculating economic value areas. In this research, we have tried to investigate the high-rise buildings growth. Since we have not had the building height data with the dynamic time, we need to use another data with the dynamic time that can indicate the high-rise building growth areas in Yangon. Also, we have also tried to find the factors that can indicate the urban growth areas in Yangon. However, the modeling high-rise building to predict high-rise building growth areas in the future has been not done yet.

8.2 Observing the estimated building types with nighttime light data

We observed the estimated building types with (1) commercial, (2) industrial and (3) residential buildings (extracted from stereo GeoEye images in 2012) (Figure A.5) with VIIRS nighttime light data in 2012 (Figure 8.2 a). We found there is a high relationship between the building types and nighttime light. Commercial buildings (high-rise buildings) has high nighttime light, and industrial buildings (high-rise buildings) have low nighttime light, and residential buildings have low nighttime light. The statistical of mean and variance of nighttime light is shown in Table 8.1 and the histogram is shown in Figure 8.1.

Table 8.1 The statistical of mean and variance of nighttime light

	Commercial buildings	Industrial buildings	Residential buildings
Mean of nighttime light	20.36	8.08	11.50
STD of nighttime light	103.66	7.83	70.92

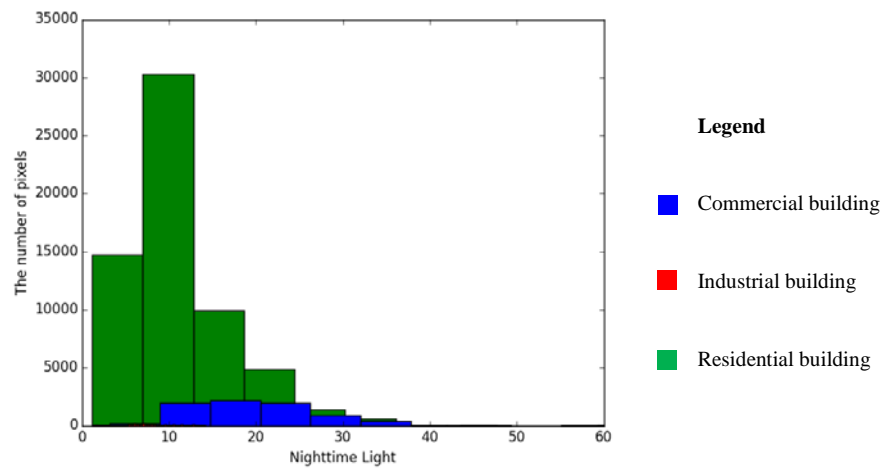


Figure 8.1 The histogram of nighttime light

8.3 Detecting the high rise building growth

We used VIIRS nighttime light in 2012 (Figure 8.2 a) and in 2015 (Figure 8.2 b) for observing nighttime light change that indicates high-rise building growth. We assumed that nighttime light change from low to high nighttime light can indicate the change from low-rise to high-rise buildings. In this research, high-rise buildings as commercial buildings can only be detected but high-rise buildings as industrial buildings can not be detected since industrial buildings have low nighttime light.

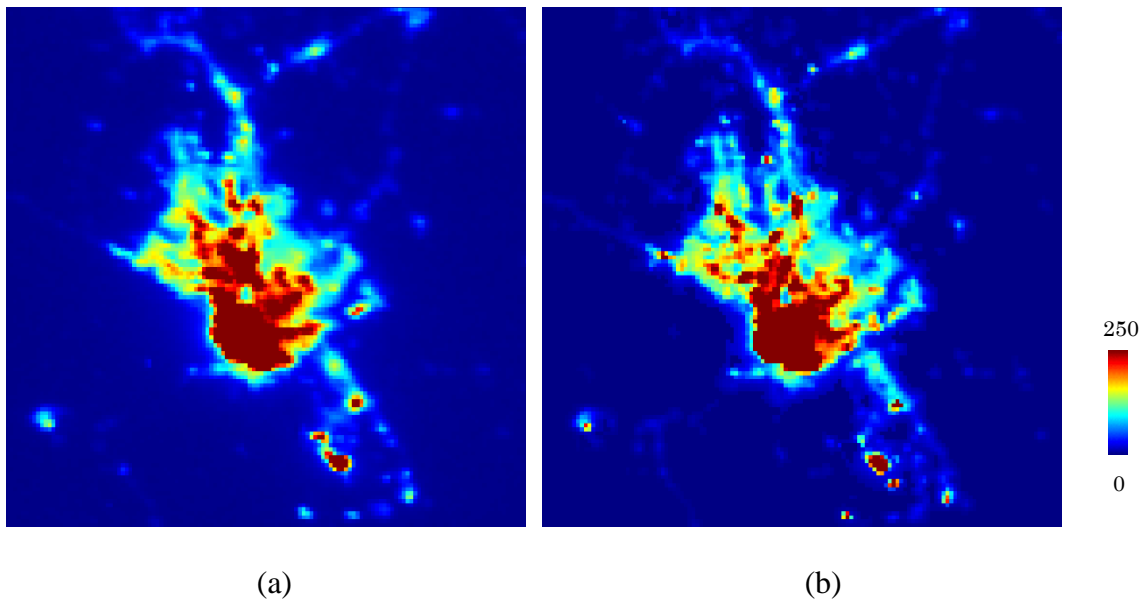


Figure 8.2 VIIRS nighttime light (a) in 2012 and (b) in 2015

After computing the change detection, the result of high-rise buildings (commercial buildings) from 2012 to 2015 is depicted in Figure 8.3.

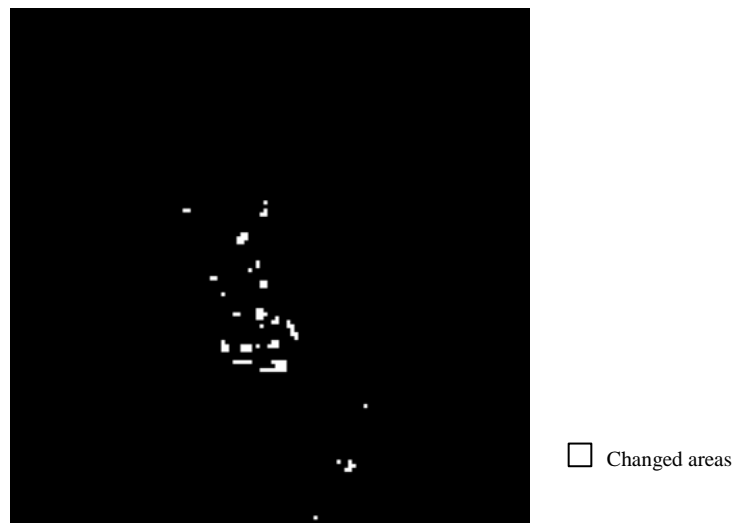


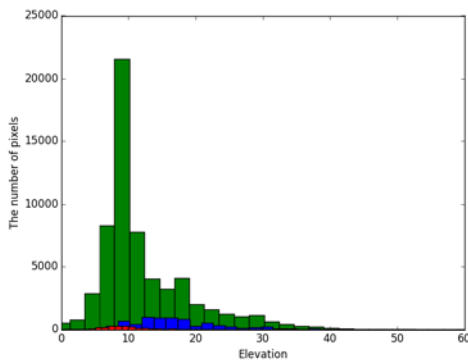
Figure 8.3 Changed areas from low to high nighttime light

In the validation step, we did not have ground surveying data of high-rise building growth. Hence, we indirectly validated by comparing the observations with three factors; (1) elevation, (2) distance from railways (3) urban areas in the past, between nighttime light change from low to high nighttime light and building types. The comparison between commercial buildings and change areas relating to elevation, distance from railways and urban areas in the past with mean and standard deviation is described in

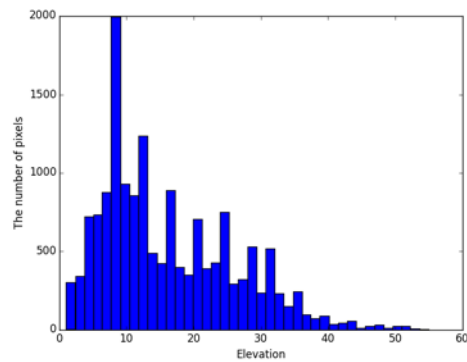
Table 8.2. The comparison of the histograms between commercial buildings and change areas is depicted in Figure 8.4.

Table 8.2 The comparison between commercial buildings and change areas relating to elevation, distance from railways and urban areas in the past

	Commercial building	Change areas
Mean of elevation	17.24	16.22
STD of elevation	51.94	96.92
Mean of distance from railway	22.68	34.12
STD of distance from railway	268.55	386.59
Mean of past urban area	0.54	0.65
STD of past urban area	0.83	1.05



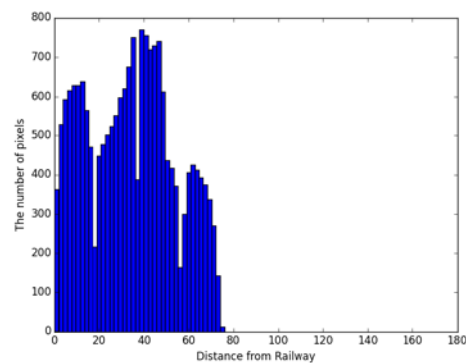
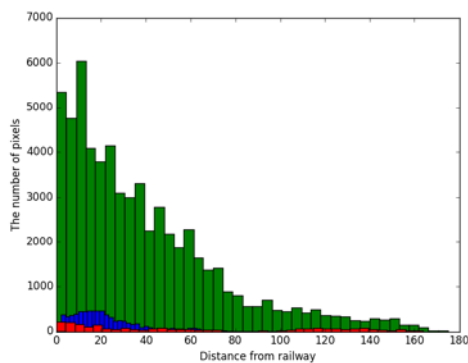
(a)



(b)

Legend

- Commercial building
- Industrial building
- Residential building



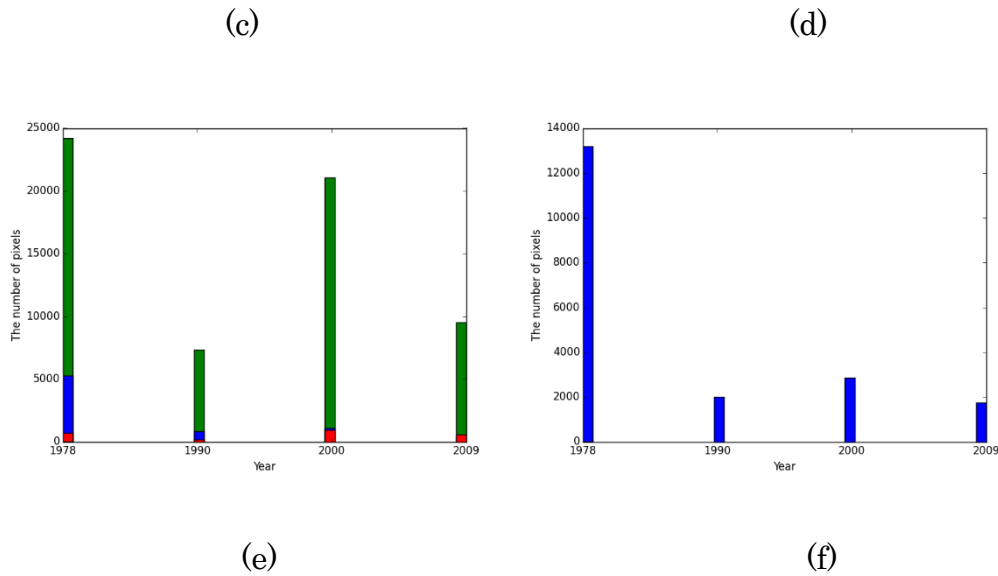


Figure 8.4 Histograms of elevation with (a) commercial buildings and (b) change areas, histograms of distance from railway with (c) commercial buildings and (d) change areas, and histograms of past urban areas with (e) commercial buildings and (f) change areas

According to Table 8.2 and Figure 8.4, we investigated that the values of the means of elevation, distance from the railway, the past urban areas between commercial buildings (high-rise buildings) and changed areas from low to high nighttime light are quite similar. It possibly indicates that changed areas from low to high nighttime light can indicate the high-rise buildings growth in term of commercial buildings.

8.4 Discussions

We investigated that in the case of the limitation of high-rise building data with dynamic time, the changed areas from low to high nighttime light could be used to indicate the high-rise building growth areas. We found that the elevation, distance from the railway and the past urban areas could be used to indicate the high-rise building growth areas. In Yangon, high-rise building has grown up on high elevations, close to railway and in the past urban areas. However, in this research, we did not have the modeling high-rise building expansion that can predict the high-rise building growth areas in the

future yet.

8.5 Remarks

Since we did not have the high-rise buildings with the dynamic time, we relied on the dynamic nighttime light data instead. We investigated that high-rise buildings as the commercial buildings have high nighttime light data but low-rise buildings as residential buildings have low nighttime light data. According to the experiment, nighttime light change from low to high nighttime light can indicate the high-rise building growth in term of commercial buildings. We found that in Yangon, Myanmar, high-rise building has grown up on high elevations, close to railway and in the past urban areas.

By using VIIRS nighttime light data, the resolution of the nighttime light data is very low with 460 m-resolution. One pixel can include both low and high-rise buildings. Hence, it possibly makes errors of high-rise building growth.

However, in this research, we did not have the modeling high-rise building expansion that can predict the high-rise building growth areas in the future yet. As a result, this chapter only shows that in the case of the limitation of high-rise building data with dynamic time, the changed areas from low to high nighttime light could be used to indicate the high-rise building growth areas. Also, the elevation, distance from the railway and the past urban areas could be used to indicate the high-rise building growth areas.

Chapter9. Conclusions and recommendations

9.1 Conclusions

Yangon is regarded as potential risks of flood and earthquake. In order to support urban development and management to mitigate the damages of flood and earthquake in the future, we proposed the methodology to reduce the flood and earthquake risks and asses flood and earthquake risks in term economic loss relating to GRDP in Yangon, Myanmar. Firstly, we proposed four fundamental methodologies with (1) flood vulnerability assessment, (2) earthquake vulnerability assessment, (3) land price estimation, (4) urban expansion modeling. Then, by combining urban expansion modeling with the master plan and relating to flood and earthquake vulnerabilities, the predicted urban areas from 2020 to 2040 with multi-scenarios were estimated in order to reduce flood and earthquake risks. Next, by integrating the predicted urban expansion with land price and relating to the prediction of GDP growth, the assessments of flood and earthquake risks in term of economic loss relating to GRDP from 2020 to 2040 with multi-scenarios were provided.

For the prediction of urban expansion in Yangon, the master plan helps to make more reliability of the prediction of the urban expansion by giving the future dataset. Unfortunately, by using the master plan, we found that some of the predicted areas are still located in the high disaster vulnerable areas. By combing the prediction of urban expansion with disaster risk reduction, the predicted urban areas can escape from the high disaster vulnerable areas.

By using the different features with the prediction model, multi-scenarios of predicted urban areas can be available to support for decision-making or policy for reducing disaster risk. We investigate that for flood risk assessment, by using master plan, total flood losses in term of economic from 2020 to 2040 are 687 million US dollars, 1,728 million US dollars, and 3,049 million US dollars, respectively. By integrating flood risk reduction, the total flood

economic losses could be reduced from 4 to 28 million US dollars. For earthquake risk assessment, by using master plan, the total earthquake losses in term of economic from 2020 to 2040 with the safest case are 1,029 million US dollars, 2,613 million US dollars, 4,673 million US dollars, respectively. By integrating earthquake risk reduction, the total earthquake economic losses with the safest case can be reduced from 1 to 7 million US dollars. by using master plan, the total earthquake losses in term of economic from 2020 to 2040 with the worst case are 1,702 million US dollars, 4,595 million US dollars, 8,673 million US dollars, respectively. By integrating earthquake risk reduction, the total earthquake economic losses with the worst case can be reduced from 10 to 64 million US dollars.

In addition, the remotely sensed data from Landsat, GeoEye, MODIS, VIIRS was used to support the assessment of flood and earthquake risks and flood and earthquake risk reductions in Yangon, Myanmar. In this research, the remotely sensed dataset helps to provide the historical water surface, indirect ages of the buildings, the building types with commercial, industrial, and residential buildings, and detecting the multi-centers of urban areas. The validated results confirm that our products by using remotely sensed data are reliable to be used in this research.

9.2 Recommendations

For disaster risk assessment, the earthquake vulnerability assessment can be compared with other works to confirm the reliability.

Land price estimation can be improved by using the other factors such as the significant structure (tourist place). In the empirical model, in the setting, the parameters, the values of parameters can be assigned in term of an exponential function instead of a linear function.

To get more reality of urban expansion, modeling high-rise building prediction should be included. The high-rise building growth areas can be detected from changed areas from low to high nighttime light. Elevation, Distance from the railway and urban areas in the past can be used to indicate the high-rise building growth areas. To improve the estimated economic value areas, the high-rise buildings expansion should be included in the land price model.

The assessment of flood and earthquake risks in term of economic loss in the future can be improved by using all input variables with the dynamic time. In this research, we proposed the equation to calculate the disaster risk in term of economic loss. For the example, the total flood loss in term economic is expressed as the below equation

$$\text{Total_FLE}(t) = C_{\text{flood}} \sum [EC(i, j, t) \times FVI(i, j)] \quad (9.1)$$

In this research, we only used the economic value areas with the dynamic time, and we used the flood impact to economic loss and flood vulnerability index without the dynamic time. To get more reality of the assessment, all input variables with the dynamic time (the flood impact to economic loss with dynamic time, the economic value areas with the dynamic time, and flood vulnerability index with the dynamic time) should be included in the below equation.

$$\text{Total_FLE}(t) = C_{\text{flood}}(t) \sum [EC(i, j, t) \times FVI(i, j, t)] \quad (9.2)$$

According to the equation, for the instance, the flood impact to economic loss

should be increased in the future time due to the implication of climate change such as increased annual rainfall and changing rainfall pattern. The economic value in the future will be increased because of population growth and urbanization. The flood vulnerable areas also would be increased due to lacking well preparation of a drainage system and land use planning. As a result, the total flood loss in term of economic will be increased (Kron, 2005).

To support to analysis with the multiple-scenarios, sensitivity analysis can be used with the multiple input variables and multiple outputs. Sensitivity analysis is the study of how the uncertainty in the output of a mathematical model or system can be apportioned to different sources of uncertainty in its inputs (Saltelli, 2002). The sensitivity analysis will help to find the boundary of the results by varying the multiple input variables and will indicate how the impacts of the changed input variables as well.

Reference

- Ahmad, N., 2015, Economic losses from disasters. PAKISTAN and National Briefing. Leadership for Environment & Development (LEAD) Pakistan. March, 2015.
- Batty, M., 1997. Cellular automata and urban form. *Journal of the American Planning Association*. Vol. 63 (3), pp. 264-274.
- Black, A. R., Burns, J. C., 2002. Re-assessing the flood risk in Scotland. *Sci. Total Environ*. Vol. 294 (1), pp. 169–184.
- Bagan H., Yamagata, Y., 2012. Landsat analysis of urban growth: How Tokyo became the world's largest megacity during the last 40 years. *Remote Sensing of Environment*. Vol. 127, pp. 210–222.
- Benenson, I., 1998. Multiagent simulations of residential dynamics in the city. *Computers Environment and Urban Systems*. Vol. 22 (1), pp. 25-42.
- Burge, G., 2014. The capitalization effects of school, residential and commercial impact fees on undeveloped land values. *Regional Science and Urban Economics*. Vol. 44, pp.1-13.
- Cho, S. H., Chen, Z., Yen, S. T., Eastwood, D. B., 2006. Estimating effects of an urban growth boundary on Land development. *Journal of Agricultural and Applied Economics*. Vol. 38 (2), pp. 287-298.
- Cinicioglu, S.F., Bozbey, I., Oztoprak, S., Kelesoglu, M.K., 2007. An integrated earthquake damage assessment methodology and its application for two districts in Istanbul, Turkey. *Eng Geol*. Vol 94, pp. 145–65.
- Clarke, K.C., Gaydos, L.J., 1998. Loose-coupling a cellular automaton

- model and GIS: long-term urban growth prediction for San Francisco and Washington/Baltimore. *International Journal of Geographical Information Science*. Vol. 12(7), pp. 699-714.
- Deaton, A. 2001. Housing, Land Prices, and Growth. *Journal of Economic Growth*. Vol. 6, pp. 87–105.
- Deza, M. M., Deza, E., 2009. *Encyclopedia of Distances*. Springer, 2009, pp. 94.
- Disaster and Climate Change (chapter 8). 2016. *Ciottone's Disaster Medicine (Second Edition)*. pp 47–52.
- earthdata.nasa.gov,
<https://earthdata.nasa.gov/earth-observation-data/near-real-time/download-nrt-data/viirs-nrt>, Accessed on 15 September 2015
- earthobservatory.nasa.gov,
<https://earthobservatory.nasa.gov/Features/MeasuringVegetation/>,
Accessed on 15 September 2015
- earthobservatory.nasa.gov,
<https://earthobservatory.nasa.gov/Features/TRMM/>, Accessed on 15 May 2016
- Estimate depends on methodology used. See World Bank. 2014. *A Systematic Country Diagnostic*.
- FEMA. HAZUSMH MR4 Earthquake model user manual. Department of Home-land Security. Federal emergency management agency. Mitigation Division. Washington, D.C. 2012.
- Gadagamma, C.K., Min, A. K.,Gokon, H., Meguro, K., 2014. Development of Seismic Fragility Functions for Reinforced Concrete (RC) Buildings in Yangon, Myanmar. rsos.royalsocietypublishing.org.
- GermanWatch. 2016. *Global Climate Risk Index 2016*.

<https://germanwatch.org/fr/download/13503.pdf>.

Greenland, S., 1995. Dose-Response and Trend Analysis in Epidemiology: Alternatives to Categorical Analysis, *Epidemiology*, Vol. 6(4), pp. 356–365.

Hartigan, J.A., Wong, M.A., 1979. Algorithm AS 136: A K-Means Clustering Algorithm. *Journal of the Royal Statistical Society*. Vol. 28, pp. 100–108.

Hoornweg, D., Pope, K., 2014. Socioeconomic Pathways and Regional Distribution of the World's 101 Largest Cities, Global Cities Institute, Working Paper No. 04.

Hu, S.; Cheng, Q.; Wang, L.; Xu, D., 2013. Modeling land price distribution using multifractal IDW interpolation and fractal filtering method. *Landscape and Urban Planning*. Vol. 110, pp.25-35.

ifrc.org,

<http://www.ifrc.org/en/what-we-do/disaster-management/about-disaster-management>, Accessed on 20 June 2016

Ihlanfeldt, K.R. 2007. The effect of land use regulation on housing and land prices. *Journal of Urban Economics*. Vol. 61, pp.420-435.

ICHARM (The International Centre for Water Hazard), 2016. Transformation of Urban Management - Part II Flood Management.

INFORM (Index for Risk Management). 2016. Results Report 2016 (<http://www.informindex.org/Portals/0/InfoRM/2016/INFORM%20Results%20Report%202016%20WEB.pdf>)

Jarvis, A., H.I. Reuter, A. Nelson, E. Guevara. 2008. Hole-filled SRTM for the globe Version 4, available from the CGIAR-CSI SRTM 90m Database (<http://srtm.csi.cgiar.org>)

JICA (Japan International Cooperation Agency), 2013. The Project for the

Strategic Urban Development Plan of the Greater Yangon.

JICA (Japan International Cooperation Agency), 2016. The Strategic Urban Development Plan and the Urban Transport Development Plan of the Greater Yangon.

Karimzadeh, S., Miyajima, M., Hassanzadeh, R., Amiraslazadeh, R., Kamel, B., 2014. A GIS based seismic hazard, building vulnerability and human loss assessment for the earthquake scenario in Tabriz. *Soil Dynamics and Earthquake Engineering*. Vol. 66, pp. 263–280.

Kazakis, N., Kougiaris, I., Patsialis, T., 2015. Assessment of flood hazard areas at a regional scale using an index-based approach and Analytical Hierarchy Process: Application in Rhodope–Evros region, Greece. *Science of the Total Environment*. Vol. 538, pp. 555–563.

Koks, E.E., Jongman, B., Husby, T.G., Botzen, W.J.W., 2015. Combining hazard, exposure and social vulnerability to provide lessons for flood risk management. *Environmental science & policy*. Vol. 47, pp. 42–52.

Kron, W., 2005. Flood Risk = Hazard • Values • Vulnerability. *Water International*, Vol. 30, pp. 58-68.

Lawson, C.L., Hanson, R.J., 1974. *Solving Least Squares Problems*. Englewood Cliffs, NJ: Prentice-Hall.

landsat.usgs.gov, <https://landsat.usgs.gov/>, Accessed on 15 March 2015

Lee, E.H., Lee, Y.S., Joo, J.G., Jung, D., Kim, J.H., 2016. Flood Reduction in Urban Drainage Systems: Cooperative Operation of Centralized and Decentralized Reservoirs. *Water* 2016, Vol 8 (10), pp. 469.

Lin R.; Zhu, D., 2014. A spatial and temporal analysis on land incremental values coupled with land rights in China. *Habitat International*. Vol. 44, pp.168-176.

lloyds.com, <https://www.lloyds.com/cityriskindex/>, Accessed on 27 June

2017

Lowry I. S., 1964. A model of metropolis Santa Monica. CA (Rand Corporation).

Lwin, A., Khaing, M. M., 2012. Yangon river geomorphology indentification and its environmental impacts analysis by optical and radsar sensing techniques. International Archives of the Photogrammetry, Remote Sensing and Spatial Information Sciences, Volume XXXIX-B8, 2012, XXII ISPRS Congress, 25 August – 01 September 2012, Melbourne, Australia.

Maesschalck, R.D., Jouan-Rimbaud, D., Massart, D.L., 2000. The Mahalanobis distance. Chemometrics and Intelligent Laboratory Systems. Vol. 50, pp. 1–18.

Meja-Navarro, M., Wohl, E. E., Oaks, S. D., 1994. Geological hazards, vulnerability, and risk assessment using GIS: model for Glenwood Springs, Colorado. Geomorphology. Vol. 10, pp. 331–354.

mmtimes.com,

<http://www.mmtimes.com/index.php/national-news/yangon/17012-yangon-flood-losses-top-k11-billion.html>, Accessed on 20 June 2016

modis.gsfc.nasa.gov, <https://modis.gsfc.nasa.gov/about/>, Accessed on 20 May 2015

Moe, S.S., 2009. Current Trends of Urban Development in Yangon City and Its Implications on the Environment. GMSARN International Journal. Vol. 3, pp. 179 - 186.

Morley, I. 2013. Rangoon, Cities. Vol. 31, pp.601–614.

Myanmar Country Report: Eric Vaughan, Mercy Corps Myanmar (https://www.accrn.net/sites/default/files/publication/attach/4._myanmar_paper.pdf)

- Nichols, D. A., 1970. Land and Economic Growth. *The American Economic Review*. Vol. 60 (3), pp. 332-340.
- Neumayer, E., Barthel, F., 2011. Normalizing economic loss from natural disasters: A global analysis. *Global Environmental Change*. Vol. 21, pp. 13-24.
- Neumayer, E., Plümper, T., Barthel, F., 2014. The political economy of natural disaster damage. *Global Environmental Change*. Vol. 24, pp. 8-19.
- Notaro, V., Marchis, M.D., Fontanazza, C.M., Loggia, G.L., Puleo, V., Freni, G., 2014. The Effect of Damage Functions on Urban Flood Damage Appraisal. *Procedia Engineering*. Vol. 70, pp. 1251-1260.
- O' conner, R., Conlon, F., 1993. Agricultural and forest land prices in Ireland. The Forest Service (Department of Agriculture, Food and Forestry).
pitt.edu, <http://www.pitt.edu/~epi2170/lecture15/sld006.htm>, Accessed on 20 May 2015
- punditcafe.com,
<http://www.punditcafe.com/science/types-of-natural-disasters-examples>, Accessed on 20 May 2015
- pwc.com, www.pwc.com/globalgoals, Accessed on 15 March 2017
- ready.gov, <https://www.ready.gov/risk-assessment>, Accessed on 20 May 2015
- reliefweb.int,
<http://reliefweb.int/report/myanmar/myanmar-cyclone-nargis-hits-rangoon>, Accessed on 20 May 2015
- Riggs, M.A., Rao, C.Y., Brown, C. M., Sickie, D.V., Cummings, K.J., Dunn, K.H., Deddens, J.A., Ferdinands, J., Callahan, D., Moolenaar, R.L., Pinkerton, L.E., 2008. Resident cleanup activities, characteristics of

- flood-damaged homes and airborne microbial concentrations in New Orleans, Louisiana, October 2005. *Environmental Research*. Vol. 106, pp. 401-409.
- Saltelli, A., 2002. Sensitivity Analysis for Importance Assessment. *Risk Analysis*. Vol. 22 (3), pp. 1–12.
- satimagingcorp.com,
<http://www.satimagingcorp.com/satellite-sensors/geoeye-1/>, Accessed on 20 May 2015
- Schumann, A.H., Funke, R., Schultz, G.A., 2000. Application of a geographic information system for conceptual rainfall–runoff modeling. *J. Hydrol.* Vol. 240 (1–2), pp. 45–61.
- Sharif, M.S., Esa, A.J. 2014. Dynamics of land price and land used change: A case of Savar Municipality, Bangladesh. *Journal of South Asian Study*. Vol. 2(01), pp. 83-89.
- Sklar, F. H., Costanza ,R., 1991. The development of dynamic spatial models for landscape ecology. A review and prognosis, pp. 239-288.
- Song, Y., Gong, J., Gao, S., Wang, D., Cui, T., Li, Y., Wei, B., 2012. Susceptibility assessment of earthquake-induced landslides using Bayesian network: A case study in Beichuan, China. *Computers & Geosciences*, Vol. 42, pp. 189–199.
- Sritarapipat, T., Takeuchi, W., 2017a. Building classification in Yangon City, Myanmar using Stereo GeoEye images, Landsat image and night-time light data. *Remote Sensing Applications: Society and Environment*, Vol. 6, pp. 46-51.
- Sritarapipat, T., Takeuchi, W., 2017b. Urban growth modeling based on the multi-centers of the urban areas and land cover change in Yangon, Myanmar. *Journal of Remote Sensing Society of Japan*, Vol. 37(3), pp. 248-260.

unisd.org, <https://www.unisd.org/who-we-are/what-is-drr>, Accessed on 20 May 2015

United Nations, 2015. World Urbanization Prospects (The 2014 Revision), Department of Economic and Social Affairs, Population Division.

Tehrany, M. S., Pradhan, B., Jebur, M. N., 2013. Spatial prediction of flood susceptible areas using rule based decision tree (DT) and a novel ensemble bivariate and multivariate statistical models. GIS. J. Hydrol. Vol. 504, pp. 69–79.

Thant, M., 2012. Probabilistic Seismic hazard assessment for Yangon region, Myanmar. ASEAN Engineering Journal. Part C, Vol 3 (2), p.131.

Thein, M., Swe, T.L., 2008. Earthquake and tsunami hazard potential along the Myanmar coastal areas. J. of Earth. and Tsunami, special issue.

The data from Planning Department. 2011. Ministry of National Planning and Economic Development (MNPED).

The EM-DAT database, an emergency events database collected by the Centre for Research on the Epidemiology of Disasters (CRED), defines the total number of people affected by a natural disaster as the sum of those people injured, homeless, or needing immediate assistance following a disaster. (<http://www.emdat.be/database>).

Tsutsumi, M.; Shimada, A.; Murakami, D., 2011. Land price maps of Tokyo Metropolitan Area. Procedia - Social and Behavioral Sciences. Vol. 21, pp.193-202.

unitar.org, <https://www.unitar.org/unosat/map/1176>, Accessed on 20 May 2015.

wcpt.org,

<http://www.wcpt.org/disaster-management/what-is-disaster-management>, Accessed on 20 May 2015.

- World Bank and Global Facility for Disaster Reduction and Recovery, 2012. ASEAN. Advancing Disaster Risk Financing and Insurance in ASEAN Member States: Framework and Options for Implementation.
- World Bank, 2016. East Asia and the Pacific. Economic Update.
- World Bank, 2017. Myanmar Southeast Asia Disaster Risk Management Project.
- Xi, L., Takeuchi, W., 2016. Land surface water coverage estimation with PALSAR and AMSR-E for large scale flooding detection. *Terrestrial, Atmospheric and Oceanic Sciences*. Vol. 27(4), pp. 473-480.
- Xu, Z.; Li, Q., 2014. Integrating the empirical models of benchmark land price and GIS technology for sustainability analysis of urban residential development. *Habitat International*. Vol. 44, pp.79-92.
- Zhang, X., Wang, Y., 2001. Spatial dynamic modeling for urban development. *Photogrammetric engineering and remote sensing*. Vol. 67 (9), pp. 1049-1057.

Appendix

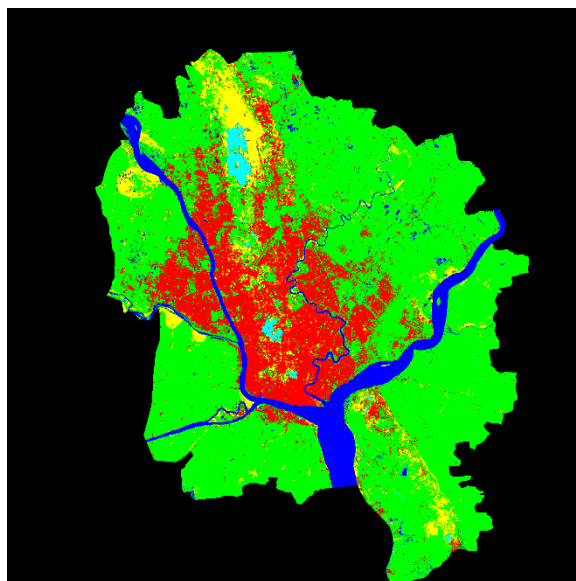


Figure A.1 Land cover image in 2015

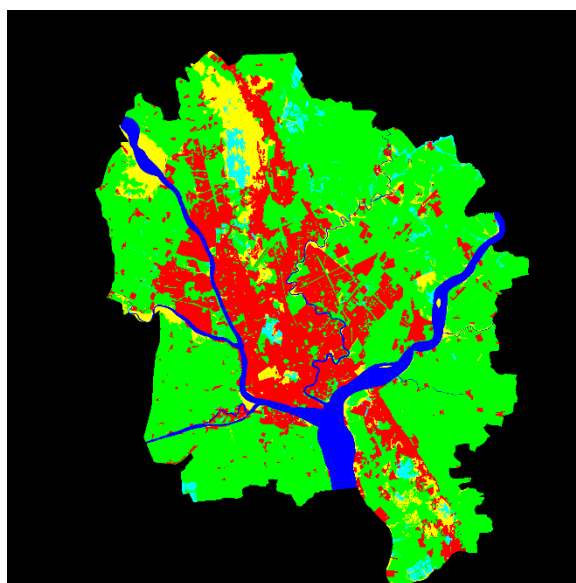


Figure A.2 Land use map in 2012 by JICA

Table A.1 The confusion matrix between land cover image in 2015 and land use map in 2012 by JICA (km²)

		Land cover map in 2012 by JICA				
		Urban	Cropland	River	Forest	Lake
Land cover result in 2015	Urban	225.82 (14.09%)	52.05 (3.24%)	1.942 (0.12%)	8.09 (0.50%)	2.25 (0.14%)
	Cropland	103.58 (6.46%)	889.65 (55.52%)	6.25 (0.39%)	47.47 (2.96%)	26.65 (1.66%)
	River	3.16 (0.19%)	12.47 (0.77%)	95.62 (5.96%)	5.85 (0.36%)	3.81 (0.23%)
	Forest	26.99 (1.68%)	23.37 (1.45%)	0.57 (0.03%)	48.87 (3.05%)	2.75 (0.17%)
	Lake	0.38 (0.02%)	0.47 (0.02%)	0.0 (0.0%)	3.13 (0.19%)	10.98 (0.68%)

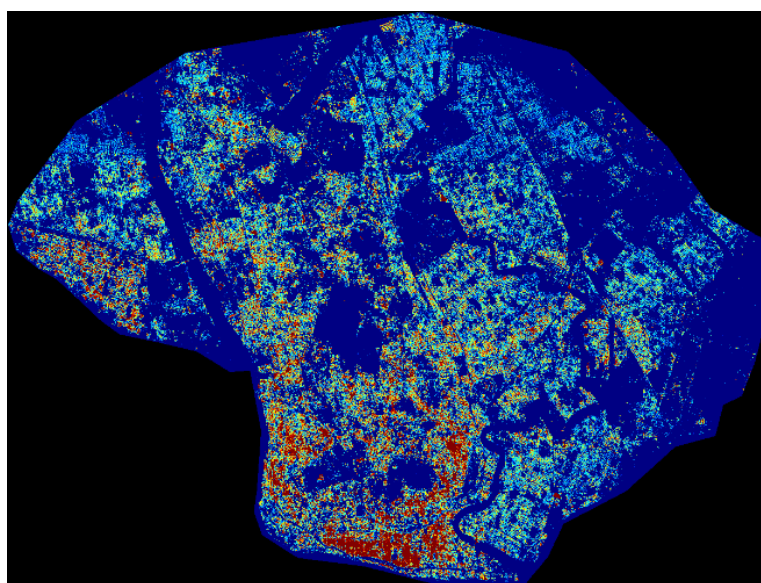


Figure A.3 Building height map in 2013

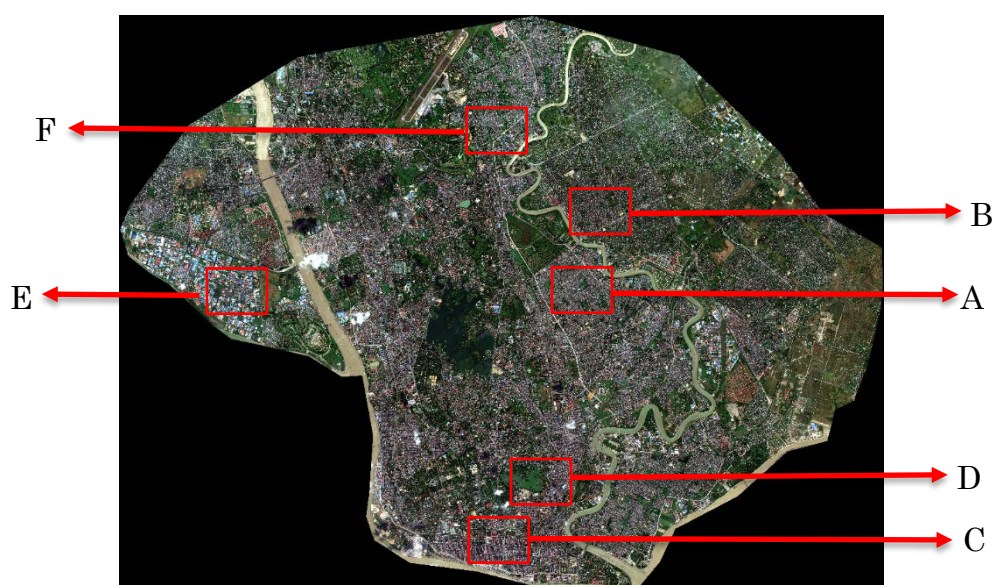


Figure A.4 The six regions of surveying building heights in 2015

Table A.2 The comparison between the estimated building heights in 2013 with the surveying building heights in 2015

Region	Type of buildings	The number of observed buildings	The average of the surveying heights of the buildings	The average of the estimated heights of the buildings
A	Residential buildings	12	5.9 m.	7.2 m.
B	Residential buildings	10	5.5 m.	6.0 m.
C	Commercial buildings	11	47.8 m.	19.3 m.
D	Commercial buildings	11	27.9 m.	19.4 m.
E	Industrial buildings	12	20.0 m.	14.6 m.
F	Industrial buildings	3	13.0 m.	10.5 m.

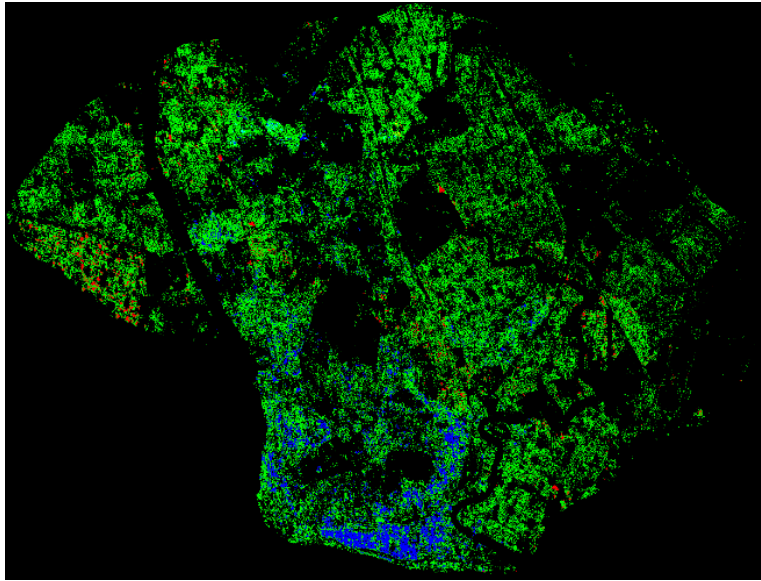


Figure A.5 Building type map in 2013

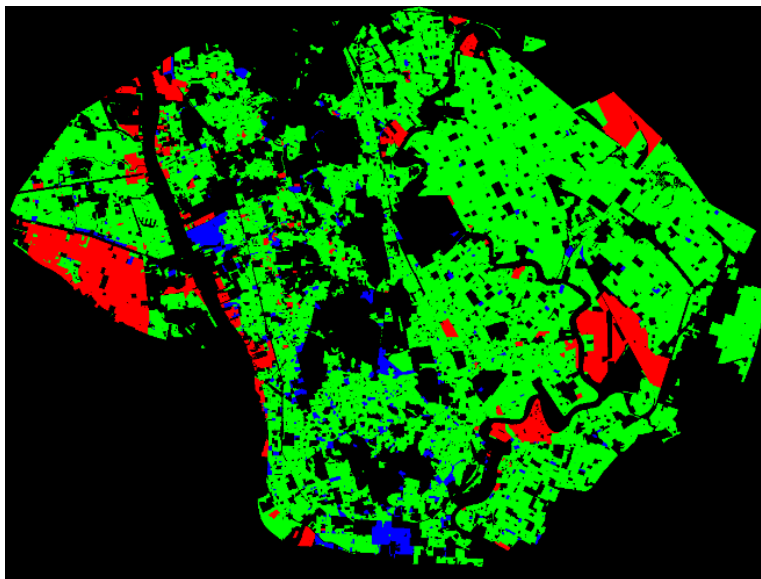


Figure A.6 Building use map in 2012 by JICA

Table A.3 The confusion matrix between building type map in 2013 and building use map in 2012 by JICA (km²)

		Land use map in 2012		
		Residential areas	Commercial areas	Industrial areas
the estimated building use map	Residential buildings	37.588 (58.63%)	2.189 (3.41%)	5.240 (8.17%)
	Commercial buildings	4.153 (6.48%)	0.994 (1.55%)	0.173 (0.27%)
	Industrial buildings	0.668 (1.04%)	0.042 (0.06%)	0.976 (1.52%)